AD_____

Award Number: DAMD17-00-1-0042

TITLE: A Novel Member of the Insulin-like Growth Factor Binding Protein Superfamily in Prostate Cancer

PRINCIPAL INVESTIGATOR: Ron G. Rosenfeld, M.D.

CONTRACTING ORGANIZATION: Oregon Health Sciences Center
Portland, Oregon 97201-3098

REPORT DATE: February 2002

TYPE OF REPORT: Annual

PREPARED FOR: U.S. Army Medical Research and Materiel Command
Fort Detrick, Maryland 21702-5012

REPORT DOCUMENTATION PAGE

Form Approved
OMB No. 074-0188

1. AGENCY USE ONLY (Leave blank)	2. REPORT DATE	3. REPORT TYPE AND DATES COVERED
	February 2002	Annual (1 Feb 01 - 31 Jan 02)

4. TITLE AND SUBTITLE
A Novel Member of the Insulin-like Growth Factor Binding Protein Superfamily in Prostate Cancer

5. FUNDING NUMBERS
DAMD17-00-1-0042

6. AUTHOR(S)
Ron G. Rosenfeld, M.D.

7. PERFORMING ORGANIZATION NAME(S) AND ADDRESS(ES)
Oregon Health Sciences Center
Portland, Oregon 97201-3098

E-Mail: rosenfer@ohsu.edu

8. PERFORMING ORGANIZATION REPORT NUMBER

9. SPONSORING / MONITORING AGENCY NAME(S) AND ADDRESS(ES)
U.S. Army Medical Research and Materiel Command
Fort Detrick, Maryland 21702-5012

10. SPONSORING / MONITORING AGENCY REPORT NUMBER

11. SUPPLEMENTARY NOTES

12a. DISTRIBUTION / AVAILABILITY STATEMENT
Approved for Public Release; Distribution Unlimited

12b. DISTRIBUTION CODE

13. ABSTRACT *(Maximum 200 Words)*
The insulin-like growth factors (IGFs) are potent mitogens for normal and cancerous prostatic cells. The IGFs are found complexed to IGF binding proteins (IGFBPs), which modulate IGF bioactivity, but may themselves act in an IGF-independent manner. We have characterized recently a series of IGFBPs in the amino-terminus, bind IGFs with low affinity, and regulate cell growth through both IGF-dependent and IGF-independent actions. This grant is directed at the study of IGFBP-rP2 (more commonly known as connective tissue growth factor) as a regulator of normal and malignant prostatic growth. The specific aims are to: 1) analyze IGFBP-rP2 mRNA and protein expression and distribution in normal and malignant prostatic tissues; 2) determine the transcriptional, translational and post-translational regulation of IGFBP-rP2; and 3) determine the mechanism by which IGFBP-rP2 regulates prostatic growth.

14. SUBJECT TERMS
growth factors, insulin-like growth factors, binding proteins, tumor suppressors

15. NUMBER OF PAGES
98

16. PRICE CODE

17. SECURITY CLASSIFICATION OF REPORT	18. SECURITY CLASSIFICATION OF THIS PAGE	19. SECURITY CLASSIFICATION OF ABSTRACT	20. LIMITATION OF ABSTRACT
Unclassified	Unclassified	Unclassified	Unlimited

Table of Contents

INTRODUCTION:

The Insulin-like growth factors (IGFs) are potent mitogens for normal and cancerous prostatic cells. The IGFs are found complexed to IGF binding proteins (IGFBPs), which modulate IGF bioactivity, but may themselves act in an IGF-independent manner. We have characterized recently a series of IGFBP-related proteins (IGFBP-rPs) which share homology with the IGFBPs in the amino-terminus, bind IGFs with low affinity, and regulate cell growth through both IGF-dependent and IGF-independent actions (1). This grant is directed at the study of IGFBP-rP2 (more commonly known as connective tissue growth factor) as a regulator of normal and malignant prostatic growth. The specific aims are to: 1) analyze IGFBP-rP2 mRNA and protein expression and distribution in normal and malignant prostatic tissues; 2) determine the transcriptional, translational and post-translational regulation of IGFBP-rP2; and 3) determine the mechanisms by which IGFBP-rP2 regulates prostatic growth.

BODY:

In our prior funding period, we listed the following accomplishments: 1) first characterization of IGFBP-rP2 mRNA and protein expression in normal and malignant prostatic cells (2); 2) first demonstration of up-regulation of IGFBP-rP2 in the prostate by TGF-beta and all-trans retinoic acid, and down-regulation by IGF-I (2); 3) first demonstration of regulation of IGFBP-rP2 mRNA and protein expression by sodium butyrate (3). We have, over the past year, extended these studies and explored new areas in the regulation of IGFBP-rP2 gene expression and action.

Since IGFBP-rP2 has been believed to play a role in fibrotic disease states, and is a potent inducer of extracellular matrix synthesis and angiogenesis, we sought to determine whether it is up-regulated by advanced glycosylation end products (AGE) in primary cultures of nonfetal human dermal fibroblasts. AGE treatment increased IGFBP-rP2 steady state mRNA levels in a time- and dose-dependent manner. In contrast, mRNAs for other IGFBP superfamily members were not up-regulated. The effect of the AGE BSA reagent was shown to be due to nonenzymatic glycosylation of BSA and, using neutralizing antisera to AGE and to the receptor for AGE (RAGE), was seen to be due to late products of nonenzymatic glycosylation and was partly mediated by RAGE. Reactive oxygen species as well as endogenous TGF-beta1 could not explain the AGE effect on IGFBP-rP2 mRNA or protein. We concluded that AGE up-regulates prefibrotic and proangiogenic IGFBP-rP2, which then plays a pivotal role in cell proliferation (4). In subsequent studies, IGFBP-rP2 was shown to be an autocrine mediator in the induction of fibronectin by AGE (5). These results have clear implications for expansion of extracellular matrix in processes such as diabetes, but clearly have importance for all proliferative actions of IGFBP-rP2.

The means by which IGFBP-rP2 acts are undoubtedly complex and have been a subject of active investigation. By affinity cross-linking studies, ligand blotting and solution binding assays, the affinity of IGFBP-rP2 for the IGFs is at least three orders of magnitude lower than that of the conventional IGFBPs. In studies employing biosensor analysis, the affinity of IGFBP-rP2 for immobilized IGFs was below the limits of detection. These studies confirm our underlying hypothesis that the actions of IGFBP-rP2 as a regulator of cell proliferation in the prostate and other tissues is not primarily related to its ability to bind IGFs with high affinity and sequester these growth factors from their receptors. On the other hand, these findings do not preclude the possibility that IGFBP-rP2 is interacting with the IGF system by some other means. Initial investigations were performed in NIH3T# cells that overexpress the type I IGF receptor, and where IGF-I reproducibly stimulates typrosine phosphorylation of the IGFIR. As expected, preincubation of IGF-I with equimolar IGFBP-3 abrogated IGF-induced IGFIR autophosphorylation and subsequent signal transduction. Under identical circumstances, however, our baculovirus-generated IGFBP-rP2 enhanced IGF-induced autophosphorylation of IGFIR. These findings were corroborated, employing avariety of different IGFBP-rP2 preparations (FLAG-tagged and nontagged, as well as heparin-column purified). These remarkable observations were supported by experiments showing: 1) that preincubation of IGF-I and IGFBP-rP2 appears to be necessary for enhanced IGF-induced signaling; 2) that the effects of IGFBP-rP2 on IGF-stimulated signaling appear to be dose-dependent; 3) that IGFBP-rP2 sustains IGF-stimulated signaling; and 4) that the effects of IGFBP-rP2 appear to be specific for the IGFs, and cannot be replicated with either insulin or EGF. Given the importance of the IGF-IGF receptor axis in normal and malignant prostatic growth, these findings have considerable potential significance.

KEY RESEARCH ACCOMPLISHMENTS OVER LAST 12 MONTHS:

- Demonstration of regulation of IGFBP-rP2 mRNA and protein by advanced glycosylation endproducts. These findings extend our previous observations of transcriptional regulation of IGFBP-rP2 by TGF-beta and by sodium butyrate.

- Demonstration that induction of fibronectin by advanced glycosylation endproducts is partly mediated by the AGE-induced up-regulation of cell-derived IGFBP-rP2. These findings have potential implications for the ability of IGFBP-rP2 to act as a pro-fibrotic and pro-angiogenic factor.

- Demonstration that IGFBP-rP2 enhances IGF-induced autophosphorylation of the IGF-I receptor, as well as post-receptor signaling.

REPORTABLE OUTCOMES:

1. Vorwerk P, Hohmann B, Oh Y, Rosenfeld RG, Shymko RM: Binding properties of insulin-like growth factor binding protein-3 (IGFBP-3), IGFBP-3 N- and C-terminal fragments, and members of the IGFBP superfamily measured using a biosensor. Endocrinology (in press)
2. Twigg SM, Chen MM, Joly AH, Chakrapani SD, Tsubaki J, Kim H-S, Oh Y, Rosenfeld RG: Advanced glycosylation end products up-regulate connective tissue growth factor (insulin-like growth factor-binding protein-related protein 2) in human fibroblasts: a potential mechanism for expansion of extracellular matrix in diabetes mellitus. Endocrinology 142:1760-1769, 2001
3. Twigg SM, Joly AH, Chen MM, Tsubaki J, Kim H-S, Hwa V, Oh Y, Rosenfeld RG: Connective tissue growth factor/IGFBP-rP2 is a mediator in the induction of fibronectin by advanced glycosylation end-products in human dermal fibroblasts. Endocrinology (in press)
4. Tsubaki J, Choi W-K, Ingermann AR, Twigg SM, Kim H-S, Rosenfeld RG, Oh Y: Effects of sodium butyrate on expression of members of the IGF-binding protein superfamily in human mammary epithelial cells. J Endocrinol 169:97-110, 2001
5. von Horn H, Hwa V, Rosenfeld RG, Hall K, The BT, Tally M, Ekstrom TJ, Gray SG: Altered expression of low affinity insulin-like growth factor binding protein related proteins I hepatoblastoma (submitted for publication)

CONCLUSIONS:

Studies over the last two years have demonstrated clearly that IGFBP-rP2 is widely expressed in prostatic cells. Depending upon the environment and the circumstances, IGFBP-rP2 appears capable of behaving as a selective tumor suppressor, while also functioning as a general pro-fibrotic and pro-angiogenic factor. These observations are supported by studies of the transcriptional and translational regulation of IGFBP-rP2 in a variety of tissues. Given the low affinity of IGFBP-rP2 for the IGFs, the major actions of IGFBP-rP2 must be independent of any ability it may have to bind and sequester IGFs. These findings are consistent with a growing body of evidence that even the high-affinity IGFBPs can function in an IGF-independent manner under select circumstances. On the other hand, the ability of IGFBP-rP2 to act in a manner independent of its affinity for IGFs does not preclude its interaction with the IGF signaling cascade,

"So what": Prostate carcinogenesis involves the loss of normal growth regulatory machinery. The IGF system has been identified as a key participant in this process and, given its complexity, we should not be surprised at the multiple interfaces between the IGF axis and other growth regulators. IGFBP-rP2 has now been demonstrated to be capable of functioning as both a potent tumor suppressor and a pro-fibrotic and pro-angiogenic factor. It is clear that further studies are required to unravel its complex regulation and actions.

REFERENCES:

1. V. Hwa et al., Endocr Rev 20, 761 (1999)
2. A. Lopez-Bermejo et al., Endocrinol 141, 4072 (2000)
3. J. Tsubaki et al., J Endocrinol 169, 97 (2001)
4. S.M. Twigg et al., Endocrinol 142, 1760, (2001)
5. S.M. Twigg et al., Endocrinol (in press)

APPENDICES: Attached

APPENDICES

Effects of sodium butyrate on expression of members of the IGF-binding protein superfamily in human mammary epithelial cells

J Tsubaki, W-K Choi, A R Ingermann, S M Twigg, H-S Kim, R G Rosenfeld and Y Oh

Department of Pediatrics, Oregon Health Sciences University, Portland, Oregon 97201, USA

(Requests for offprints should be addressed to Y Oh, Department of Pediatrics, School of Medicine, NRC 5, Oregon Health Sciences University, 3181 Southwest Sam Jackson Park Road, Portland, Oregon 97201–3042, USA; Email: ohy@ohsu.edu)

Abstract

Dietary factors play an important role in both the development and prevention of human cancers, including breast carcinoma. One dietary micronutrient, sodium butyrate (NaB), is a major end product of dietary starch and fiber, produced naturally during digestion by anaerobic bacteria in the cecum and colon. NaB is a potent growth inhibitor and initiates cell differentiation for many cell types *in vitro*. In this study, we investigated the effects of NaB on three human mammary epithelial cells and regulation of the IGF axis, specifically, IGF-binding protein-3 (IGFBP-3), a known growth regulator in human mammary cells, and IGFBP-related protein 2 (IGFBP-rP2)/connective tissue growth factor.

NaB inhibited DNA synthesis, as measured by [^{3}H]thymidine incorporation, in estrogen-responsive (MCF-7) and estrogen-non-responsive (Hs578T) breast cancer cells, and normal human mammary epithelial cells (HMEC) to a similar degree (up to 90% inhibition at 1–10 mM concentrations). Treatment of cells with NaB induced histone hyperacetylation, suggesting that NaB exerts its biological effects, at least in part, as a histone deacetylase inhibitor in mammary epithelial cells. Treatment of Hs578T cells with NaB caused an induction of apoptotic cell death. NaB treatment resulted in increased levels of $p21^{Waf1/Cip1}$ mRNA and protein in Hs578T cells and distinct upregulation of $p27^{Kip1}$ in HMEC, suggesting that NaB activates different genes involved in cell cycle arrest, depending upon the cell type. In the same context, among the IGFBP superfamily members tested, NaB specifically upregulated the expression of IGFBP-3 and IGFBP-rP2. These two proteins are known to be involved in inhibition of mammary epithelial cell replication. Northern blot analysis showed that NaB treatment at 1–10 mM concentrations caused a dose-dependent stimulation of IGFBP-3 mRNA expression in cancerous cells and IGFBP-rP2 mRNA expression in both cancerous and non-cancerous cells. Protein data from Western ligand blot and immunoblot analyses demonstrated parallel results.

In summary, we have demonstrated that NaB (i) uniformly suppresses DNA synthesis in both cancerous and non-cancerous mammary cells, and (ii) upregulates IGFBP-3 and IGFBP-rP2 mRNA and protein levels in cancerous and non-cancerous mammary cells. These results provide the first demonstration that butyrate regulates the IGFBP system in the human mammary system.

Journal of Endocrinology (2001) **169**, 97–110

Introduction

Butyric acid is a 4-carbon fatty acid which is the major product from microbial fermentation of dietary fibers in the large intestine (Velázquez *et al.* 1997). It is a potent growth inhibitor and initiates cell differentiation in several cell types, including breast cancer cells *in vitro* (Coradini *et al.* 1997, Velázquez *et al.* 1997, Gleave *et al.* 1998, Yamamoto *et al.* 1998). Although the molecular mechanisms by which butyrate exerts its effects are still unclear, it is known to induce a number of alterations within the nucleus, including histone hyperacetylation (de Haan *et al.* 1986, Archer & Hodin 1999).

It has been reported that butyrate, as well as trichostatin A (TSA), a specific histone deacetylase inhibitor (Yoshida *et al.* 1990), modulates specific genes involved in cell cycle regulation and apoptosis. These include the cyclin-dependent kinase (cdk) inhibitor $p21^{Waf1/Cip1}$ (Archer *et al.* 1998), $p16^{INK4}$ (Schwartz *et al.* 1998), $p27^{Kip1}$ (Litvak *et al.* 1998), retinoblastoma protein (Vaziri *et al.* 1998), cyclin D1 (Lallemand *et al.* 1996, Siavoshian *et al.* 1997), Bcl-2 and Bax (Mandal & Kumar 1996, Hague *et al.* 1997). Furthermore, butyrate has also been reported to upregulate the expression of transforming growth factor-β (TGF-β) (Staiano-Coico *et al.* 1990), which is known to be involved in growth suppression of various

0022–0795/01/0169–097

cancer cells, including breast cancer cells (Knabbe *et al.* 1987).

Insulin-like growth factors (IGFs) are potent mitogens for several cell types (Macaulay 1992, Resnicoff *et al.* 1995). The IGF system consists of IGF-I and IGF-II ligands, the transmembrane type I and type II IGF receptors, the IGF-binding proteins (IGFBPs) and IGFBP proteases (Hwa *et al.* 1999). Recently, the concept of the IGFBP superfamily has been proposed (Baxter *et al.* 1998); it consists of high affinity IGF binders (IGFBP-1 to -6) and low affinity IGF binders (IGFBP-related proteins (IGFBP-rPs)). The IGFBPs modulate IGF bioactivity, and bind with differential affinities to IGFs in serum and various biological fluids (Kelley *et al.* 1996, Rajaram *et al.* 1997). In addition, recent evidence suggests that some IGFBPs may have direct receptor-mediated effects independent of IGFs (Oh *et al.* 1993). IGFBP-3, for example, has been demonstrated to be an important mediator of other growth inhibitory agents, such as retinoic acid (Gucev *et al.* 1996), vitamin D (Colston *et al.* 1998), TGF-β (Oh *et al.* 1995, Gucev *et al.* 1996, Rajah *et al.* 1997), anti-estrogens (Huynh *et al.* 1996), tumor necrosis factor-α (Rozen *et al.* 1998) and p53 (Buckbinder *et al.* 1995), independently of the IGF signaling system. Furthermore, the importance of IGF-independent biological effects of the IGFBP superfamily, such as IGFBP-3 (Oh *et al.* 1993), IGFBP-rP1 (Burger *et al.* 1998) and -rP2 (Hishikawa *et al.* 1999) on cell replication has been demonstrated in human breast cancer cell systems.

In this study, we have investigated the effects of sodium butyrate (NaB) on members of the IGFBP superfamily in human mammary epithelial cells, using estrogen-responsive (MCF-7) and estrogen-non-responsive (Hs578T) breast cancer cells, and normal human mammary epithelial (HMEC) cells. We report here that NaB upregulates IGFBP-3 and IGFBP-rP2 mRNA and protein in mammary epithelial cells.

Materials and Methods

Materials

NaB, TSA, BSA and 0·4% trypan blue solution were purchased from Sigma Chemical Co. (St Louis, MO, USA). ^{125}I-labeled IGF-I was kindly provided by Diagnostic Systems Laboratories (Webster, TX, USA). Polyclonal anti-IGFBP-3, anti-IGFBP-rP1, anti-IGFBP-rP2 and anti-HEC1 (specific for both human IGFBP-2 and -3) antisera were generated as previously described (Rosenfeld *et al.* 1990, Oh *et al.* 1993, Wilson *et al.* 1997, Yang *et al.* 1998). Polyclonal anti-IGFBP-5 antibody was purchased from Austral Biologicals (San Ramon, CA, USA). Polyclonal anti-acetyl-lysine, anti-acetylated histone H3 and anti-acetylated histone H4 antibodies were purchased from Upstate Biotechnology (Lake Placid, NY, USA). Polyclonal anti-poly(ADP-ribose)polymerase (PARP) antibody was purchased from Santa Cruz Biotechnology (Santa Cruz, CA, USA). Monoclonal antibodies, anti-p21$^{Waf1/Cip1}$, anti-p16^{INK4} and anti-p27^{Kip1} were purchased from Transducion Laboratories (Lexington, KY, USA), PharMingen (San Diego, CA, USA) and Calbiochem (Cambridge, MA, USA) respectively.

Cell culture

Hs578T estrogen-non-responsive human breast cancer cells and MCF-7 estrogen-responsive human breast cancer cells were purchased from ATCC (Manassas, VA, USA). Both cell lines were maintained in DMEM supplemented with 4·5 g/l glucose, 110 mg/l sodium pyruvate, and 10% fetal bovine serum. HMEC (normal human mammary epithelial cells) were purchased from Clonetics (San Diego, CA, USA), and maintained in mammary epithelium basal medium (MEBM) with growth supplements (bovine pituitary extract (BPE), human epidermal growth factor, insulin, hydrocortisone, gentamicin and amphotericin-B) as directed by the manufacturer.

[^{3}H]thymidine incorporation assay

Cells were seeded into 24-well dishes at 37 °C in 5% CO_2. At 90% confluence, cells were placed in serum-free media for 12 h, then treated as indicated in the text. After 22 h, 0·1 μCi [^{3}H]thymidine (NEN, Boston, MA, USA) in a volume of 25 μl PBS was added to each well, and the plate was incubated for 4 h at 37 °C. Cells were washed with cold PBS twice, treated with 10% trichloroacetic acid (TCA) for 10 min at − 20 °C, washed with 10% TCA followed by 95% ethanol, and lysed with 400 μl 0·25 N NaOH per well. Cell lysates (CL) from each well were transferred to scintillant vials, then 10 ml scintillation fluid with 100 μl 2 N HCl were added to the vials, and the radioactivity was measured in a scintillation counter.

MTS assay

Hs578T cells were seeded into 96-well plates. At 80% confluence, they were incubated for 12 h in serum-free DMEM, then treated with various concentrations of NaB as indicated in the text in serum-free media. After a further incubation of 1–4 days, the MTS reagent (Promega Co., Madison, WI, USA) was added in the ratio recommended by the manufacturer. At 15 min intervals, the absorbance of the formazan product at 490 nm was read with a plate reader (Spectra Shell Reader; SLT Labinstruments GmbH, Austria). On the same plate, cells were dispensed at the differential confluency. These cells were left untreated in serum-free media, and then the MTS reagent was added at the same time as to the butyrate-treated wells. After the reading, cells were trypsinized, then the cell number was counted with a

hemacytometer. Using this method, a linear correlation was obtained between direct cell counts from 1×10^3 to 1×10^4 per well and the absorbance ($r=0{\cdot}85$, $n=70$) (data not shown). The experiment was repeated three times in conditions where the starting untreated control cell number was 8×10^3 per well, and the absorbance at 490 nm read at 45 min after adding the MTS reagent to the wells was ~0·8.

Quantitation of apoptosis

To quantitate apoptotic cell death, the Cell Death Detection ELISA^{PLUS} kit (Roche Molecular Biochemicals, Mannheim, Germany), which measures cytoplasmic histone-bound DNA fragments produced during apoptotic DNA fragmentation, was used (Mandal & Kumar 1996). Hs578T cells were seeded into a 96-well plate at 80% confluence, they were incubated for 12 h in serum-free DMEM, then treated with various concentrations of NaB in serum-free media. After 72 h, cytoplasmic extracts were made from attached cells by adding 100 µl lysis buffer to 5×10^3 cells per well. Supernatant (20 µl from 100 µl) was analyzed in the ELISA, as directed by the manufacturer's protocol. Briefly, the samples were placed into streptavidin-coated multi-well plates, a mixture of anti-histone-biotin and anti-DNA-peroxidase was added and incubated. The ELISA was developed with peroxidase substrate, and the absorbance at 405 nm was measured against 490 nm as a reference wavelength. The experiment was performed from duplicate samples for each data point generated, and was repeated twice independently.

Preparation of conditioned media (CM) and CL

Cells were seeded in 12-well plates. At 95% confluence, they were incubated for 12 h in serum-free DMEM (Hs578T and MCF-7) or supplement-free MEBM with added BPE (HMEC), then treated as indicated in the text in serum- or supplement-free media. CM samples were collected after 72 h and centrifuged at 1000 *g* for 10 min to remove debris. The harvested CM from duplicate wells within each experiment were pooled and stored at − 20 °C until assay. Proteins in 40 µl CM per lane were examined by Western immunoblot or Western ligand blot under non-reducing conditions.

CL samples were harvested at 24 h post-treatment by washing with PBS, and then adding 150 µl cold RIPA lysis buffer (20 mM Tris, pH 8·0, 150 mM NaCl, 1% NP-40, 0·5% NaDOC, 0·1% SDS) plus protease inhibitors cocktail (Roche Molecular Biochemicals) directly to each well. Plates were rocked for 30 min at 4 °C, and the lysates were collected and centrifuged at 10 000 *g* for 10 min at 4 °C. The supernatants from duplicate wells within each experiment were pooled and stored at − 20 °C until assay. Total protein concentration was determined for each sample using DC Protein Assay Reagent (Bio-Rad, Hercules, CA, USA), and 20 µg total protein per sample were examined by Western immunoblot under reducing conditions.

Western ligand blot analysis

Proteins from CM samples were size-fractionated by 12% SDS-PAGE under non-reducing conditions and electroblotted onto nitrocellulose filters (Hybond; Amersham Pharmacia Biotech, Piscataway, NJ, USA). Filters were washed in 3% NP-40/ddH_2O for 30 min, blocked with 1% BSA/TBS-T (20 mM Tris–HCl, pH 7·6, 150 mM NaCl, 0·1% Tween-20) for 2 h, and incubated overnight with $2{\cdot}0 \times 10^6$ c.p.m. ^{125}I-labeled IGF-I. The membranes were washed, dried and exposed to film (Kodak BioMax MS, Eastman Kodak Co., Rochester, NY, USA) for 12–18 h.

Western immunoblot analysis

For IGFBP-3, IGFBP-rP1 and IGFBP-rP2 detection, CM samples were separated on non-reducing 12 or 15% SDS-PAGE. For $p21^{Waf1/Cip1}$ detection, CL samples were separated on reducing 15% SDS-PAGE. Proteins were electrotransferred onto nitrocellulose, and membranes were blocked with 5% non-fat dry milk/TBS-T for 1 h at room temperature, then incubated in 1:3000 dilution of primary antibody at 4 °C overnight. Immunoreactive proteins were detected using enhanced chemiluminescence (NEN, Boston, MA, USA).

Total RNA isolation and Northern blot analysis

Cells were grown in 6-well plates until 95% confluent. Cells were then incubated in serum-free media for 12 h, then treated for 18 h in serum- or supplement-free media as indicated in the text. Total RNA was isolated from duplicate wells, using the RNeasy Kit (Qiagen, Valencia, CA, USA), and 5 µg total RNA per sample were separated on a 1% formaldehyde agarose gel and transferred to nylon membranes (GeneScreenPlus; NEN). Membranes were stained with 0·02% methylene blue in 0·3 M NaOAc, pH 5·5, and 18S and 28S rRNA bands were used as internal controls to adjust for sample loading. The blot was then hybridized at 65 °C with full length cDNA probes random-labeled with [^{32}P]dCTP (Prime-It II; Stratagene, Cedar Creek, TX, USA), washed and autoradiographed.

Densitometric analysis

To quantitate the relative induction after Western blot analyses or Northern blot analyses, densitometric measurement was performed by using a GS-700 imaging densitometer with Multi-Analyst software (Bio-Rad).

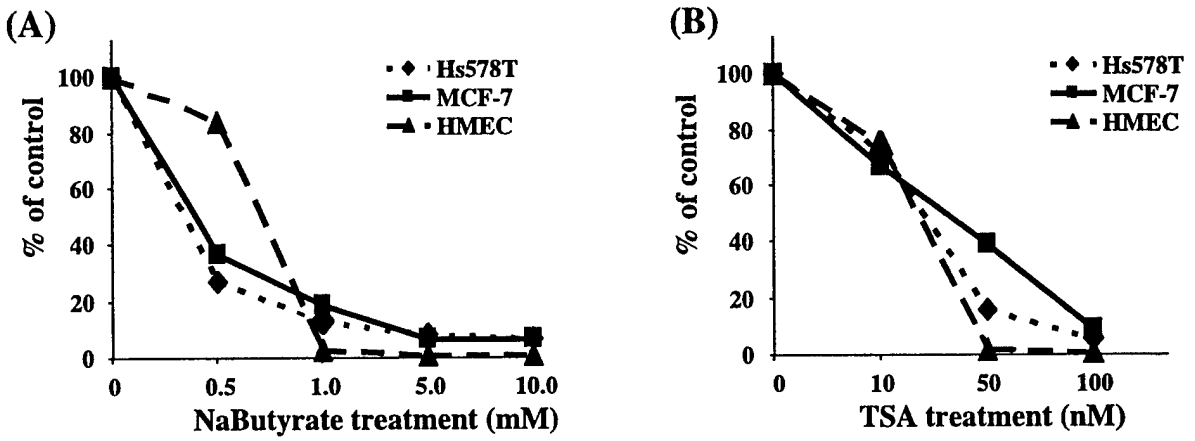

Figure 1 Effect of NaB (A) and TSA (B) on DNA synthesis in Hs578T, MCF-7 and HMEC cells. Serum-starved cells (85–90% confluent) were incubated in basal medium for 22 h in the absence or presence of various concentrations of NaB or TSA as indicated. [^{3}H]Thymidine was added, and the incubation was continued for another 4 h. The incorporation of [^{3}H]thymidine was determined relative to control cells incubated without the addition of these reagents. Results represent the average of two independent experiments each performed in triplicate.

Results

NaB treatment inhibits DNA synthesis and causes histone hyperacetylation in human mammary epithelial cells

Since it has been demonstrated that treatment of NaB resulted in growth inhibition in a variety of cell systems *in vitro*, we first examined the effect of NaB on DNA synthesis in normal (HMEC) and cancerous (Hs578T, MCF-7) human mammary epithelial cells, using the [^{3}H]thymidine incorporation assay. NaB suppressed DNA synthesis in both cancerous and non-cancerous human mammary epithelial cells in a dose-dependent manner, with 90–100% inhibition at NaB concentrations of 5 mM (Fig. 1A). One major function of NaB is inhibition of histone deacetylase activity, resulting in histone hyperacetylation. In order to determine whether NaB-induced inhibition of DNA synthesis might be due to histone hyperacetylation, we treated the cells with TSA, a specific histone deacetylase inhibitor, and compared its effect on DNA synthesis. As shown in Fig. 1B, TSA also suppressed DNA synthesis, with 90–100% inhibition at TSA concentrations of 100 nM in these cells. This suggests that butyrate-induced suppression of DNA synthesis in these human mammary cells may involve histone hyperacetylation, as is shown by Western immunoblot with an anti-acetyl-lysine antibody (Fig. 2). The CL 24 h after treatment with NaB showed an increase of acetylated proteins in a dose-dependent manner, as indicated by the appearance of 11 and 16 kDa bands, which were identified as H4 and H3 histones respectively by Western immunoblot with specific antibodies (data not shown). Histone hyperacetylation was similarly demonstrated by treatment with TSA (Fig. 2). Interestingly, only the 11 kDa band was seen at concentrations over 100 nM.

Effects of NaB on reducing cell number and the induction of apoptosis in human mammary epithelial cells

As NaB inhibits DNA synthesis almost completely by 24 h treatment, cell viability over 4 days after NaB treatment in Hs578T cells was then studied. The MTS assay was used, as described in Materials and Methods, as a marker of relative viable cell number. A progressive reduction in cell number by MTS assay was observed from day 2 onwards using 10 mM NaB, and from day 3 onwards after 5 mM NaB treatment (Fig. 3). In parallel wells, when cell numbers were counted after trypsinizing by direct visualization using a hemacytometer, the attached cell numbers were reduced over the same time course and concentrations of NaB as was detected in the MTS assay above (data not shown). Using trypan blue exclusion during hemacytometer counting, when counted at the same time point, the same number of attached cells were shown to take up trypan blue in the NaB-treated wells compared with the control wells, throughout the full 4 days of the study (data not shown). This trypan blue staining pattern indicates that cell plasma membrane integrity was maintained in the attached cells after NaB treatment compared with the control.

As a reduction in viable cell number by NaB was occurring over time, the possibility that apoptosis was being induced by NaB in the mammary epithelial cells was then addressed. Two independent methods of analysis were used to detect apoptosis: first, nuclear enzyme cleavage, and secondly, DNA fragmentation. The nuclear enzyme PARP is proteolytically cleaved during apoptosis *in vitro* in many cell types, including breast cancer cells (Kaufmann *et al.* 1993). Figure 4A shows Western immunoblots with an anti-PARP antibody after treatment of Hs578T and MCF-7 cells with NaB followed by

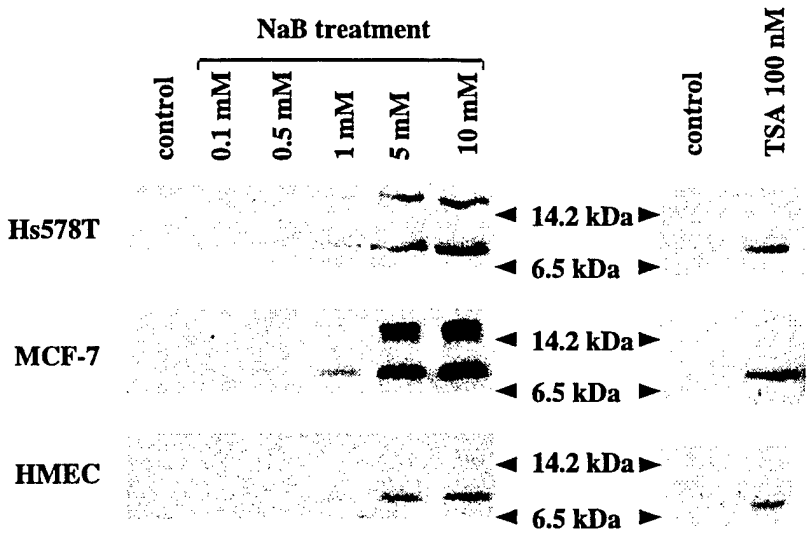

Figure 2 Effect of NaB on protein acetylation. Serum-starved cells were treated for 24 h with various concentrations of NaB as indicated. CL harvested from duplicate wells within each experiment were pooled, and 20 μg protein per lane were loaded onto 15% SDS-PAGE under reducing conditions. Gels were immunoblotted with an anti-acetyl-lysine antibody as described in Materials and Methods. The immunoblots of CL treated with 100 nM TSA are shown on the right. Molecular mass markers are also shown. The results are representative of two independent experiments.

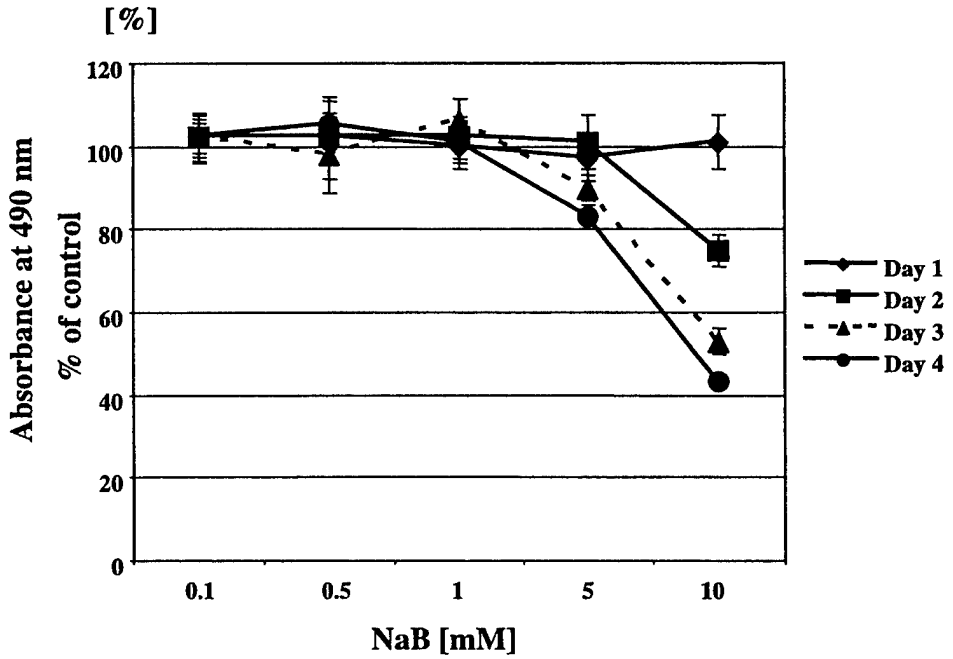

Figure 3 Growth inhibition by NaB. Hs578T cells were seeded into 96-well plates, then serum-starved cells were treated with various concentrations of NaB as indicated. On subsequent days, cell proliferation was measured using the MTS assay. A dose–response effect with added NaB is seen over 4 days. Results are expressed in absorbance readings at 490 nm as percent of the untreated controls ± S.E. ($n=16$).

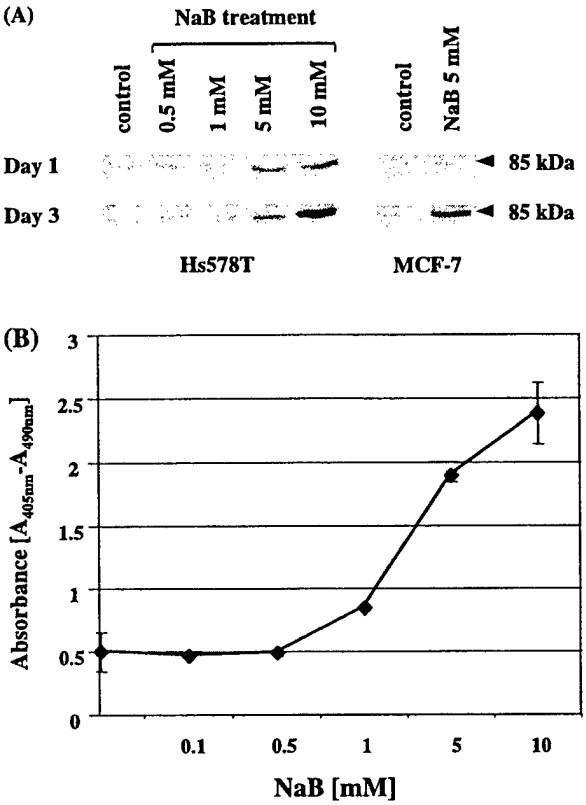

Figure 4 Effect of NaB on apoptosis. (A) Immunoblot analysis of PARP in Hs578T and MCF-7 CL obtained during treatment with NaB (day 1 and day 3). The 85 kDa fragment characteristic of apoptosis is shown. The data shown are representative of two independent experiments. (B) Induction of apoptosis in Hs578T cells treated with increasing doses (0–10 mM) of NaB for 72 h. Cytoplasmic extracts were prepared from attached cells, and apoptotic cell death was quantitated by ELISA measuring cytoplasmic histone-bound DNA complexes characteristic of apoptosis, as described in Materials and Methods. Results are expressed as mean absorbance ± S.D. of two independent experiments performed in duplicate ($n=4$).

analysis of CL. The ~85 kDa carboxy-terminal fragment of PARP detected by Western immunoblotting is indicative of apoptosis occurring in the lysates sampled (Kaufmann *et al.* 1993, Lazebnik *et al.* 1994). In Hs578T cells, some induction of the fragment was already observed by day 1 at concentrations of 5 mM NaB and above, and was more marked in the day 3 lysates, particularly after 10 mM NaB. Detectable increases in the PARP fragment were also seen in the day 3 CL of MCF-7 cells (Fig. 4A).

To verify and more accurately quantitate the apoptosis induced by NaB, an ELISA kit that detects histone-associated DNA fragments (mono- and oligonucleosomes) in the cytoplasmic fraction of CL was used, as described in Materials and Methods. In the Hs578T cytoplasmic extracts from attached cells studied at 3 days post-treatment, NaB induced apoptosis in a dose-dependent manner (Fig. 4B). This sensitive assay demonstrated apoptotic effects initially commencing at 1 mM NaB. Taken together, the two methods of measuring apoptosis show that NaB induces apoptosis in the cells studied, in a more delayed time course compared with the earlier effects on [^{3}H]thymidine incorporation. The apoptosis induced by NaB would be expected to reduce the viable cell number, which was observed, as described earlier.

NaB upregulates expression of p21$^{Waf1/Cip1}$ mRNA and protein levels in human mammary epithelial cells

As the major mechanism for butyrate-induced growth inhibition in various cell systems is known to be through upregulation of cdk inhibitors, in particular p21$^{Waf1/Cip1}$, the induction of p21$^{Waf1/Cip1}$ in mammary epithelial cells was next investigated. Figure 5A is a Northern blot of p21$^{Waf1/Cip1}$ from Hs578T, MCF-7 and HMEC cells treated with or without NaB. p21$^{Waf1/Cip1}$ mRNA expression was upregulated in all three cell lines, and was most marked in Hs578T cells. As shown in Fig. 5B, an upregulation of p21$^{Waf1/Cip1}$ protein levels occurred in these cells, with the greatest increase in p21$^{Waf1/Cip1}$ observed in Hs578T cells, which parallels the mRNA data. As the degree of induction was different between Hs578T cells and the other two cell lines, the NaB effect on cdk inhibitors p27^{Kip1} and p16^{INK4} was further investigated. A distinct upregulation of p27^{Kip1} by NaB treatment (a 2·5-fold increase at 5 mM treatment) was reproducibly seen in HMEC cells, but not in the cancerous cell lines (Fig. 5B). We did not detect p16^{INK4} in Hs578T and MCF-7 cells, and only a slight induction of this protein was seen in HMEC cells. Taken together, these data suggest that differential cdk inhibitors are induced by NaB treatment, in a cell-type-dependent manner.

Butyrate upregulates IGFBP-3 mRNA and protein levels in cancerous, but not in non-cancerous mammary cells

To investigate any correlation between the effect of NaB and the regulation of IGFBP system, we first examined IGFBP-3, a known growth suppressor in human mammary cells. Northern blotting was firstly performed to measure steady-state mRNA levels. Figure 6A shows the time-course effect of NaB treatment on steady-state levels of IGFBP-3 mRNA in Hs578T cells. NaB induced the expression of IGFBP-3 mRNA in a time-dependent manner, with increases first detectable at 6 h after treatment, and with a 2·5-fold increase after treating cells with 5 mM NaB for 24 h, whereas in the non-cancerous HMEC cells, only a slight induction (<1·2-fold) was observed (Fig. 6B). In MCF-7 cells, IGFBP-3 mRNA was not detected in these analyses.

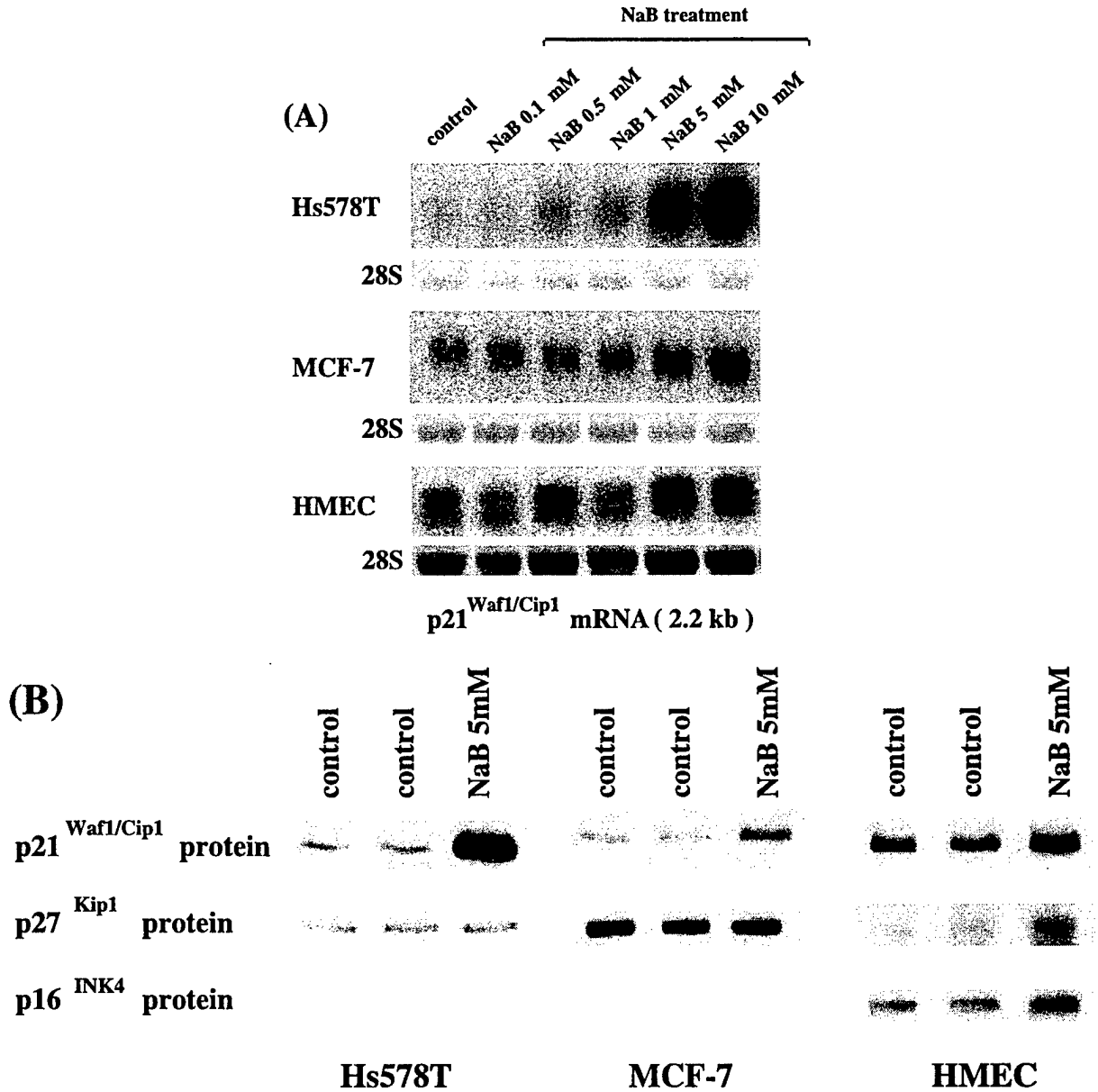

Figure 5 Effect of NaB on expression of $p21^{Waf1/Cip1}$ mRNA (A), and protein of $p21^{Waf1/Cip1}$, $p27^{Kip1}$ and $p16^{INK4}$ (B). (A) Representative Northern blots. Serum-starved cells were treated for 18 h with various concentrations of NaB as indicated. Total RNA was harvested, and 5 μg per lane were electrophoresed. The membrane was probed with labeled cDNA fragments for $p21^{Waf1/Cip1}$. The 28S rRNA is presented as an indicator of loading. The data shown are representative of at least three separate experiments. (B) Representative Western immunoblots. Twenty micrograms total protein from whole CL obtained at 24 h post-treatment per lane were loaded onto 15% SDS-PAGE under reducing conditions, and immunoblotted with anti-$p21^{Waf1/Cip1}$, anti-$p27^{Kip1}$ and anti-$p16^{INK4}$, as indicated in Materials and Methods. Two sets of untreated controls were derived from different wells in the same culture plates. The data shown represent two separate experiments. $p16^{INK4}$ was only detectable in the CL of HMEC cells.

The CM were then examined for changes in IGFBP-3 protein levels after NaB treatment. In order to ascertain a suitable time point to collect CM samples, the time-course induction of media IGFBP-3 protein in Hs578T cells was studied by Western ligand blot analysis, using ^{125}I-labeled IGF-I as the ligand, as described in Materials and Methods. The IGFBP-3 level in the CM was detectably increased at 24 h, even after 1 mM NaB, was further increased at 48 h,

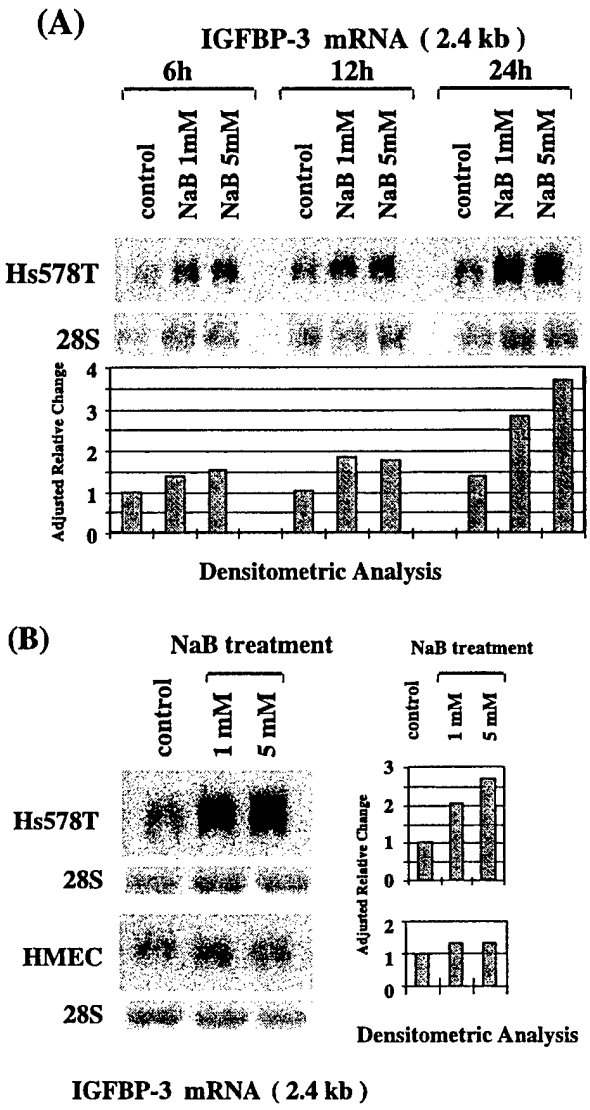

Figure 6 Northern blot analysis of the effect of NaB on the expression of IGFBP-3 mRNA. Total RNA was harvested, and 5 μg per lane were electrophoresed. The membrane was subsequently probed with labeled cDNA fragments of IGFBP-3. (A) Time-course expression of IGFBP-3 mRNA in Hs578T cells. Serum-starved cells were treated for 6, 12 and 24 h, with or without NaB as indicated. (B) Representative Northern blots for IGFBP-3 mRNA expression at 18 h (HMEC) and 24 h (Hs578T) post-treatment. 28S rRNA methylene blue membrane staining is presented as an indicator of equal loading. Densitometric analysis adjusted for 18S and 28S rRNA is also shown. Each result represents at least three independent experiments. In MCF-7 cells, IGFBP-3 mRNA was not detected in 10 μg total RNA.

and peaked at 72 h following NaB treatment (Fig. 7A). Subsequently, CM at 72 h post-treatment were analyzed in further studies. As shown in Fig. 7B, various IGFBPs could be detected by the IGF ligand blot. The identity of these IGFBPs was confirmed by Western immunoblots using IGFBP-3, -2 and -5 specific antibodies, showing the 42–46 kDa doublet bands to be IGFBP-3, the broad 29–36 kDa bands to contain IGFBP-2 and -5, and the 24 kDa band to be IGFBP-4 (data not shown). In HMEC cells, the Western ligand blot did not reveal an IGFBP-5 band, whereas the Western immunoblot with IGFBP-5 antibody revealed a low intensity band of the predicted molecular mass for IGFBP-5 (data not shown) (Adamo *et al.* 1992, Sheikh *et al.* 1992). IGFBP-3 protein levels were upregulated in both Hs578T (2·1-fold over the control) and MCF-7 (12·6-fold over the control) cells, each after 5 mM NaB treatment (Fig. 7B). Further Western immunoblotting analyses demonstrated no detected IGFBP-3 fragments in all samples tested in these cells (data not shown). As the basal level of IGFBP-3 in MCF-7 cells was nearly undetectable, the induction of IGFBP-3 protein by NaB was more conspicuous in this cell line. In contrast, only slight upregulation of IGFBP-3 (<1·5-fold) was observed in HMEC cells, mirroring the mRNA data (shown earlier in Fig. 6B). Levels of IGFBP-2/-5 and -4 showed no significant change up to 10 mM NaB treatment, after accounting for effects of NaB on cell number (not shown). The effect of TSA treatment on IGFBP-3 protein levels by Western ligand blot and immunoblot was also studied. TSA treatment of both Hs578T and MCF-7 cells caused a dose-dependent increase in IGFBP-3 protein levels (not shown), suggesting that NaB-induced upregulation of IGFBP-3 is, at least in part, through histone hyperacetylation. This effect was not seen in the HMEC cells (data not shown).

NaB upregulates IGFBP-rP2 mRNA and protein expression in both cancerous and non-cancerous mammary cells

The induction of the low affinity IGF binders, especially IGFBP-rP2, was then investigated, as this protein also has recently been shown to have a growth suppressive effect in human mammary cells (Hishikawa *et al.* 1999). The effect of NaB treatment on IGFBP-rP2 mRNA expression was potent, particularly in Hs578T cells, where effects occurred with 0·5 mM NaB. As seen in Fig. 8A, a 10-fold induction of IGFBP-rP2 by 5 mM NaB treatment was observed in Hs578T cells, whereas a maximal 2- to 3-fold induction occurred in HMEC cells. IGFBP-rP2 mRNA was not detected in MCF-7 cells.

Western immunoblot analysis against IGFBP-rP2 and -rP1 was then performed. As shown in Fig. 8B, NaB highly upregulated IGFBP-rP2 protein levels in all three cell lines in a dose-dependent manner (>10-fold at 10 mM NaB over the control in all three cell lines). Increases in media IGFBP-rP2 were initially detectable within 24 h, even after only 1 mM NaB (data not shown). In contrast to the effects on IGFBP-rP2, the IGFBP-rP1 band intensity was not increased by NaB treatment. The apparent reduction in IGFBP-rP1 by NaB treatment

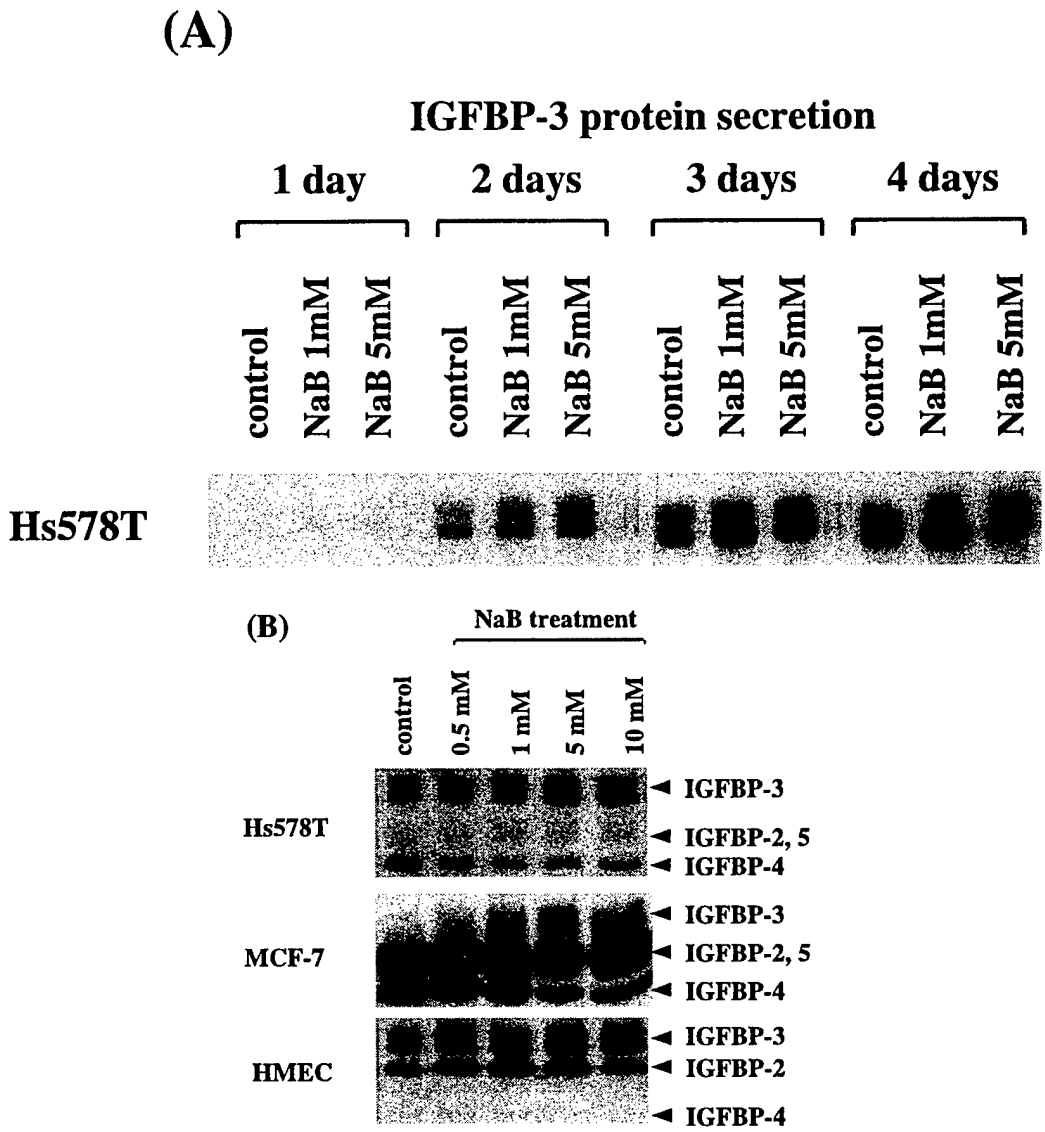

Figure 7 Effect of NaB on IGFBP production in Hs578T, MCF-7 and HMEC cells analyzed by Western ligand blotting. Serum-starved cells were treated with various concentrations of NaB. CM harvested from duplicate wells within each experiment were pooled, size-fractionated using 12% SDS-PAGE under non-reducing conditions, electroblotted onto nitrocellulose membranes, and treated with ^{125}I-labeled IGF-I, as indicated in Materials and Methods. (A) Time-course expression of IGFBP-3 protein in Hs578T cells. Serum-starved cells were treated with or without NaB as indicated and Western ligand blot was performed over 4 days. (B) Representative Western ligand blots using 72 h CM in Hs578T, MCF-7 and HMEC cells. The data shown were derived from at least three independent experiments.

compared with control, especially in Hs578T CM, was 52% on average using densitometric analysis at day 3 after 10 mM NaB. This reduction in IGFBP-rP1 could be fully accounted for by considering the effects of NaB on cell number, as shown earlier in Fig. 3, where 40–50% of the cells are non-viable by this time of NaB treatment compared with control. IGFBP-rP1 was not detected in MCF-7 cells. These results show that IGFBP-rP2 mRNA and protein are specifically induced by NaB in both cancerous and non-cancerous breast epithelial cells.

Discussion

In this study, NaB effects in the human mammary cell system including cancerous and non-cancerous cells, was

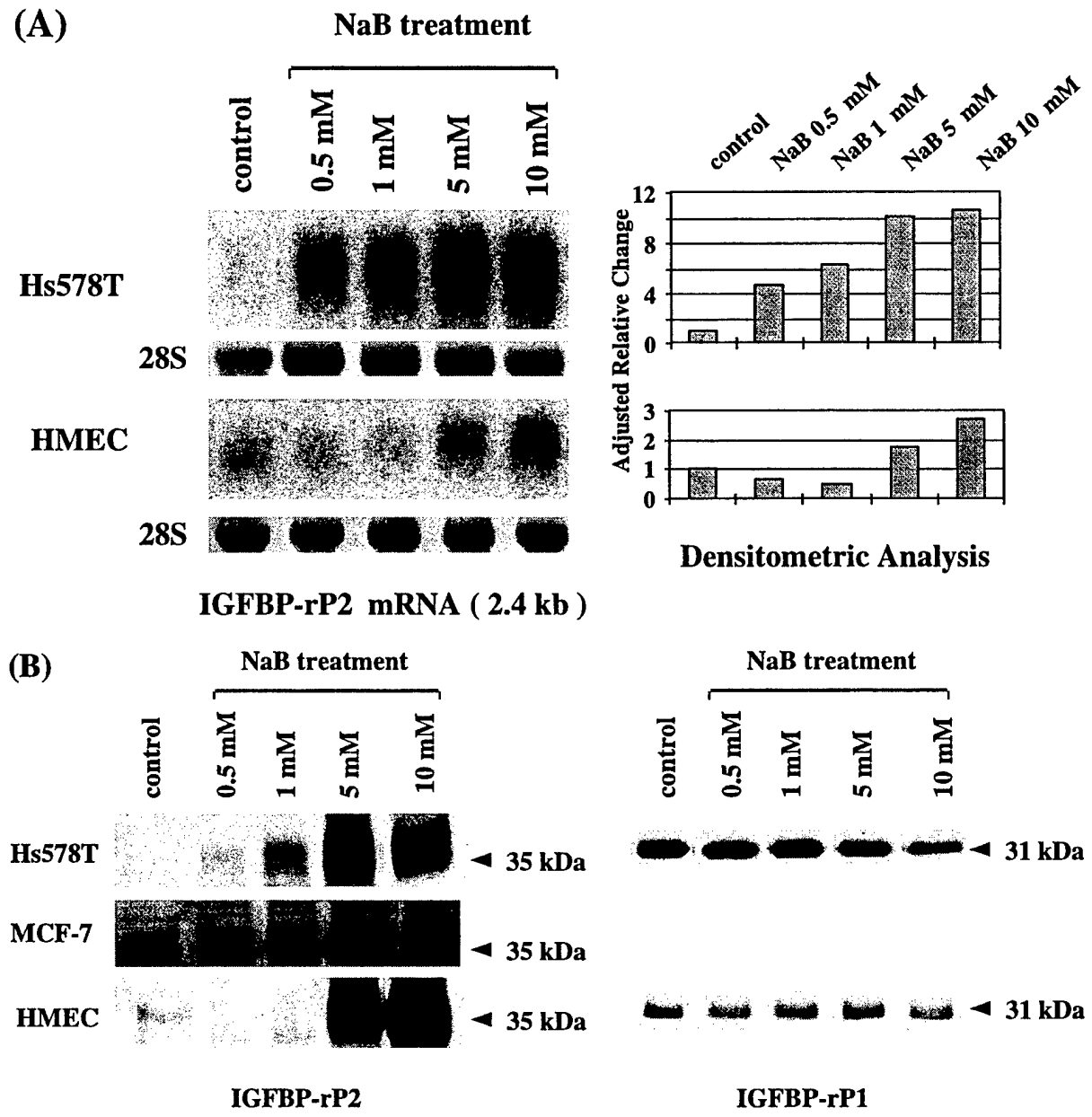

Figure 8 Effect of NaB on (A) IGFBP-rP2 mRNA expression, and (B) IGFBP-rP2 and -rP1 protein expression in Hs578T, MCF-7 and HMEC cells. (A) Representative Northern blots. Total RNA was harvested at 18 h post-treatment, and 5 μg per lane were electrophoresed. The membrane was subsequently probed with labeled cDNA fragments of IGFBP-rP2. 28S rRNA methylene blue membrane staining is presented as an indicator of equal loading. Densitometric analysis adjusted for 18S and 28S rRNA is also shown. Each result represents two independent experiments. In MCF-7 cells, IGFBP-rP2 mRNA was not detected in 10 μg total RNA. (B) Representative Western immunoblot analysis. Serum-starved cells were treated with various concentrations of NaB for 72 h. CM harvested from duplicate wells within each experiment were pooled, size-fractionated using 12% (for IGFBP-rP2) or 15% (for IGFBP-rP1) SDS-PAGE under non-reducing conditions, electroblotted onto nitrocellulose membranes, and treated with appropriate antibodies, as indicated in Materials and Methods. IGFBP-rP1 was not detected in the CM of MCF-7 cells.

investigated, in order to obtain a greater understanding of the cellular mechanism of action of NaB in this cell type. NaB was found to cause an initial inhibition in new DNA synthesis, followed by apoptotic changes, and a reduction in viable cell number. Subsequently, the cdk inhibitors studied showed some cellular specificity in their

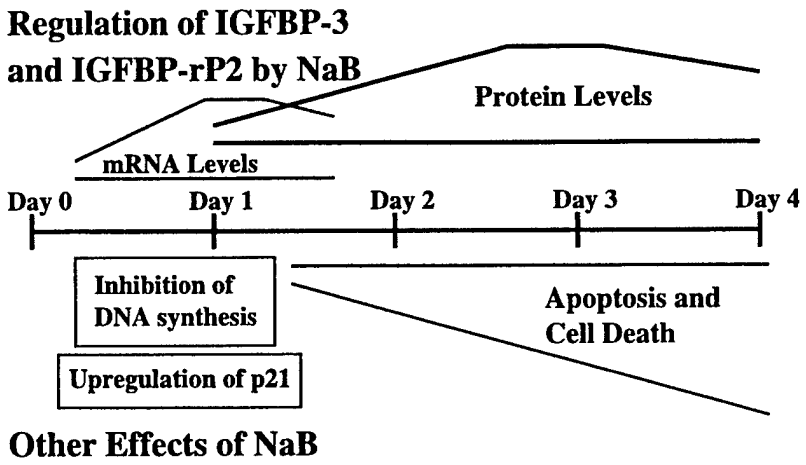

Figure 9 Schematic diagram showing a summary of sequential effects of NaB in Hs578T cells observed in this study. The upregulation of IGFBP-3 and IGFBP-rP2 is shown above the time line and other effects of NaB including cell growth inhibition and cell death are shown below. For further description refer to the discussion in the text.

upregulation by NaB. IGFBP superfamily members known to induce growth inhibition and apoptosis in breast epithelial cells were also upregulated by NaB.

A schematic summary of our observations in Hs578T cells is shown in Fig. 9. We first studied the general effects of NaB on cell growth regulation. Butyrate induces diverse and reversible biological effects on cell differentiation, apoptosis and cell growth *in vitro* (Pouillart 1998). In colonic epithelial cells, butyrate is known to exert paradoxical effects, with induction of proliferation in normal cells and growth inhibition in neoplastic phenotypes (Hassig *et al.* 1997, Archer & Hodin 1999). In the mammary system studied here, butyrate inhibits DNA synthesis in both normal and cancerous cells as measured by [^{3}H]thymidine incorporation at 24 h after treatment. Also, as shown in Fig. 9, after 24 h of NaB treatment at concentrations over 1 mM, cell numbers became reduced in a dose- and time-dependent manner. This reduction in cell number was explained, at least in part, by NaB-induced apoptosis. The observed induction of apoptosis is consistent with previous reports of NaB-induced apoptosis in other cell systems (Hague *et al.* 1993, Carducci *et al.* 1996, Coradini *et al.* 1997). In summary, NaB was found to induce both inhibition of DNA synthesis and programmed cell death, in Hs578T cells.

It is known that butyrate induces a variety of changes within the nucleus (Siavoshian *et al.* 1997, Schwartz *et al.* 1998), including histone hyperacetylation, especially of H3 and H4 (Archer & Hodin 1999), and DNA methylation (de Haan *et al.* 1986). Previous studies indicate that the effect of butyrate and other histone deacetylase inhibitors on cells closely corresponds to the effects of $p21^{Waf1/Cip1}$ expression in the regulation of G1 (Hunter & Pines 1994), S (Ogryzko *et al.* 1997) and G2 (Coradini *et al.* 1997, Lallemand *et al.* 1999) phases of the cell cycle (Hassig *et al.* 1997). The major mechanism for butyrate-induced cell cycle arrest is reported to be through upregulation of $p21^{Waf1/Cip1}$ in various cell systems, including hepatocellular carcinoma cells (Yamamoto *et al.* 1998), colon cancer cells (Nakano *et al.* 1997, Siavoshian *et al.* 1997, Archer *et al.* 1998, Litvak *et al.* 1998), prostate cancer cells (Huang *et al.* 1999) and breast cancer cells (Lallemand *et al.* 1999). In contrast, Vaziri *et al.* (1998) demonstrated $p21^{Waf1/Cip1}$-independent G1 cell cycle arrest by butyrate in 3T3 fibroblasts. In our present studies, the prominent induction of $p21^{Waf1/Cip1}$ was observed in estrogen-non-responsive Hs578T cancer cells, whereas modest induction was observed in estrogen-responsive MCF-7 cancer cells and non-cancerous HMEC cells. Interestingly, butyrate upregulated $p27^{Kip1}$ expression only in HMEC cells. The $p16^{INK4}$ protein was detected only in HMEC cells and no further regulation was observed after butyrate treatment. Taken together, these data imply that the biological function of butyrate is mediated through more than one mechanism, even in butyrate-induced cell cycle arrest, suggesting that butyrate possesses multifunctional mechanisms of action.

This is the first demonstration that butyrate upregulates members of the IGFBP superfamily in human mammary cells. One previous report showed that only IGFBP-2 was upregulated by butyrate in colon cancer cells (Nishimura *et al.* 1998). In contrast, our studies demonstrate that among the six IGFBPs and IGFBP-rP-1 and -2, only IGFBP-3 and IGFBP-rP2 are upregulated by butyrate in cancerous and non-cancerous mammary epithelial cells. Recent evidence has suggested that, in addition to modulating the access of IGFs to their receptors, IGFBP-3 has the ability to suppress proliferation in various cell systems, including

human breast cancer cells, working through IGF-independent mechanisms (Valentinis *et al.* 1995, Oh 1998). Further studies have demonstrated that IGFBP-3 directly induces apoptosis through an IGF-independent pathway in PC-3 human prostatic adenocarcinoma cells (Rajah *et al.* 1997) as well as in other cell systems (Nickerson *et al.* 1997). We, therefore, hypothesized that IGFBP-3 may be a major downstream effector of growth inhibitory and apoptosis-inducing agents.

Indeed, NaB treatment significantly upregulated IGFBP-3 steady-state mRNA and protein levels in a time- and dose-dependent manner in Hs578T and MCF-7 human breast cancer cells, while levels of IGFBP-2 and -4 were unaffected. As summarized in Fig. 9, we observed that the mRNA induction had already started at 6 h after treatment and peaked by 24 h after treatment, while the presence of the protein in CM was barely detectable at the 24 h time point and gradually increased up to day 3. Notably, both the mRNA and protein induction by NaB were detectable earlier than the reduction in cell number and apoptosis, consistent with a specific regulation of these IGFBP superfamily members by NaB rather than effects on these IGFBPs occurring secondary to cell death. In contrast to effects seen in these cancer cell lines, the NaB regulation of IGFBP-3 in normal human mammary epithelial cells was less marked. Additionally, treatment with TSA gave similar results, indicating that histone hyperacetylation may be involved. The differential regulation of IGFBP-3 by NaB in cancerous versus non-cancerous cells may point to an important mechanism for growth inhibition by IGFBP-3 in cancer.

It has been demonstrated that TGF-β, which is a potent growth suppressing factor in human breast cancer cells (Zugmaier *et al.* 1989, Oh *et al.* 1995), induces expression of IGFBP-rP2 mRNA and protein levels (Yang *et al.* 1998). In addition, recent studies have demonstrated that IGFBP-rP2 has a direct apoptotic effect in MCF-7 cells (Hishikawa *et al.* 1999). Our present data show that IGFBP-rP2 was significantly upregulated by NaB treatment in a time- and dose-dependent manner in both cancerous and non-cancerous human mammary epithelial cell lines, suggesting that IGFBP-rP2 may also play a role in the bioactivity of butyrate on cells. In Hs578T cells, the induction of IGFBP-rP2 mRNA was already marked at 0·5 mM, while the protein levels were significantly increased at 5 mM. One potential explanation for this dose discrepancy is that some post-transcriptional modification by NaB of IGFBP-rP2 may also be occurring.

On the basis of this work, it can be speculated that the IGFBP superfamily members, IGFBP-3 and IGFBP-rP2, participate in butyrate-induced sequential cell growth inhibition, particularly in the later event of apoptosis. Detailed studies involving regulation of IGFBP-3 and IGFBP-rP2 bioactivity following butyrate treatment in breast epithelial cells are now required to formally address this issue. It is hoped that exploration of butyrate-induced biological effects subsequent to the cell cycle arrest in this cell system and the investigation of the interaction between butyrate and the IGF axis will lead to a more complete understanding of the complex mechanisms of cell growth control, and to the development of better therapeutic reagents.

Acknowledgements

This research was supported by NIH grants R01 DK51513 (R G R) and CA58110 (R G R), and by US Army grants DAMD17-00-1-0042 (R G R), DAMD17–96–1–6204 (Y O) and DAMD17–96–1–7204 (Y O).

References

Adamo ML, Shao ZM, Lanau F, Chen JC, Clemmons DR, Roberts CT Jr, LeRoith D & Fontana JA 1992 Insulin-like growth factor-I (IGF-I) and retinoic acid modulation of IGF-binding proteins (IGFBPs): IGFBP-2, -3, and -4 gene expression and protein secretion in a breast cancer cell line. *Endocrinology* **131** 1858–1866.

Archer SY & Hodin RA 1999 Histone acetylation and cancer. *Current Opinion in Genetics and Development* **9** 171–174.

Archer SY, Meng S, Shei A & Hodin RA 1998 $p21^{WAF1}$ is required for butyrate-mediated growth inhibition of human colon cancer cells. *PNAS* **95** 6791–6796.

Baxter RC, Binoux MA, Clemmons DR, Conover CA, Drop SL, Holly JM, Mohan S, Oh Y & Rosenfeld RG 1998 Recommendations for nomenclature of the insulin-like growth factor binding protein superfamily. *Journal of Clinical Endocrinology and Metabolism* **83** 3213.

Buckbinder L, Talbott R, Velasco-Miguel S, Takenaka I, Faha B, Seizinger BR & Kley N 1995 Induction of the growth inhibitor IGF-binding protein 3 by p53. *Nature* **377** 646–649.

Burger AM, Zhang X, Li H, Ostrowski JL, Beatty B, Venanzoni M, Papas T & Seth A 1998 Down-regulation of T1A12/mac25, a novel insulin-like growth factor binding protein related gene, is associated with disease progression in breast carcinomas. *Oncogene* **16** 2459–2467.

Carducci MA, Nelson JB, Chan-Tack KM, Ayyagari SR, Sweatt WH, Campbell PA, Nelson WG & Simons JW 1996 Phenylbutyrate induces apoptosis in human prostate cancer and is more potent than phenylacetate. *Clinical Cancer Research* **2** 379–387.

Colston KW, Perks CM, Xie SP & Holly JM 1998 Growth inhibition of both MCF-7 and Hs578T human breast cancer cell lines by vitamin D analogues is associated with increased expression of insulin-like growth factor binding protein-3. *Journal of Molecular Endocrinology* **20** 157–162.

Coradini D, Biffi A, Costa A, Pellizzaro C, Pirronello E & Di Fronzo G 1997 Effect of sodium butyrate on human breast cancer cell lines. *Cell Proliferation* **30** 149–159.

Gleave ME, Sato N, Sadar M, Yago V, Bruchovsky N & Sullivan L 1998 Butyrate analogue, isobutyramide, inhibits tumor growth and time to androgen-independent progression in the human prostate LNCaP tumor model. *Journal of Cellular Biochemistry* **69** 271–281.

Gucev ZS, Oh Y, Kelley KM & Rosenfeld RG 1996 Insulin-like growth factor binding protein 3 mediates retinoic acid- and transforming growth factor β2-induced growth inhibition in human breast cancer cells. *Cancer Research* **56** 1545–1550.

de Haan JB, Gevers W & Parker MI 1986 Effects of sodium butyrate on the synthesis and methylation of DNA in normal cells and their transformed counterparts. *Cancer Research* **46** 713–716.

Hague A, Manning AM, Hanlon KA, Huschtscha LI, Hart D & Paraskeva C 1993 Sodium butyrate induces apoptosis in human colonic tumour cell lines in a p53-independent pathway: implications for the possible role of dietary fibre in the prevention of large-bowel cancer. *International Journal of Cancer* **55** 498–505.

Hague A, Díaz GD, Hicks DJ, Krajewski S, Reed JC & Paraskeva C 1997 bcl-2 and bak may play a pivotal role in sodium butyrate-induced apoptosis in colonic epithelial cells; however overexpression of bcl-2 does not protect against bak-mediated apoptosis. *International Journal of Cancer* **72** 898–905.

Hassig CA, Tong JK & Schreiber SL 1997 Fiber-derived butyrate and the prevention of colon cancer. *Chemistry and Biology* **4** 783–789.

Hishikawa K, Oemar BS, Tanner FC, Nakaki T, Lüscher TF & Fujii T 1999 Connective tissue growth factor induces apoptosis in human breast cancer cell line MCF-7. *Journal of Biological Chemistry* **274** 37461–37466.

Huang H, Reed CP, Zhang JS, Shridhar V, Wang L & Smith DI 1999 Carboxypeptidase A3 (CPA3): a novel gene highly induced by histone deacetylase inhibitors during differentiation of prostate epithelial cancer cells. *Cancer Research* **59** 2981–2988.

Hunter T & Pines J 1994 Cyclins and cancer. II: cyclin D and CDK inhibitors come of age. *Cell* **79** 573–582.

Huynh H, Yang X & Pollak M 1996 Estradiol and antiestrogens regulate a growth inhibitory insulin-like growth factor binding protein 3 autocrine loop in human breast cancer cells. *Journal of Biological Chemistry* **271** 1016–1021.

Hwa V, Oh Y & Rosenfeld RG 1999 Insulin-like growth factor binding proteins: a proposed superfamily. *Acta Paediatrica. Supplement* **428** 37–45.

Kaufmann SH, Desnoyers S, Ottaviano Y, Davidson NE & Poirier GG 1993 Specific proteolytic cleavage of poly (ADP-ribose) polymerase: an early marker of chemotherapy-induced apoptosis. *Cancer Research* **53** 3976–3985.

Kelley KM, Oh Y, Gargosky SE, Gucev Z, Matsumoto T, Hwa V, Ng L, Simpson DM & Rosenfeld RG 1996 Insulin-like growth factor-binding proteins and their regulatory dynamics. *International Journal of Biochemistry and Cell Biology* **28** 619–637.

Knabbe C, Lippman ME, Wakefield LM, Flanders KC, Kasid A, Derynck R & Dickson RB 1987 Evidence that transforming growth factor-β is a hormonally regulated negative growth factor in human breast cancer cells. *Cell* **48** 417–428.

Lallemand F, Courilleau D, Sabbah M, Redeuilh G & Mester J 1996 Direct inhibition of the expression of cyclin D1 gene by sodium butyrate. *Biochemical and Biophysical Research Communications* **229** 163–169.

Lallemand F, Courilleau D, Buquet-Fagot C, Atfi A, Montagne MN & Mester J 1999 Sodium butyrate induces G2 arrest in the human breast cancer cells MDA-MB-231 and renders them competent for DNA rereplication. *Experimental Cell Research* **247** 432–440.

Lazebnik YA, Kaufmann SH, Desnoyers S, Poirier GG & Earnshaw WC 1994 Cleavage of poly (ADP-ribose) polymerase by a proteinase with properties like ICE. *Nature* **371** 346–347.

Litvak DA, Evers M, Hwang KO, Hellmich MR, Ko TC & Townsend CM Jr 1998 Butyrate-induced differentiation of Caco-2 cells is associated with apoptosis and early induction of $p21^{Waf1/Cip1}$ and $p27^{Kip1}$. *Surgery* **124** 161–170.

Macaulay VM 1992 Insulin-like growth factors and cancer. *British Journal of Cancer* **65** 311–320.

Mandal M & Kumar R 1996 Bcl-2 expression regulates sodium butyrate-induced apoptosis in human MCF-7 breast cancer cells. *Cell Growth and Differentiation* **7** 311–318.

Nakano K, Mizuno T, Sowa Y, Orita T, Yoshino T, Okuyama Y, Fujita T, Ohtani-Fujita N, Matsukawa Y, Tokino T, Yamagishi H, Oka T, Nomura H & Sakai T 1997 Butyrate activates the *WAF1/Cip1* gene promoter through Sp1 sites in a p53-negative human colon cancer cell line. *Journal of Biological Chemistry* **272** 22199–22206.

Nickerson T, Huynh H & Pollak M 1997 Insulin-like growth factor binding protein-3 induces apoptosis in MCF7 breast cancer cells. *Biochemical and Biophysical Research Communications* **237** 690–693.

Nishimura A, Fujimoto M, Oguchi S, Fusunyan RD, MacDermott RP & Sanderson IR 1998 Short-chain fatty acids regulate IGF-binding protein secretion by intestinal epithelial cells. *American Journal of Physiology* **275** E55–E63.

Ogryzko VV, Wong P & Howard BH 1997 WAF1 retards S-phase progression primarily by inhibition of cyclin-dependent kinases. *Molecular and Cellular Biology* **17** 4877–4882.

Oh Y 1998 IGF-independent regulation of breast cancer growth by IGF binding proteins. *Breast Cancer Research and Treatment* **47** 283–293.

Oh Y, Müller HL, Lamson G & Rosenfeld RG 1993 Insulin-like growth factor (IGF)- independent action of IGF-binding protein-3 in Hs578T human breast cancer cells. Cell surface binding and growth inhibition. *Journal of Biological Chemistry* **268** 14964–14971.

Oh Y, Müller HL, Ng L & Rosenfeld RG 1995 Transforming growth factor-β-induced cell growth inhibition in human breast cancer cells is mediated through insulin-like growth factor-binding protein-3 action. *Journal of Biological Chemistry* **270** 13589–13592.

Pouillart PR 1998 Role of butyric acid and its derivatives in the treatment of colorectal cancer and hemoglobinopathies. *Life Sciences* **63** 1739–1760.

Rajah R, Valentinis B & Cohen P 1997 Insulin-like growth factor (IGF)-binding protein-3 induces apoptosis and mediates the effects of transforming growth factor-β1 on programmed cell death through a p53- and IGF-independent mechanism. *Journal of Biological Chemistry* **272** 12181–12188.

Rajaram S, Baylink DJ & Mohan S 1997 Insulin-like growth factor-binding proteins in serum and other biological fluids: regulation and functions. *Endocrine Reviews* **18** 801–831.

Resnicoff M, Abraham D, Yutanawiboonchai W, Rotman HL, Kajstura J, Rubin R, Zoltick P & Baserga R 1995 The insulin-like growth factor I receptor protects tumor cells from apoptosis *in vivo*. *Cancer Research* **55** 2463–2469.

Rosenfeld RG, Lamson G, Pham H, Oh Y, Conover C, De Leon DD, Donovan SM, Ocrant I & Giudice L 1990 Insulin-like growth factor binding proteins. *Recent Progress in Hormone Research* **46** 99–159.

Rozen F, Zhang J & Pollak M 1998 Antiproliferative action of tumor necrosis factor-alpha on MCF-7 breast cancer cells is associated with increased insulin-like growth factor binding protein-3 accumulation. *International Journal of Oncology* **13** 865–869.

Schwartz B, Avivi-Green C & Polak-Charcon S 1998 Sodium butyrate induces retinoblastoma protein dephosphorylation, p16 expression and growth arrest of colon cancer cells. *Molecular and Cellular Biochemistry* **188** 21–30.

Sheikh MS, Shao ZM, Clemmons DR, LeRoith D, Roberts CT Jr & Fontana JA 1992 Identification of the insulin-like growth factor binding proteins 5 and 6 (IGFBP-5 and 6) in human breast cancer cells. *Biochemical and Biophysical Research Communications* **183** 1003–1010.

Siavoshian S, Blottiere HM, Cherbut C & Galmiche JP 1997 Butyrate stimulates cyclin D and p21 and inhibits cyclin-dependent kinase 2 expression in HT-29 colonic epithelial cells. *Biochemical and Biophysical Research Communications* **232** 169–172.

Staiano-Coico L, Khandke L, Krane JF, Sharif S, Gottlieb AB, Krueger JG, Heim L, Rigas B & Higgins PJ 1990 TGF-α and TGF-β expression during sodium-n-butyrate-induced differentiation of human keratinocytes: evidence for subpopulation-specific up-regulation of TGF-β mRNA in suprabasal cells. *Experimental Cell Research* **191** 286–291.

Valentinis B, Bhala A, DeAngelis T, Baserga R & Cohen P 1995 The human insulin-like growth factor (IGF) binding protein-3 inhibits the growth of fibroblasts with a targeted disruption of the IGF-I receptor gene. *Molecular Endocrinology* **9** 361–367.

Vaziri C, Stice L & Faller DV 1998 Butyrate-induced G1 arrest results from p21-independent disruption of retinoblastoma protein-mediated signals. *Cell Growth and Differentiation* **9** 465–474.

Velázquez OC, Lederer HM & Rombeau JL 1997 Butyrate and the colonocyte. Production, absorption, metabolism, and therapeutic implication. *Advances in Experimental Medicine and Biology* **427** 123–134.

Wilson EM, Oh Y & Rosenfeld RG 1997 Generation and characterization of IGFBP-7 antibody: identification of 31 kD IGFBP-7 in human biological fluids and Hs578T human breast cancer conditioned media. *Journal of Clinical Endocrinology and Metabolism* **82** 1301–1303.

Yamamoto H, Fujimoto J, Okamoto E, Furuyama J, Tamaoki T & Hashimoto-Tamaoki T 1998 Suppression of growth of hepatocellular carcinoma by sodium butyrate *in vitro* and *in vivo*. *International Journal of Cancer* **76** 897–902.

Yang DH, Kim HS, Wilson EM, Rosenfeld RG & Oh Y 1998 Identification of glycosylated 38-kDa connective tissue growth factor (IGFBP-related protein 2) and proteolytic fragments in human biological fluids, and up-regulation of IGFBP-rP2 expression by TGF-β in Hs578T human breast cancer cells. *Journal of Clinical Endocrinology and Metabolism* **83** 2593–2596.

Yoshida M, Kijima M, Akita M & Beppu T 1990 Potent and specific inhibition of mammalian histone deacetylase both *in vivo* and *in vitro* by trichostatin A. *Journal of Biological Chemistry* **265** 17174–17179.

Zugmaier G, Ennis BW, Deschauer B, Katz D, Knabbe C, Wilding G, Daly P, Lippman ME & Dickson RB 1989 Transforming growth factors type β1 and β2 are equipotent growth inhibitors of human breast cancer cell lines. *Journal of Cellular Physiology* **141** 353–361.

Received 21 November 2000
Accepted 8 December 2000

0013-7227/01/$03.00/0
Endocrinology

Vol. 142, No. 5
Printed in U.S.A.

Advanced Glycosylation End Products Up-Regulate Connective Tissue Growth Factor (Insulin-Like Growth Factor-Binding Protein-Related Protein 2) in Human Fibroblasts: A Potential Mechanism for Expansion of Extracellular Matrix in Diabetes Mellitus*

STEPHEN M. TWIGG, MICHELLE M. CHEN, ALISON H. JOLY, SANJAY D. CHAKRAPANI, JUNKO TSUBAKI, HO-SEONG KIM, YOUNGMAN OH, AND RON G. ROSENFELD

Department of Pediatrics, Oregon Health Sciences University (S.M.T., S.D.C., J.T., H.-S.K., Y.O., R.G.R.), Portland, Oregon 97201; and Cardiorenal Cell Biology, Scios, Inc. (M.M.C., A.H.J.), Sunnyvale, California 94086

ABSTRACT

Expansion of extracellular matrix with fibrosis occurs in many tissues as part of the end-organ complications in diabetes, and advanced glycosylation end products (AGE) are implicated as one causative factor in diabetic tissue fibrosis. Connective tissue growth factor (CTGF), also known as insulin-like growth factor-binding protein-related protein-2 (IGFBP-rP2), is a potent inducer of extracellular matrix synthesis and angiogenesis and is increased in tissues from rodent models of diabetes. The aim of this study was to determine whether CTGF is up-regulated by AGE *in vitro* and to explore the cellular mechanisms involved. AGE treatment of primary cultures of nonfetal human dermal fibroblasts in confluent monolayer increased CTGF steady state messenger RNA (mRNA) levels in a time- and dose-dependent manner. In contrast, mRNAs for other IGFBP superfamily members, IGFBP-rP1 (mac 25) and IGFBP-3, were not up-regulated by AGE. The effect of the AGE BSA reagent on CTGF mRNA was due to nonenzymatic glycosylation of BSA and, using neutralizing antisera to AGE and to the receptor for AGE, termed RAGE, was seen to be due to late products of nonenzymatic glycosylation and was partly mediated by RAGE. Reactive oxygen species as well as endogenous transforming growth factor-β1 could not explain the AGE effect on CTGF mRNA. AGE also increased CTGF protein in the conditioned medium and cell-associated CTGF. Thus, AGE up-regulates the profibrotic and proangiogenic protein CTGF (IGFBP-rP2), a finding that may have significance in the development of diabetic complications. (*Endocrinology* **142:** 1760–1769, 2001)

MULTIPLE MECHANISMS have been described by which chronic hyperglycemia might contribute to the pathological end-organ complications that occur in diabetes mellitus. These include direct effects of elevated glucose on cells, hyperosmolality, oxidant stress, and nonenzymatic glycosylation (1, 2). Advanced glycosylation end products (AGE) are biochemical end products of nonenzymatic glycosylation that are formed irreversibly (3). AGE is elevated in serum (4) and in many tissues in patients with diabetes (5), including skin (6), and has the ability to covalently cross-link and biochemically modify protein structure and affect protein function (7). Additionally, in recent years cell surface receptors for AGE have been identified (8), and postreceptor signaling pathways are being defined (9, 10). Through an AGE receptor-dependent mechanism, AGE induction of cytokines and growth factors has been implicated in contributing to end-organ changes that occur in tissues in patients with diabetes (11–13).

Pathological hallmarks in most tissues where diabetes complications occur include expansion of extracellular matrix (ECM) and angiogenesis (1). The ECM expansion has been proposed to be due to a combination of increased ECM production (14) (15) and biochemically modified matrix, with a reduction in ECM breakdown (16). Connective tissue growth factor (CTGF), also known as insulin-like growth factor (IGF)-binding protein-related protein-2 (IGFBP-rP2) (17), is a potent inducer of ECM in fibroblasts (18, 19) and a potent angiogenic factor (20, 21). A potential role for CTGF in fibrotic disease states is increasingly being described (22–24), suggesting that CTGF may be a mediator of ECM expansion and fibrosis in diabetes. The aim of this study was to determine whether CTGF is up-regulated by AGE and subsequently to explore the cellular mechanism(s) that might be responsible for this effect.

Received October 3, 2000.

Address all correspondence and requests for reprints to: Dr. Stephen M. Twigg, Department of Pediatrics, NRC-5, Mark O. Hatfield Research Center, Oregon Health Sciences University, 3181 SW Sam Jackson Park Road, Portland Oregon 97201. E-mail: twiggs@ohsu.edu.

* This work was supported by the National Health and Medical Research Council of Australia (C. J. Martin Postdoctoral Fellowship to S.T.), and the NIH [Summer Student's Scholarship (to S.C.) and Grants CA-58110 and DK-51513 (to R.G.)]. This work was presented in part at the 82nd Annual Meeting of The Endocrine Society, Toronto, Canada, 2000.

Materials and Methods

Reagents

Polyclonal anti-IGFBP-rP2 (CTGF) antibodies (8799 and 8800) were generated in New Zealand White rabbits, as previously described (25). The anti-AGE antibody, which neutralizes the activity of AGE BSA (26),

was a gift from Dr. H. Miyata, Kissei Pharmaceutical Co. Ltd. (Nagano, Japan). The antihuman polyclonal antibody generated in rabbits against the receptor for AGE (RAGE) was provided as an IgG fraction (gift from Dr. A.M. Schmidt, Columbia University, New York, NY). This antibody inhibits ligand-stimulated activation of RAGE by AGE (27, 28). The transforming growth factor-β1 (TGFβ1) affinity-purified IgG antibody generated in chickens that neutralizes TGFβ1 bioactivity was purchased from R&D Systems, Inc. (Minneapolis, MN). Nonimmune rabbit IgG, D-glucose, glycolaldehyde, BSA (fraction V, fatty acid and endotoxin free), and aminoguanidine were purchased from Sigma (St. Louis, MO). TGFβ1 was purchased from Austral Biologicals (San Ramon, CA).

Intact carboxyl-terminal flag-tagged IGFBP-rP2 (CTGF), used as a standard in the Western immunoblots and in the CTGF enzyme-linked immunosorbent assay (ELISA), was purified from a baculovirus expression system, and pure IGFBP-rP2 (CTGF) protein was quantitated using Coomassie-stained gels with BSA as standard, all as previously described (29). The approximately 14-kDa fragment of IGFBP-rP2 (CTGF), described in Fig. 7A, was purified from a highly proteolyzed preparation of pure IGFBP-rP2 (CTGF) protein, using late-harvested SF-9 insect cell lysates. After initial purification of this preparation by means of flag protein-Sepharose affinity chromatography (29), the fragment was separated from any remaining intact IGFBP-rP2 (CTGF) using a high performance size-fractionation gel permeation column (HR-75, Pharmacia Biotech, Piscataway, NJ) with PBS as buffer, with fast performance liquid chromatography, eluting at 0.5 ml/min with 0.5-ml fractions. Pure, approximately 14-kDa fragment was confirmed by Coomassie staining and Western immunoblot using IGFBP-rP2 (CTGF) primary antibody (not shown).

AGE synthesis

Advanced glycosylation end products were synthesized *in vitro*, following methods previously described (26, 30, 31). BSA (Sigma, RIA grade, fraction V) at 10 mM was coincubated in sterile PBS with either 0.5 M D-glucose for 10 weeks or 25 mM glycolaldehyde for 3 days, each with 1.5 mM phenylmethylsulfonylfluoride under aerobic conditions at 37 C. To generate control BSA for comparison with AGE treatments, tubes were prepared with simultaneous incubations under the same conditions without the addition of the respective reducing sugar or aldehyde. Additionally, in parallel preparations, aminoguandine at 100 mM, as an inhibitor of formation of products of nonenzymatic glycosylation (13), was added to the BSA and glucose. All preparations were extensively dialyzed in PBS, using a low M_r cut-off membrane (6–8 kDa, Spectrapor 1, Spectrum Industries, Los Angeles, CA) (13).

The AGE content in the preparations was assessed by means of fluorescence, SDS-PAGE analysis, and ELISA. The fluorescence content, measured with a fluorescence spectrometer at 390 nm emission after 450 nm excitation in relative fluorescence units per mg BSA, was 11.2 ± 2.5 for control BSA, 67.1 ± 12.5 for AGE BSA from glycolaldehyde, 52.3 ± 6.3 for AGE BSA from glucose, and 9.7 ± 1.2 for aminoguanidine added to BSA and glucose (termed aminoguanidine BSA) (31). By SDS-PAGE analysis under reducing conditions, followed by Coomassie staining, the AGE BSA produced from D-glucose and glycolaldehyde was shown to have high M_r species consistent with the intermolecular cross-linking ability of AGE, as previously described (26). In contrast, the control BSA and aminoguanidine BSA preparations did not have these high M_r forms (data not shown). By competitive ELISA (32), performed by Dr. P. Foiles (Alteon, Inc., Ramsey, NJ), using a synthetic *N*-ε-carboxymethyl lysine (CML) analog as the standard, the CML content of the preparations (picomoles of CML per μg BSA ± 95% confidence interval) was 82 ± 8.5 for AGE BSA from glycolaldehyde and 13 ± 1.4 for AGE BSA from glucose and was undetectable (<1) for control BSA and also undetectable when aminoguanidine at 100 mM was coincubated with BSA and glucose. Unless otherwise indicated in the text, the data described refer to the use of AGE BSA synthesized from glucose.

Cell culture

Primary cell cultures of nonfetal human dermal fibroblasts, CRL-2097 and CRL-1474, were purchased from American Type Culture Collection (Manassas, VA). Cells were maintained in MEM supplemented with 10% FBS and were used in these studies between passages 4 and 12. The human primary cultures of dermal fibroblasts, designated A35 (derived from the forearm of a 70-yr-old male) and A305 (newborn foreskin fibroblasts), were gifts from Dr. S. Goldstein, Memorial Veteran's Hospital (Little Rock, AR). These cells were maintained in DMEM with 15% FBS.

Cell treatment

After trypsinization, cells were grown in 12-well plates for 5 days in their respective media with FBS until they were confluent. For experiments requiring the use of blocking antibodies to RAGE and AGE, cells were grown in 24-well plates under the same conditions. Cells were then incubated in their respective serum-free medium for 16 h and then treated with additions on day 0 under serum-free conditions, using fresh media. Unless otherwise indicated in the text, the conditioned media were not changed after adding the treatments. When cells were transiently treated for 8 h with reagents, they were washed with PBS, and fresh serum-free medium with 0.05% BSA was added. Cell lysates and conditioned media were harvested up to 3 days after treatments. For experiments involving the use of blocking antibodies or antioxidants, cells were preincubated with the antibody or reagent for 2 h under serum-free conditions before adding AGE or control BSA directly to the medium.

Total RNA isolation and analysis by quantitative real-time RT-PCR

Total RNA was isolated from duplicate wells using the RNeasy Mini-kit from QIAGEN (Valencia, CA) and was then analyzed by quantitative real-time PCR using an ABI Prism 7700 Sequence Detection System (PE Applied Biosystems, Foster City, CA). This system is based on the ability of the 5′-nuclease activity of *Taq* polymerase to cleave a nonextendable dual labeled fluorogenic hybridization probe during the extension phase of PCR. The following sequence-specific primers and probes for human CTGF, IGFBP-rP1, IGFBP-3, and 18S ribosomal RNA were designed using Primer Express Software 1.0 (PE Applied Biosystems): for CTGF: forward, 5′-GAGGAAAACATTAAGAAGGGCAAA-3′; reverse, 5′-CGGCACAGGTCTTGATGA-3′; and probe, 5′-6FAM-TTTGAGCTTTCTGGCTGCACCAGTGT-TAMRA-3′; for IGFBP-rP1: forward, 5′-GCGGAAAATGGCAGACAATT-3′; reverse, 5′-CTTGAGGGTTTGGGTTTCCA-3′; and probe, 5′-6FAM-TTCGCTCCATGATGCGTTATCTGGGTAMRA-3′; for IGFBP-3: forward, 5′-AAGGTGGGTAGGCACGTTGTAG-3′; reverse, 5′-ATATCAAAACCCGAATCCACTTTACT-3′; and probe, 5′-6FAM-CAAAGCAATGTCTAGTCCCGGTATGTCCAA-TAMRA-3′; for 18S: forward, 5′-CGGCTACCACATCCAAGGAA-3′; reverse, 5′-GCTGGAATTACCGCGGCT-3′; and probe, 5′-6FAM-TGCTGGCACCAGACTTGCCCTC-TAMRA-3′. Primers were used at a concentration of 200 nM and probes at 100 nM in each reaction. Multiscribe reverse transcriptase and AmpliTaq Gold polymerase (PE Applied Biosystems) were used in all RT-PCR reactions. Each RNA sample was analyzed in triplicate. Relative quantitation of 18S ribosomal RNA and human CTGF, IGFBP-rP1, and IGFBP-3 messenger RNAs (mRNAs) was calculated using the comparative threshold cycle number for each sample fitted to a five-point standard curve (ABI prism 7700 User Bulletin 2, PE Applied Biosystems). The standard curve was constructed using a serial dilution of total RNA extracted from human cardiac fibroblasts that had been treated with TGFβ1 at 1 ng/ml for 24 h. Expression levels were normalized to 18S ribosomal RNA and related to relevant controls, as indicated in the text.

Preparation of conditioned media and cell lysates

Cell lysate samples were harvested after treatment, by washing cells with PBS, then adding 100 μl cold RIPA lysis buffer [20 mM Tris (pH 8.0), 150 mM NaCl, 1% Nonidet P-40, 0.5% sodium deoxycholate, and 0.1% SDS] plus a protease inhibitor cocktail (Roche Molecular Biochemicals, Mannheim, Germany) directly to each well. Plates were rocked for 15 min at 4 C, and lysates were collected and centrifuged at 10,000 × *g* for 10 min at 4 C. The supernatants from duplicate wells within each experiment were pooled and stored at −20 C until analysis. The total protein concentration was determined for each sample by use of the DC Protein Assay reagent (Bio-Rad Laboratories, Inc., Hercules, CA). Then 20 μg total protein were loaded per lane for SDS-PAGE analysis, and 5 μg total protein were added to each ELISA well for CTGF quantitation.

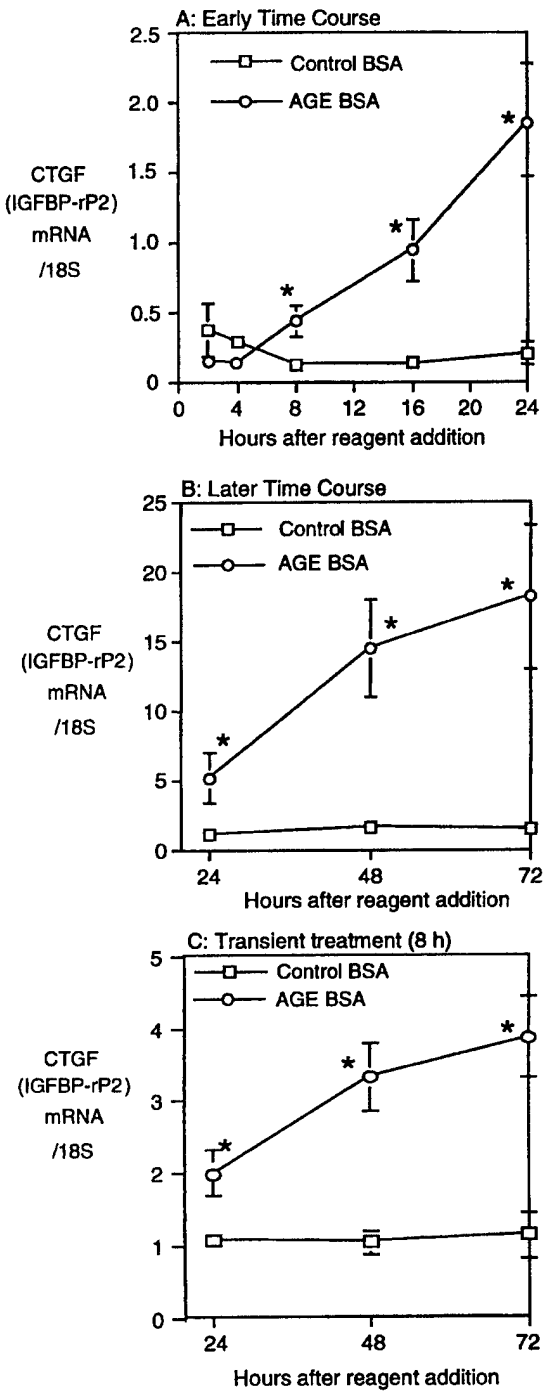

FIG. 1. Time-course induction of CTGF (IGFBP-rP2) mRNA by AGE BSA. Soluble AGE BSA at 100 μg/ml was added to duplicate wells of confluent primary cultures of human fibroblasts (CRL-2097 cells) under serum-free conditions, and total RNA was collected at the time points shown. Control BSA at the same concentration was added to other wells, also in duplicate. CTGF mRNA was then determined by quantitative RT-PCR in triplicate for each sample, as described in *Materials and Methods*. The CTGF mRNA level is expressed in arbitrary units normalized to 18S. A, Time course up to 24 h. B, Time course from 1–3 days. C, Treatment for 8 h only with AGE BSA or control BSA at 100 μg/ml, followed by RNA analysis on days 1–3. Data in A–C are the mean ± 1 SD from three independent experiments. *, $P < 0.05$ *vs.* the respective control BSA.

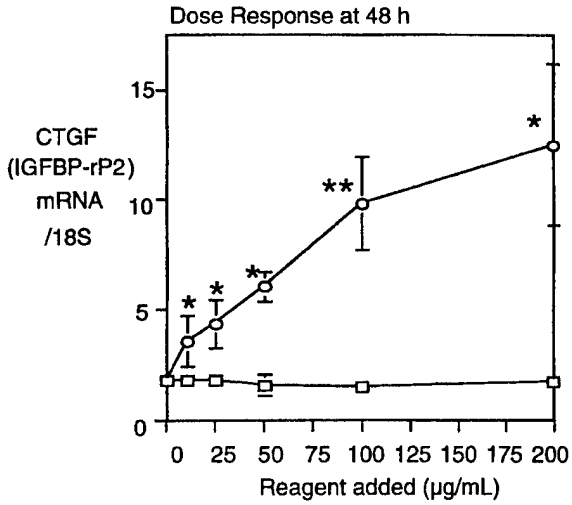

FIG. 2. Dose-dependent induction of CTGF (IGFBP-rP2) mRNA by AGE BSA. Dose response with AGE BSA or control BSA treatment from 0–200 μg/ml added to wells of confluent human fibroblasts (CRL-2097 cells), with RNA collection at 48 h. CTGF mRNA was determined by quantitative RT-PCR in triplicate for each sample, and the CTGF mRNA level is expressed in arbitrary units normalized to 18S. Data are the mean ± 1 SD from three independent experiments. *, $P < 0.05$, **, $P < 0.01$ *vs.* the respective control BSA.

Western immunoblot analysis

Conditioned medium samples were separated on 15% nonreducing SDS-PAGE. Proteins were electrotransferred onto nitrocellulose, and membranes were blocked with 5% nonfat dry milk/TBS with 0.1% (vol/vol) Tween 20 for 1 h at 22 C, then incubated in IGFBP-rP2 (CTGF) antiserum at 1:1000 dilution at 4 C overnight. After incubation of membranes with a horseradish peroxidase (HRP)-labeled secondary antibody for 1 h at 22 C, immunoreactive proteins were detected by use of enhanced chemiluminescence (NEN Life Science Products, Boston, MA).

CTGF (IGFBP-rP2) ELISA

The anti-IGFBP-rP2 (CTGF) antibody (8800) (25) was biotinylated by incubating protein A affinity-purified 8800 (0.8 μg) with 150 μg sulfo-NHS-LC biotin (Pierce Chemical Co., Rockford, IL) for 2 h at 22 C, followed by separation from unreacted biotin through a size-fractionation and desalting column with PBS as buffer according to the manufacturer's instructions. Affinity-purified 8800 antibody (600 ng/well) in 10 mM sodium carbonate, pH 9.6, was adsorbed to 96-well immunoplates (Nalge Nunc International, Rochester, NY) by a 20-h incubation at 4 C. The unbound antibody was removed, and the wells were blocked by incubation with PBS and 0.1% (vol/vol) Triton X-100 (buffer A) containing 10 g/liter BSA for 2 h at 37 C, then washed four times with buffer A. Purified intact recombinant human (rh) IGFBP-rP2 (CTGF) in buffer A and 1 g/liter BSA was used to generate standard curves. Standard and samples (100 μl/well) were incubated in duplicate at 4 C for 20 h. The plate was washed, then incubated with biotinylated IGFBP-rP2 (CTGF) antibody (80 ng/well) for 20 h at 4 C. After washing, the plate was incubated with streptavidin-HRP (1:500) for 30 min at 22 C, followed by substrate [0.1 g/liter 3,3′,5,5′-tetramethylbenzidine in 0.2 M sodium acetate (pH 6) containing 0.06% (wt/wt) H_2O_2] for 30 min at 22 C. The reaction was stopped by the addition of 2 M H_2SO_4, and the absorbance was measured at 450 nm using a microplate reader. The interassay coefficient of variation was 8.1% for the middle concentration (10 ng/well) of rhIGFBP-rP2 (CTGF) standard used. No cross-reactivity was detected with 1 μg/well purified rhIGFBP-3, rhIGFBP-rP1 (mac 25), or rhIGFBP-rP3 (Nov H; not shown).

CTGF (IGFBP-rP2) cell association assay

To determine whether increases in rhIGFBP-rP2 (CTGF) in the whole cell lysates after AGE treatment are due to increases in rhIGFBP-rP2

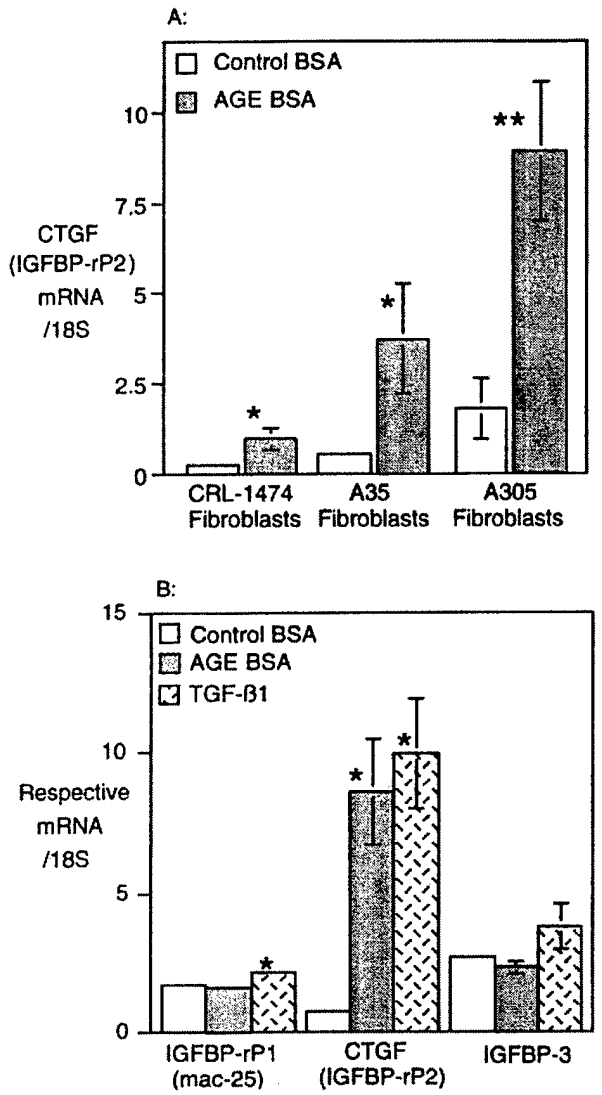

FIG. 3. Generalizability of the AGE BSA effect on CTGF (IGFBP-rP2) mRNA to multiple sources and donors of human skin fibroblasts, and specificity of the effect to CTGF (IGFBP-rP2). A, Soluble AGE BSA or control BSA at 100 μg/ml was added to duplicate wells of confluent primary cultures of human skin fibroblasts from multiple donors under serum-free conditions, and total RNA was collected at the time points shown. IGFBP-rP2 (CTGF) mRNA was then determined by quantitative RT-PCR in triplicate for each sample. The IGFBP-rP2 (CTGF) mRNA level is expressed in arbitrary units, normalized to 18S. The donor age and skin site of the fibroblasts studied are: 7-yr-old male abdomen (CRL-1474 cells), 70-yr-old male forearm (A35), and newborn foreskin (A305). Data are the mean ± 1 SD from three independent experiments. B, Soluble AGE BSA or control BSA at 100 μg/ml or TGFβ1 at 1 ng/ml was added to duplicate wells of confluent primary cultures of human fibroblasts (CRL-2097) under serum-free conditions. Total RNA was collected at 48 h, and CTGF (IGFBP-rP2) mRNA, IGFBP-rP1 (mac-25) mRNA, and IGFBP-3 mRNA levels were determined by quantitative RT-PCR in triplicate for each sample. The mRNA levels are expressed in arbitrary units. Data are the mean ± 1 SD from three independent experiments. *, $P < 0.05$; **, $P < 0.01$ (*vs.* the respective control BSA).

(CTGF) at a cell-associated site either on the cell surface or in the extracellular matrix, rather than intracellularly, 2097 fibroblasts in confluent monolayer were treated under serum-free conditions with AGE or control BSA (each at 100 μg/ml) for 3 days in replicates of four. After washing twice with PBS at 4 C, biotinylated rhIGFBP-rP2 (CTGF) antibody (800 ng/well) together with streptavidin-HRP (1:500) was added for 2 h at 22 C in PBS and 0.1% BSA. In some wells the streptavidin-HRP (1:500) was added in the absence of primary antibody to determine nonspecific binding and endogenous cellular peroxidase activity. After two further (gentle) PBS washes, developing substrate was added, and absorbance was read as described for the IGFBP-rP2 (CTGF) ELISA above.

Densitometric analysis

To quantify the relative induction of CTGF after Western immunoblots, densitometric measurement was performed using GS-700 Imaging Densitometer with Mutli-Analyst Software (Bio-Rad Laboratories, Inc.).

Statistical analysis

Results are expressed as the mean ± SD or the mean ± SEM as indicated in the text. All data were pooled from three or four independent experiments, each performed in triplicate. Differences between groups were assessed using Student's two-tailed paired *t* test in Excel 98 (Microsoft Corp., Redmond, WA). $P < 0.05$ was considered statistically significant.

Results

To determine whether CTGF mRNA steady state levels are up-regulated by AGE in primary cultures of human dermal fibroblasts, confluent monolayers of CRL-2097 fibroblasts were treated with soluble AGE BSA under serum-free conditions. In response to 100 μg/ml AGE BSA, an increase in CTGF mRNA was initially detectable after 8 h of AGE treatment (Fig. 1A), and a progressive increase occurred over the 3-day time course of the study (Fig. 1B). In contrast, no change in CTGF mRNA over time was seen with the same concentration of control BSA (Fig. 1, A and B). These results were confirmed by Northern analysis (not shown). Transient treatment of cells with AGE for 8 h, followed by washing of cells with PBS and replacement with fresh serum-free medium, also caused a progressive increase in CTGF mRNA over subsequent days (Fig. 1C), with a clear persistence of the effect for at least 72 h after AGE addition.

A dose-response study with AGE BSA from 0–200 μg/ml, with continuous AGE treatment and RNA collection at 48 h after initial AGE addition, showed that increases in CTGF mRNA were significant using 10 μg/ml or more AGE BSA, whereas increasing concentrations of control BSA did not produce any change in CTGF mRNA compared with no addition of BSA (Fig. 2).

Primary human skin fibroblasts from other donors were studied to assess whether the changes seen in CTGF mRNA in human foreskin fibroblast CRL-2097 cells are generalizable to human dermal fibroblasts. When these other cells were treated with 100 μg/ml AGE BSA, increases in CTGF mRNA were observed 48 h after treatment, compared with the control BSA, in all of the fibroblast cell lines studied whether they were derived from neonatal foreskin (A305), a child's abdomen (CRL-1474), or the forearm of a mature adult (A35; Fig. 3A).

To address whether the changes seen in CTGF mRNA were relatively specific, other members of the IGFBP superfamily were analyzed in the same cell system. In contrast to the observed regulation of CTGF mRNA by AGE, IGFBP-rP1 (mac 25) mRNA was not up-regulated by AGE BSA (Fig. 3B). IGFBP-3 is the predominant IGFBP present in human fibro-

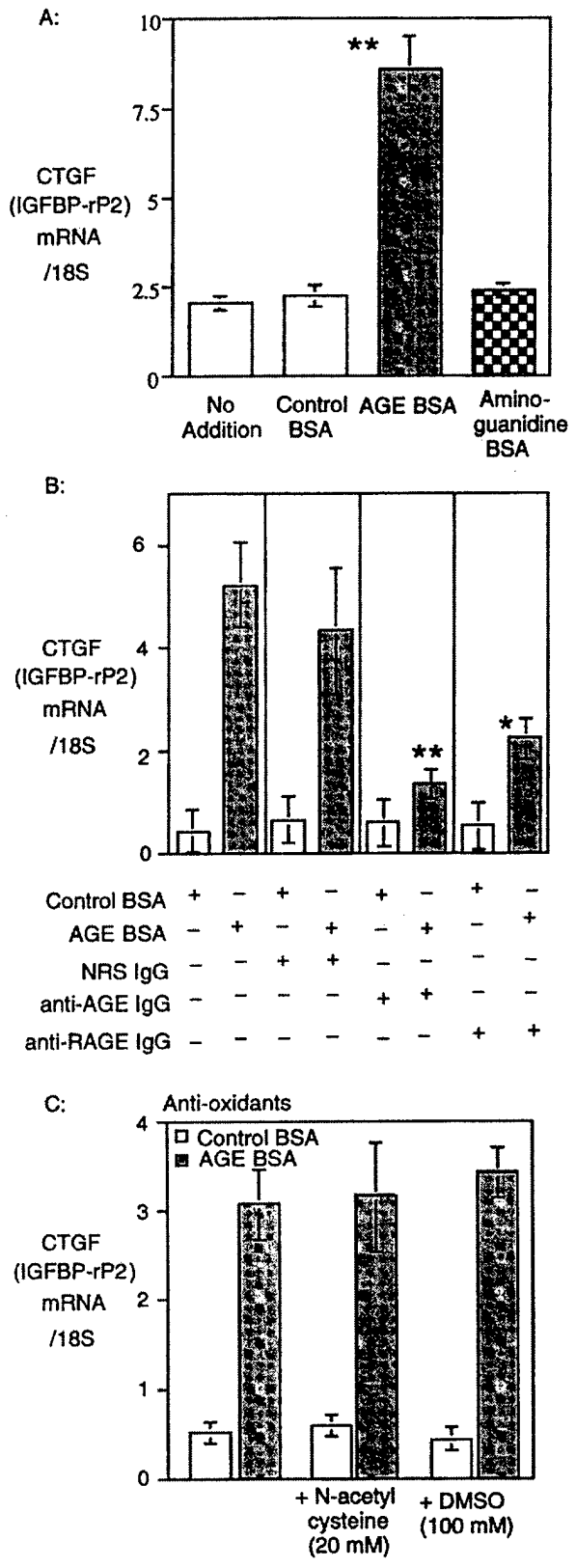

FIG. 4. The AGE effect on CTGF (IGFBP-rP2) occurs through non-enzymatic glycosylation of BSA, is blocked by an anti-AGE-neutralizing antibody, is partially mediated through the AGE receptor, RAGE, and is not inhibited by oxygen free radical scavengers. A, Soluble AGE BSA or control BSA at 100 μg/ml, or no treatment, was added to duplicate wells of confluent primary cultures of human fibroblasts (CRL-2097 cells) under serum-free conditions. In other wells BSA was added that had previously been coincubated with glucose and aminoguanidine before dialysis, as described in *Materials and Methods*. Total RNA was collected at 48 h, and CTGF mRNA was determined by quantitative RT-PCR in triplicate for each sample. The CTGF mRNA level is expressed in arbitrary units. Data are the mean ± 1 SD from three independent experiments. **, $P < 0.01$ *vs.* all other treatments. B, Wells were preincubated with anti-AGE polyclonal neutralizing IgG, anti-RAGE polyclonal neutralizing IgG (each at 100 μg/ml IgG), or 100 μg/ml normal rabbit serum (NRS) IgG for 2 h. Soluble AGE BSA or control BSA at 100 μg/ml was then added to the wells. Total RNA was collected at 48 h, and IGFBP-rP2 (CTGF) mRNA was determined by quantitative RT-PCR in triplicate for each sample. Data are the mean ± 1 SD from four independent experiments. *, $P < 0.05$; **, $P < 0.01$ (*vs.* AGE BSA added alone). C, Duplicate wells of human fibroblasts under serum-free conditions were incubated with serum-free medium alone, 20 mM *N*-acetyl cysteine, or 100 mM dimethylsulfoxide (DMSO) for 2 h. Soluble AGE BSA or control BSA at 100 μg/ml was then added to the wells. Total RNA was collected at 48 h, and CTGF (IGFBP-rP2) mRNA was determined by quantitative RT-PCR in triplicate for each sample. The mRNA levels are expressed in arbitrary units. Data are the mean ± 1 SD from three independent experiments.

blast conditioned medium (33), and its mRNA also was not increased by AGE (Fig. 3B). In comparison with the lack of effect of AGE treatment, TGFβ1 treatment modestly up-regulated IGFBP-rP1, and possibly IGFBP-3 mRNA, at 48 h (Fig. 3B), as previously described (33, 34). Also consistent with previous observations in cultured human fibroblasts (35), a pronounced up-regulation of CTGF mRNA occurred after TGFβ1 addition (Fig. 3B).

Formation of products of nonenzymatic glycosylation was inhibited by the dihydrazine compound, aminoguanidine (13). When cells were treated with BSA that had been coincubated for 10 weeks with both glucose and aminoguanidine as described in *Materials and Methods*, no increase in CTGF mRNA was observed compared with control BSA treatment alone or with serum-free medium without any addition (Fig. 4A). This result confirms that the active component in the AGE reagent used is a product of nonenzymatic glycosylation.

To determine whether early or advanced glycosylation end products are mediating the effect on CTGF in this cell system, cells were preincubated with anti-AGE IgG before addition of the AGE reagent. Using the anti-AGE antibody, the AGE induction of CTGF mRNA was inhibited, on the average, by 86.2% (Fig. 4B). As this antibody is specific to AGE and it does not bind to amadori products (26), which are early products of nonenzymatic glycosylation, these results show that AGE is the active component in the synthesized reagent responsible for increasing CTGF in these studies.

AGE may bind to and activate one or more of the defined cell surface receptors for AGE (8). The AGE receptor subtype, termed RAGE, has recently been shown to be present on the surface of human fibroblasts (27), and in some cell systems the induction of growth factors by AGE has been shown to be mediated by RAGE (36). When cells were preincubated with a blocking antibody of RAGE activation by AGE ligand, the induction of CTGF mRNA by AGE was attenuated by the

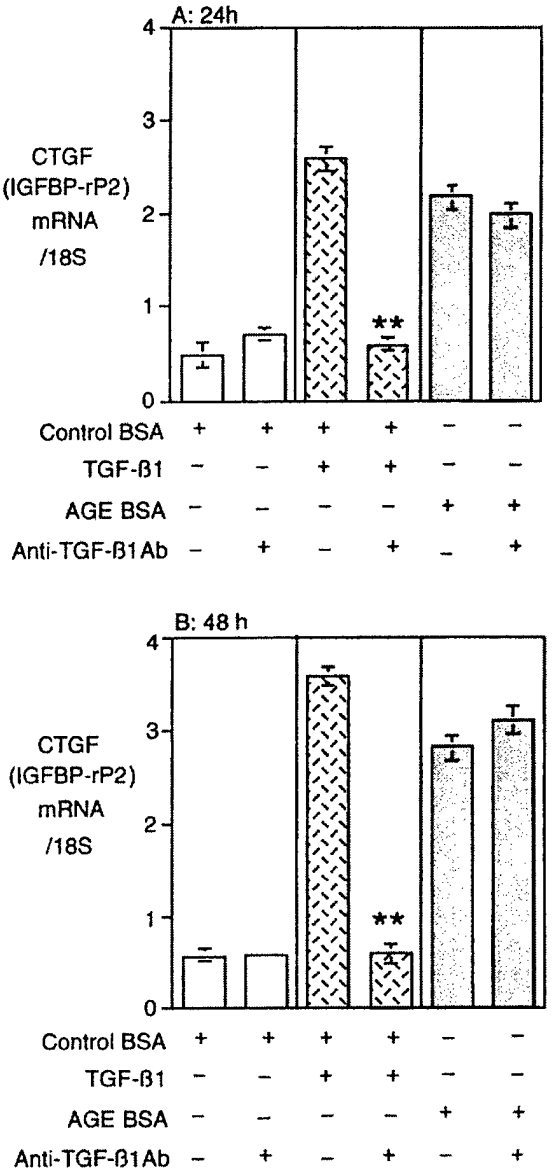

FIG. 5. AGE induction of CTGF (IGFBP-rP2) mRNA is independent of endogenous TGFβ1 activity. Duplicate wells of confluent primary cultures of human fibroblasts (CRL-2097 cells) under serum-free conditions were incubated with AGE BSA or control BSA at 100 μg/ml or with TGFβ1 at 1 ng/ml for 24 h (A) or 48 h (B), and in some wells a chicken antihuman TGFβ1-neutralizing antibody (200 ng/ml) was added simultaneously as indicated. Total RNA was collected at 24 h (A) and 48 h (B), and CTGF mRNA was determined by quantitative RT-PCR in triplicate for each sample. The mRNA levels are expressed in arbitrary units. Data are the mean ± 1 SD from three independent experiments in A and B. **, $P < 0.01$ *vs.* TGFβ1 added without neutralizing antibody.

anti-RAGE IgG by 64.1%, on the average (Fig. 4B). Higher concentrations of anti-RAGE IgG did not have any additional effect (not shown). In contrast, the AGE effect was not significantly inhibited by normal rabbit serum IgG (Fig. 4B). These results show that RAGE is at least partly mediating the AGE induction of CTGF mRNA in the fibroblasts.

As reactive oxygen (RO) species are commonly generated in cells after activation of AGE receptors by its ligand (9, 37), an effect of inhibiting RO species formation during AGE treatment was studied. Preincubation of the fibroblasts with the antioxidants dimethylsulfoxide or *N*-acetyl cysteine, however, did not inhibit the increases in CTGF mRNA (Fig. 4C). These results imply that RO species are unlikely to play a role in the observed AGE effect on CTGF.

A potential role for autocrine TGFβ1 in CTGF mRNA induction by AGE was then examined. TGFβ1 is a potent inducer of CTGF gene expression in this cell system (Fig. 3A), and in addition, AGE may induce TGFβ1 mRNA and protein in some cells (13). Induction of CTGF mRNA by rhTGFβ1 added to the cultured fibroblasts was fully inhibited by a TGFβ1-neutralizing antibody at 24 h (Fig. 5A) and 48 h (Fig. 5B). In contrast, when the same antibody was added under the same conditions in parallel wells, no significant inhibition of the CTGF mRNA increase induced by AGE occurred (Fig. 5, A and B), indicating that the effect of AGE is TGFβ1 independent in this cell system.

The fibroblast cellular protein from CRL-2097 skin fibroblasts was then analyzed to determine whether AGE treatment causes increases in CTGF protein as well as increases in steady state CTGF mRNA levels. By Western immunoblot after SDS-PAGE, using a polyclonal IGFBP-rP2 (CTGF) antiserum (25), CTGF steady state protein levels over days 1–3 in the conditioned medium were increased in response to AGE BSA, compared with control BSA treatment (Fig. 6A). A progressive increase in intact CTGF as well as previously described lower M_r immunoreactive forms, at approximately 14 and 20 kDa (38), occurred (Fig. 6A). High M_r immunoreactive material (>80 kDa) was also more prominent in the AGE-treated medium, which may include CTGF covalently cross-linked by AGE. All of these increases were more marked using AGE BSA synthesized from glycolaldehyde compared with AGE BSA synthesized from glucose (not shown). Using densitometric analysis from three independent experiments, the intact CTGF in the medium was increased by AGE compared with control BSA treatment (mean ± SEM) by 3.6 ± 1.1-fold on day 1, 8.0 ± 1.3-fold on day 2, and 14.5 ± 3.1-fold on day 3 ($P < 0.05$ for all days of AGE treatment compared with control BSA treatment).

As CTGF is an extracellular matrix and cell-associated signaling protein and also exists in cell media (38), analysis of whole cell lysates for CTGF protein after AGE treatment was performed. Western immunoblot analysis of the whole cell lysates after SDS-PAGE showed that intact CTGF was increased by AGE treatment from day 3 compared with control BSA treatment (Fig. 6B). There was no CTGF fragment or high M_r immunoreactive material observed in the lysates (not shown). Densitometric analysis of CTGF from lysates from four independent experiments (mean ± SEM) gave the following results for fold change with AGE treatment compared with control BSA treatment: 0.89 ± 0.33 on day 1, 0.97 ± 0.17 on day 2, and 1.53 ± 0.25 on day 3 ($P < 0.05$ for day 3 only for AGE compared with control BSA on the respective day).

Considering that the increase in CTGF in whole cell lysates on day 3 after AGE treatment was relatively modest, changes in cell lysate CTGF were further determined by a CTGF ELISA, as described in *Materials and Methods*. This assay can measure endogenous intact CTGF, which is present in whole cell lysates, but due to a lack of parallelism with the intact

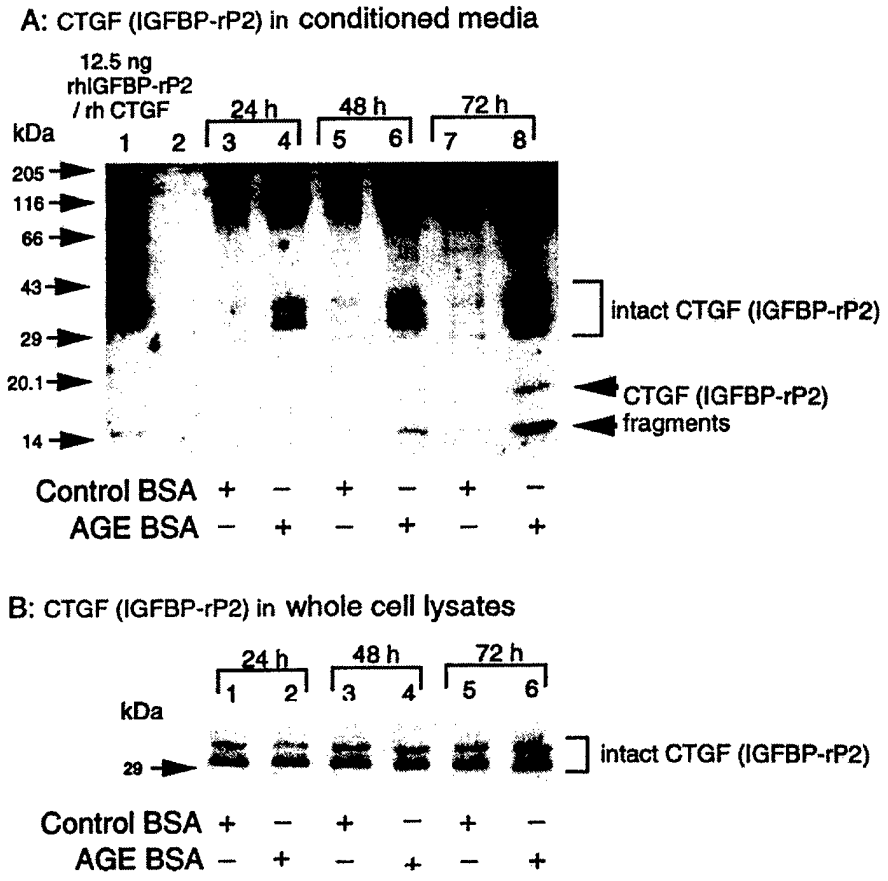

FIG. 6. CTGF (IGFBP-rP2) protein up-regulation by AGE BSA in conditioned media and whole cell lysates. Soluble AGE BSA or the respective control BSA was added to duplicate wells of confluent primary cultures of human fibroblasts (CRL-2097 cells) under serum-free conditions. After 24–72 h, as indicated, conditioned media and whole cell lysates were collected and subjected to SDS-PAGE and then Western immunoblotted using IGFBP-rP2 (CTGF) antiserum, as described in *Materials and Methods*. A, Conditioned medium; lane 2, unconditioned serum-free medium loaded alone. B, Whole cell lysates, with 20 μg total protein loaded in each sample lane. In A and B one representative immunoblot is shown from three and four independent experiments, respectively, with each experiment showing equivalent results.

rhCTGF used as the standard, it cannot be used to accurately measure the 14-kDa CTGF fragment (Fig. 7A), which is present in the fibroblast-conditioned media (Fig. 6A). Consistent with the Western immunoblots of cell lysates (Fig. 6B), the ELISA also showed that AGE treatment reproducibly increased CTGF in the fibroblast whole cell lysates on day 3 (Fig. 7B). Thus, in contrast to the increases in CTGF protein observed in the conditioned media, there was no increase in CTGF protein in the first 2 days after AGE treatment in the whole cell lysates compared with control, and there was only a modest and delayed increase in CTGF in the lysates, which was much less striking than the increases in CTGF protein observed in the conditioned media (Fig. 6A).

To determine whether the increase in CTGF in the whole cell lysates seen by day 3 of AGE treatment was accessible to the extracellular environment, a cell association assay for CTGF was performed, as described in *Materials and Methods*. This assay uses binding of a biotinylated CTGF primary antibody to endogenous CTGF protein, followed by antibody detection using a streptavidin-HRP system. As no plasma membrane-permeabilizing agents were used in the protocol, the specific signal detected by the CTGF primary antibody was due to CTGF present on the cell surface or in the extracellular matrix, rather than CTGF present in an intracellular compartment. As shown in Fig. 7C, at 72 h AGE at 100 μg/ml specifically increased the absorbance signal compared with control ($P < 0.05$ for analysis of combined data from four independent experiments). In parallel wells, under the same conditions of confluent cell monolayers in serum-free media, cell number determined by hemocytometer counting and trypan blue exclusion was not changed by AGE treatment compared with control BSA (not shown). Thus, these results indicate that at 72 h, AGE treatment increases cell-associated CTGF compared with BSA control treatment alone.

Discussion

This study describes the up-regulation of CTGF mRNA and protein by treatment of human skin fibroblasts with advanced glycosylation end products. The effect of AGE on CTGF induction was caused by products of nonenzymatic glycosylation, as coincubation of aminoguanidine, an inhibitor of nonenzymatic glycosylation, with glucose and BSA did not have an effect on CTGF mRNA, nor was an effect seen with increasing control BSA alone. The up-regulation of CTGF in this cell model was mediated by AGE rather than by earlier products of nonenzymatic glycosylation, such as amadori products, as the use of an antibody specific for AGE that does not bind amadori products inhibited the induction of CTGF gene expression. The effect was at least partly mediated through the AGE receptor known as RAGE, as an anti-RAGE antibody significantly attenuated the effect of AGE on CTGF.

The up-regulation of CTGF by AGE appears to be specific for CTGF and is generalizable to skin fibroblasts from dif-

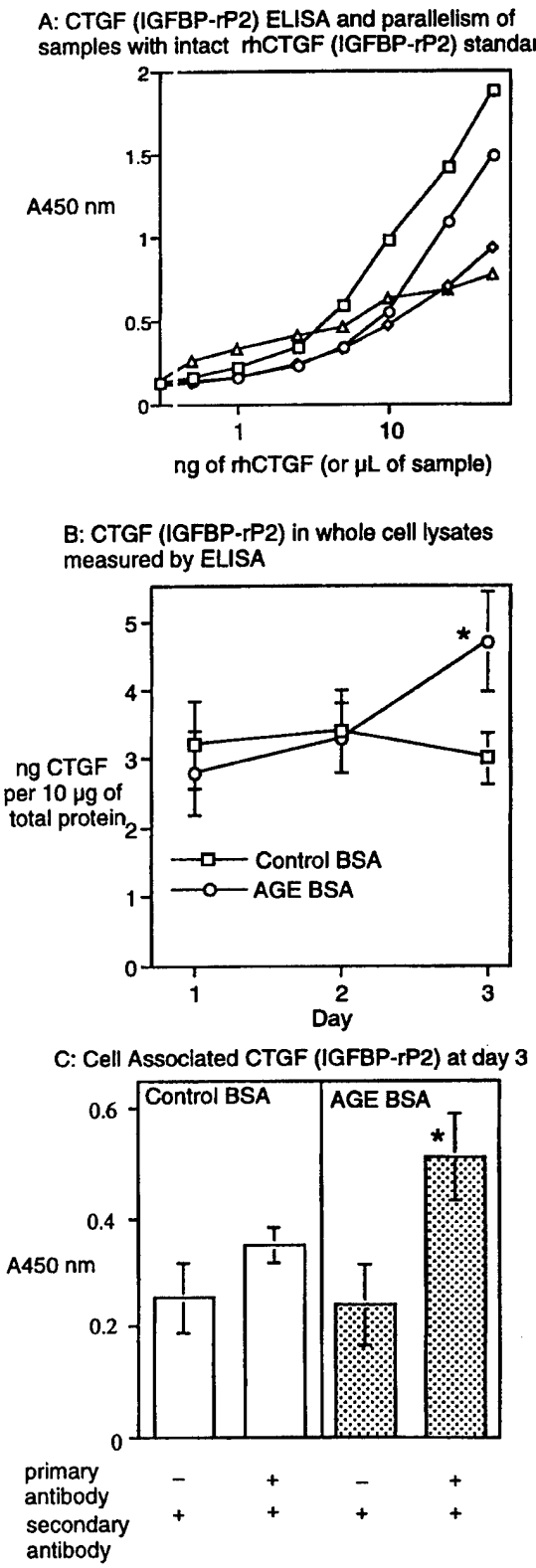

FIG. 7. Whole cell lysate and cell-associated increases in CTGF (IGFBP-rP2) after AGE BSA treatment. A, CTGF (IGFBP-rP2) ELISA as described in *Materials and Methods*, showing the standard curve generated for intact CTGF (IGFBP-rP2; □) compared with the curves generated with a 14-kDa fragment of CTGF (IGFBP-rP2; △), endogenous intact CTGF present in 2097 cell-conditioned medium (◇), and 2097 cell whole cell lysates (○). B, Results of analysis of CTGF in the whole cell lysates by CTGF ELISA after treatment up to 72 h with AGE or control BSA, each at 100 µg/ml. Data are the mean ± 1 SD of four independent experiments. *, $P < 0.05$ *vs.* control BSA on day 3. C, Results showing cell-associated CTGF after AGE treatment compared with control BSA (100 µg/ml) at 72 h, using biotinylated anti-CTGF IgG primary antibody followed by HRP-labeled secondary antibody or the secondary antibody alone, as described in *Materials and Methods*. Data are the mean ± 1 SD of four independent experiments. *, $P < 0.05$ *vs.* all other groups.

fering sources and passage number. In each of the four fibroblast cell lines studied, AGE up-regulated CTGF. In the cell line most extensively studied, CRL-2097, CTGF was regulated by AGE in early passages (passage 4) and also at later passages (passage 12). In contrast to effects on CTGF, the two other members of the IGFBP superfamily that were studied, IGFBP-3 and IGFBP-rP1, were not up-regulated by AGE. Further studies will be required to determine whether AGE affects other members of the CCN (CTGF, Cyrbl, Nov) family.

The concentrations of AGE BSA used in these experiments approximate those used *in vitro* in other studies exploring biological effects of AGE on cells (13, 27). Although there is no universal standard method for measuring specific AGE components at this time, and the AGE antibodies used in assays measuring AGE differ (39), the AGE BSA concentrations studied are in the broad range for AGE concentrations found in diabetic serum (40).

Few AGE components have been defined biochemically to date, and the specific end-product(s) that might be mediating the effect on CTGF was not identified in this work. AGE adducts existing in diabetic tissues that have been shown to signal through AGE receptors include mainly CML (28) and imidazoline-based products (41). Considering that CML adduct is a ligand for RAGE (28), that our AGE reagent contained CML, and that at least part of the AGE effect on CTGF has been shown to be mediated through RAGE, it is plausible that CML adducts are one of the AGE components operative in this study. In the current work, when AGE BSA synthesized from glycolaldehyde was studied in experiments where AGE BSA synthesized from glucose was also used in treatments, each at the same AGE concentration of 100 µg/ml BSA with mRNA measurements over 3 sequential days, the induction of CTGF mRNA by these reagents did not differ (data not shown). As these two AGE reagents contain differing amounts of CML (as described in *Materials and Methods*), the CML adduct cannot be the only explanation for the observed AGE effect on CTGF mRNA in these AGE preparations. Further experiments with pure CML and other pure AGE adducts, when available, will be required to address this issue.

A number of subtypes of cell surface receptor bind AGE specifically and are responsible for mediating multiple cellular effects of AGE (42). These receptors exist in four main classes: RAGE, AGE-R1, AGE-R2, and AGE-R3 (8). In the diabetic environment, the increased AGE present is hypothesized to bind and activate AGE receptors, and in some studies, the induction of growth factors by AGE has been shown to be mediated by AGE receptors, including RAGE (43). Our studies indicate that RAGE is responsible for mediating at least part of the effect of AGE on CTGF mRNA. The

possibility that other AGE receptors might also contribute to these effects is not excluded by this work.

A role for growth factors in contributing to chronic diabetes-related end-organ complications, particularly vascular endothelial growth factor (VEGF), TGFβ1, IGF-I, and platelet-derived growth factor, is under increasing evaluation, and a potential role for CTGF in chronic diabetic complications is emerging. CTGF is a potent profibrotic agent (18, 44), which is reflected in its ability to induce ECM components and increase fibroblast DNA synthesis (18) and to promote angiogenesis (20, 21). CTGF mRNA levels are up-regulated in many chronic disease states where fibrosis is prominent (22–24). Two separate studies involving renal mesangial cells and differing diabetic rat models recently reported that CTGF gene expression (45) as well as protein (46) are increased in mesangial cells after exposure to high glucose and *in vivo* in diabetic rat kidneys. Immunohistochemical studies of kidney tissue in human end-stage renal disease showed increased CTGF protein in diabetic kidneys as well as other nephropathies (47), and CTGF mRNA is markedly increased in advanced atheromatous lesions (48).

This is the first report of CTGF induction by advanced glycosylation end products, and it provides a potentially critical linkage among AGE, growth factors, and fibrosis. AGE induction of growth factors and cytokines has been described for VEGF, TGFβ1, IGF-I and platelet-derived growth factor, TNFα, IL-1β, and IL-6 (3) mainly in various endothelial and mesenchymal cultured cells and in some cases by AGE administration *in vivo* (15). CTGF appears to fit well into this group of proinflammatory and/or profibrotic proteins.

The striking persistent effect over 3 days of AGE on CTGF mRNA even after transient treatment suggests that regulation of CTGF by the AGE reagent tested is complex and may involve multiple interrelated intracellular signals. The cellular mechanism of AGE induction of CTGF mRNA was not defined in this study. RO species were not implicated, because antioxidants were ineffective in inhibiting AGE induction of CTGF. TGFβ1 is a known potent inducer of CTGF gene expression, and CTGF is implicated as a downstream mediator of TGFβ1 effects (49), particularly in fibrosis (44). We were unable to show, however, that TGFβ1 is a mediator in the AGE induction of CTGF. In the current work, both the early time course of initial induction of CTGF mRNA by AGE at 8 h as well as the inability of TGFβ1-neutralizing antibodies to inhibit AGE induction of CTGF suggest that AGE is operating through mechanisms that are independent of TGFβ1. Although studies involving the use of exogenously added neutralizing antibodies have potential limitations in assessing the role of endogenous protein bioactivity, that total TGFβ1 measurements in conditioned media measured by TGFβ1 ELISA (Promega Corp., Madison, WI) in these cells were not increased by AGE compared with control BSA treatment (data not shown) is also supportive that TGFβ1 is not a mediator of AGE induction of CTGF in this work. These results contrast with studies describing TGFβ-dependent effects of glucose on CTGF up-regulation in human mesangial cells (45, 46), but are consistent with other studies showing that various reagents can potently up-regulate CTGF mRNA independently of TGFβ1 (50).

In human fibroblast primary cultures, CTGF exists at very low levels in conditioned medium and is often present in low M_r fragment forms, which may also have bioactivity (38). That intact CTGF was readily detectable in the medium after AGE treatment may be partly related to posttranslational modification of CTGF, with cross-linking of CTGF protein by AGE into a high M_r immunoreactive form and redistribution of CTGF from a cell-associated site into the conditioned medium. In addition to the CTGF increases in the conditioned medium and consistent with the progressive increase in CTGF mRNA after AGE treatment, AGE caused increases in intact CTGF in whole cell lysates at 72 h. Further analysis showed that the CTGF increase in the lysates included protein that was cell associated and in a site accessible to the extracellular environment. To what extent the bioactivity of CTGF protein is affected by its presence in the medium compared with a cell-associated site is an important issue for future study of CTGF bioactivity.

There is a rationale to potentially link AGE effects and diabetic complications with the induction of CTGF in skin and, by association, with pathology in other tissues. A feature commonly present in human diabetes, even in late childhood and adolescence, is skin thickening and contracture (51), termed diabetic sclerosis. This process affects mainly the distal extremities and is characterized by expansion of extracellular matrix, fibroblast proliferation, and angiogenesis (52). The presence of overt diabetic sclerosis of skin is correlated with the presence and future development of end-organ complications, particularly diabetic nephropathy and retinopathy (53). AGE products are increased in human diabetic skin (6), and the levels of AGE in skin also correlate positively with the presence of diabetic microvascular kidney and eye disease (5, 6). That the ability of CTGF to induce fibrosis has been well characterized in skin (18, 44) makes skin fibroblasts a relevant cell model for the current study.

Clearly, *in vivo* and longer term studies are required to substantiate a more definitive role for induction of CTGF by AGE in potentially mediating diabetic fibrotic complications in skin and other organs. Activation of receptors for AGE, particularly RAGE (54), has also been implicated in the pathogenesis of fibrosis that develops in chronic diseases other than diabetes (42, 54, 55). That AGE up-regulates CTGF in nontransformed human fibroblasts suggests that CTGF may be a factor mediating the observed AGE and RAGE effects, which is a hypothesis that requires further testing.

Acknowledgments

We thank Alteon Inc., for measuring the CML adduct concentration in the AGE reagent with their CML ELISA. The generous gifts of anti-AGE antiserum from Dr. Miyata, Kissei Pharmaceutical Co. Ltd. (Hotaka, Japan), and the anti-RAGE antiserum from Dr. Anne-Marie Schmidt, at Columbia University (New York, NY), are gratefully acknowledged.

References

1. **King GL, Wakasaki H** 1999 Theoretical mechanisms by which hyperglycemia and insulin resistance could cause cardiovascular diseases in diabetes. Diabetes Care 22:C31–C37
2. **Nishikawa T, Edelstein D, Du XL, Yamagishi S, Matsumura T, Kaneda Y, Yorek MA, Beebe D, Oates PJ, Hammes HP** 2000 Normalizing mitochondrial superoxide production blocks three pathways of hyperglycaemic damage. Nature 404:787–790
3. **Bierhaus A, Hofmann MA, Ziegler R, Nawroth PP** 1998 AGEs and their interaction with AGE-receptors in vascular disease and diabetes mellitus. I. The AGE concept. Cardiovasc Res 37:586–600
4. **Chiarelli F, de Martino M, Mezzetti A, Catino M, Morgese G, Cuccurullo F, Verrotti A** 1999 Advanced glycation end products in children and adolescents with diabetes: relation to glycemic control and early microvascular complications. J Pediatr 134:486–491

5. **Beisswenger PJ, Makita Z, Curphey TJ, Moore LL, Jean S, Brinck-Johnsen T, Bucala R, Vlassara H** 1995 Formation of immunochemical advanced glycosylation end products precedes and correlates with early manifestations of renal and retinal disease in diabetes. Diabetes 44:824–829
6. **Sell DR, Lapolla A, Odetti P, Fogarty J, Monnier VM** 1992 Pentosidine formation in skin correlates with severity of complications in individuals with long-standing IDDM. Diabetes 41:1286–1292
7. **Vlassara H, Brownlee M, Cerami A** 1986 Nonenzymatic glycosylation: role in the pathogenesis of diabetic complications. Clin Chem 32:B37–B41
8. **Thornalley PJ** 1998 Cell activation by glycated proteins. AGE receptors, receptor recognition factors and functional classification of AGEs. Cell Mol Biol 44:1013–1023
9. **Schmidt AM, Hori O, Brett J, Yan SD, Wautier JL, Stern D** 1994 Cellular receptors for advanced glycation end products. Implications for induction of oxidant stress and cellular dysfunction in the pathogenesis of vascular lesions. Arterioscler Thromb 14:1521–1528
10. **Brownlee M** 2000 Negative consequences of glycation. Metabolism 49:9–13
11. **Vlassara H** 1992 Receptor-mediated interactions of advanced glycosylation end products with cellular components within diabetic tissues. Diabetes [Suppl 2] 41:52–56
12. **Hirata C, Nakano K, Nakamura N, Kitagawa Y, Shigeta H, Hasegawa G, Ogata M, Ikeda T, Sawa H, Nakamura K** 1997 Advanced glycation end products induce expression of vascular endothelial growth factor by retinal Muller cells. Biochem Biophys Res Commun 236:712–715
13. **Pugliese G, Pricci F, Romeo G, Pugliese F, Mene P, Giannini S, Cresci B, Galli G, Rotella CM, Vlassara H** 1997 Upregulation of mesangial growth factor and extracellular matrix synthesis by advanced glycation end products via a receptor-mediated mechanism. Diabetes 46:1881–1887
14. **Striker LJ, Striker GE** 1996 Administration of AGEs in vivo induces extracellular matrix gene expression. Nephrol Dial Transplant 11:62–65
15. **Yang CW, Vlassara H, Peten EP, He CJ, Striker GE, Striker LJ** 1994 Advanced glycation end products up-regulate gene expression found in diabetic glomerular disease. Proc Natl Acad Sci USA 91:9436–9440
16. **Paul RG, Bailey AJ** 1999 The effect of advanced glycation end-product formation upon cell-matrix interactions. Int J Biochem Cell Biol 31:653–660
17. **Baxter RC, Binoux MA, Clemmons DR, Conover CA, Drop SL, Holly JM, Mohan S, Oh Y, Rosenfeld RG** 1998 Recommendations for nomenclature of the insulin-like growth factor binding protein superfamily. Endocrinology 139:4036
18. **Frazier K, Williams S, Kothapalli D, Klapper H, Grotendorst GR** 1996 Stimulation of fibroblast cell growth, matrix production, and granulation tissue formation by connective tissue growth factor. J Invest Dermatol 107:404–411
19. **Grotendorst GR** 1997 Connective tissue growth factor: a mediator of TGF-β action on fibroblasts. Cytokine Growth Factor Rev 8:171–179
20. **Shimo T, Nakanishi T, Kimura Y, Nishida T, Ishizeki K, Matsumura T, Takigawa M** 1998 Inhibition of endogenous expression of connective tissue growth factor by its antisense oligonucleotide and antisense RNA suppresses proliferation and migration of vascular endothelial cells. J Biochem 124:130–140
21. **Babic AM, Chen CC, Lau LF** 1999 Fisp12/mouse connective tissue growth factor mediates endothelial cell adhesion and migration through integrin $\alpha_v\beta_3$, promotes endothelial cell survival, and induces angiogenesis in vivo. Mol Cell Biol 19:2958–2966
22. **Igarashi A, Nashiro K, Kikuchi K, Sato S, Ihn H, Grotendorst GR, Takehara K** 1995 Significant correlation between connective tissue growth factor gene expression and skin sclerosis in tissue sections from patients with systemic sclerosis. J Invest Dermatol 105:280–284
23. **Dammeier J, Brauchle M, Falk W, Grotendorst GR, Werner S** 1998 Connective tissue growth factor: a novel regulator of mucosal repair and fibrosis in inflammatory bowel disease? Int J Biochem Cell Biol 30:909–922
24. **di Mola FF, Friess H, Martignoni ME, Di Sebastiano P, Zimmermann A, Innocenti P, Graber H, Gold LI, Korc M, Buchler MW** 1999 Connective tissue growth factor is a regulator for fibrosis in human chronic pancreatitis. Ann Surg 230:63–71
25. **Yang DH, Kim HS, Wilson EM, Rosenfeld RG, Oh Y** 1998 Identification of glycosylated 38-kDa connective tissue growth factor (IGFBP-related protein 2) and proteolytic fragments in human biological fluids, and up-regulation of IGFBP-rP2 expression by TGF-β in Hs578T human breast cancer cells. J Clin Endocrinol Metab 83:2593–2596
26. **Yamagishi S, Yonekura H, Yamamato Y, Katsuno K, Sato F, Mita I, Ooka H, Satozawa N, Kawakami T, Nomura M** 1997 Advanced glycation end-products driven angiogenesis in vitro: induction of the growth and tube formation of human microvascular endothelial cells through. J Biol Chem 272:8723–8730
27. **Owen Jr WF, Hou FF, Stuart RO, Kay J, Boyce J, Chertow GM, Schmidt AM** 1998 β_2-Microglobulin modified advanced glycation end products modulates collagen synthesis in human fibroblasts. Kidney Int 53:1365–1373
28. **Kislinger T, Fu C, Huber B, Qu W, Taguchi A, Du Yan S, Hofmann M, Yan SF, Pischetsrieder M, Stern D** 1999 $N(\epsilon)$-(Carboxymethyl)lysine adducts of proteins are ligands for receptor for advanced glycation end products that activate cell signaling pathways and modulate gene expression. J Biol Chem 274:31740–31749
29. **Kim HS, Nagalla SR, Oh Y, Wilson E, Roberts Jr CT, Rosenfeld RG** 1997 Identification of a family of low-affinity insulin-like growth factor binding proteins (IGFBPs): characterization of connective tissue growth factor as a member of the IGFBP superfamily. Proc Natl Acad Sci USA 94:12981–12986
30. **Lander HM, Tauras JM, Ogiste JS, Hori O, Moss RA, Schmidt AM** 1997 Activation of the receptor for advanced glycation end products triggers a $p21^{ras}$-dependent mitogen activated protein kinase pathway regulated by oxidant stress. J Biol Chem 272:17810–17814
31. **Lu M, Kuroki M, Amano S, Tolentino M, Keough K, Kim I, Bucala R, Adamis AP** 1998 Advanced glycation end products increase retinal vascular endothelial growth factor expression. J Clin Invest 101:1219–1224
32. **Koschinsky T, He CJ, Mitsuhashi T, Bucala R, Liu C, Buenting C, Heitmann K, Vlassara H** 1997 Orally absorbed reactive glycation products (glycotoxins): an environmental risk factor in diabetic nephropathy. Proc Natl Acad Sci USA 94:6474–6479
33. **Martin JL, Ballesteros M, Baxter RC** 1992 Insulin-like growth factor-I (IGF-I) and transforming growth factor-β1 release IGF-binding protein-3 from human fibroblasts by different mechanisms. Endocrinology 131:1703–1710
34. **Damon SE, Haugk KL, Swisshelm K, Quinn LS** 1997 Developmental regulation of Mac25/insulin-like growth factor-binding protein-7 expression in skeletal myogenesis. Exp Cell Res 237:192–195
35. **Igarashi A, Okochi H, Bradham DM, Grotendorst GR** 1993 Regulation of connective tissue growth factor gene expression in human skin fibroblasts and during wound repair. Mol Biol Cell 4:637–645
36. **Bierhaus A, Illmer T, Kasper M, Luther T, Quehenberger P, Tritschler H, Wahl P, Ziegler R, Muller M, Nawroth PP** 1997 Advanced glycation end product (AGE)-mediated induction of tissue factor in cultured endothelial cells is dependent on RAGE. Circulation 96:2262–2271
37. **Lalla E, Lamster IB, Schmidt AM** 1998 Enhanced interaction of advanced glycation end products with their cellular receptor RAGE: implications for the pathogenesis of accelerated periodontal disease in diabetes. Ann Periodontol 3:13–19
38. **Steffen CL, Ball-Mirth DK, Harding PA, Bhattacharyya N, Pillai S, Brigstock DR** 1998 Characterization of cell-associated and soluble forms of connective tissue growth factor (CTGF) produced by fibroblast cells in vitro. Growth Factors 15:199–213
39. **Munch G, Keis R, Wessels A, Riederer P, Bahner U, Heidland A, Niwa T, Lemke HD, Schinzel R** 1997 Determination of advanced glycation end products in serum by fluorescence spectroscopy and competitive ELISA. Eur J Clin Chem Clin Biochem 35:669–677
40. **Makita Z, Vlassara H, Cerami A, Bucala R** 1992 Immunochemical detection of advanced glycosylation end products *in vivo*. J Biol Chem 267:5133–5138
41. **Al-Abed Y, Bucala R** 2000 Structure of a synthetic glucose derived advanced glycation end product that is immunologically cross-reactive with its naturally occurring counterparts. Bioconjug Chem 11:39–45
42. **Park L, Raman KG, Lee KJ, Lu Y, Ferran Jr LJ, Chow WS, Stern D, Schmidt AM** 1998 Suppression of accelerated diabetic atherosclerosis by the soluble receptor for advanced glycation endproducts. Nat Med 4:1025–1031
43. **Yan SD, Stern D, Schmidt AM** 1997 What's the RAGE? The receptor for advanced glycation end products (RAGE) and the dark side of glucose. Eur J Clin Invest 27:179–181
44. **Duncan MR, Frazier KS, Abramson S, Williams S, Klapper H, Huang X, Grotendorst GR** 1999 Connective tissue growth factor mediates transforming growth factor beta-induced collagen synthesis: down-regulation by cAMP. FASEB J 13:1774–1786
45. **Murphy M, Godson C, Cannon S, Kato S, Mackenzie HS, Martin F, Brady HR** 1999 Suppression subtractive hybridization identifies high glucose levels as a stimulus for expression of connective tissue growth factor and other genes in human mesangial cells. J Biol Chem 274:5830–5834
46. **Riser BL, Denichilo M, Cortes P, Baker C, Grondin JM, Yee J, Narins RG** 2000 Regulation of connective tissue growth factor activity in cultured rat mesangial cells and its expression in experimental diabetic glomerulosclerosis. J Am Soc Nephrol 11:25–38
47. **Ito Y, Aten J, Bende RJ, Oemar BS, Rabelink TJ, Weening JJ, Goldschmeding R** 1998 Expression of connective tissue growth factor in human renal fibrosis. Kidney Int 53:853–861
48. **Oemar BS, Werner A, Garnier JM, Do DD, Godoy N, Nauck M, Marz W, Rupp J, Pech M, Luscher TF** 1997 Human connective tissue growth factor is expressed in advanced atherosclerotic lesions. Circulation 95:831–839
49. **Grotendorst GR, Okochi H, Hayashi N** 1996 A novel transforming growth factor beta response element controls the expression of the connective tissue growth factor gene. Cell Growth Differ 7:469–480
50. **Dammeier J, Beer HD, Brauchle M, Werner S** 1998 Dexamethasone is a novel potent inducer of connective tissue growth factor expression. Implications for glucocorticoid therapy. J Biol Chem 273:18185–18190
51. **Huntley AC** 1989 Cutaneous manifestations of diabetes mellitus. Dermatol Clin 7:531–546
52. **Hanna W, Friesen D, Bombardier C, Gladman D, Hanna A** 1987 Pathologic features of diabetic thick skin. J Am Acad Dermatol 16:546–553
53. **Seibold JR** 1982 Digital sclerosis in children with insulin-dependent diabetes mellitus. Arthritis Rheum 25:1357–1361
54. **Schmidt AM, Yan SD, Wautier JL, Stern D** 1999 Activation of receptor for advanced glycation end products: a mechanism for chronic vascular dysfunction in diabetic vasculopathy and atherosclerosis. Circ Res 84:489–497
55. **Vlassara H, Fuh H, Donnelly T, Cybulsky M** 1995 Advanced glycation endproducts promote adhesion molecule (VCAM-1, ICAM-1) expression and atheroma formation in normal rabbits. Mol Med 1:447–456

Altered expression of low affinity insulin-like growth factor binding protein related proteins in Hepatoblastoma

Henrik von Horn[a,b], Vivian Hwa[c], Ron G. Rosenfeld[c], Kerstin Hall[b], Bin Tean Teh[d], Michael Tally[b], Tomas. J. Ekström[a] and Steven G. Gray[a,d,*].

a) Laboratory for Molecular Development and Tumour Biology Experimental Alcohol and Drug Addiction Section, Dept. of Clinical Neuroscience, Karolinska Institute, CMM, L8:01, S-171 76 Stockholm, Sweden.

b) Endocrinology and Diabetes Unit, Department of Molecular Medicine, Karolinska Hospital, S-171 76 Stockholm, Sweden.

c) Department of Pediatrics, Oregon Health Sciences University, Portland, Oregon 97201, USA.

d) Van Andel Research Institute, 333 Bostwick Ne, Grand Rapids, MI 49503, USA

* Address correspondence to:
Dr. Steven Gray
Van Andel Research Institute
333 Bostwick NE
Grand Rapids
MI 49503
USA
Telephone: (616) 234 5576
Fax: (616) 234 5577
e-mail: steven.gray@vai.org

Abstract

Hepatoblastoma is a poorly understood rare pediatric liver tumour. We have previously shown that the IGF-axis is seriously disrupted in this tumour type. With the recent discovery that several other proteins also have the potential to bind to IGFs called insulin-like growth factor binding protein related proteins (IGFBP-rPs), we undertook an examination of several such genes in a series of hepatoblastomas with matched normal liver tissue. The expression profiles obtained reveal that the expression of these genes are also disturbed in these tumours, and may have implications for our understanding of the IGF-axis and its importance in this disease.

Keywords

Hepatoblastoma; Insulin-like growth factor binding protein related protein; Gene expression

1. Introduction.

Hepatoblastoma is a rare pediatric liver disease with an incidence of between 0.5 - 1.5 per million children [1]. Most hepatoblastomas are sporadic, but some familial inherited disorders, most notably Beckwith-Wiedemann (BWS), and familial Adenomatous polyposis (FAP), are associated with an increased risk for developing hepatoblastomas. Pre-operative chemotherapy regimes have proven to be extremely successful for treating this disease, but an understanding of the molecular processes behind the development of hepatoblastoma has lagged.

Gene expression studies have revealed that several genes show altered expression in hepatoblastomas. These include genes involved with modifying chromatin, cell growth and cell cycle control [2-5]. We and others have shown that the insulin-like growth factor axis is greatly altered in hepatoblastoma not only at the level of the growth factors themselves but also to their receptors and binding proteins [6-8]. Because the IGF-axis plays an important role in many diverse cellular functions including the promotion of cell growth and cell survival, such alterations may be critical to this tumour type. Recently an increasing number of proteins have been identified to have the ability to bind to the insulin-like growth factors albeit with low affinity. This has led to them being called insulin-like growth factor binding related proteins or IGFBP-rPs, although some controversy exists as to them being renamed [9-12]. These include the proteins CTGF, NovH and TAF all of which have been shown to have altered expression in cancer [9]. Because these genes may have functional roles with regard to the IGF-axis and have been shown to have altered expression in various cancers we sought to examine their

expression in series of hepatoblastoma for which matched normal liver was available and in which the IGF-axis has been shown to be altered, in an attempt to assess whether their expression may also be altered as a consequence of the tumour.

2. Materials and Methods

2.1 Samples

Twelve sporadic hepatoblastomas were examined in this study. For eight of these, matched normal liver tissue was available. All of the tumours with the exception of cases 6 and 7 were freeze-sectioned into 1 mm portions interrupted by 5 μm sections. The 1-mm sections were used for RNA isolation, while the interrupted thin sections were prepared for histopathological evaluation. These samples were fixed in formalin, stained and processed with hematoxylin and eosin in the usual manner. The results of this evaluation are presented in Table I, along with particulars for each sample. Human fetal livers (14- and 18- week) were obtained from therapeutic terminations, with the permission of the local ethical committee. Due to the nature of such procedures, limited amounts of tisuue were obtained, and where available the mRNA was included in the analyses.

2.2 *Nucleic Acid Isolation*

Total RNA was prepared as described previously [13].

2.3 *Preparation of Probe and RNase Protection Analysis*

T3, T7 and Sp6 RNA polymerases (Invitrogen) were used to make antisense RNA probes from the following templates according to the protocol provided in the RPA II kit (Ambion).When incorporating radioactivity into the probe, radioactive 32P-UTP with a specific activity of 800 Ci/mmol was used. Cold UTP was added such that final UTP specific-activity was 80 Ci/mmol for the *GAPDH* probe and 400 Ci/mmol for the others.

The probes used in this study were prepared as follows:

To measure *IGFBP-rP1* (*Mac25/TAF/PSF*) expression, a *Sma* I/*Kpn* I fragment from the full length cDNA contained in pcDNA3.1 (ref for pcDNA3.1.rP1?)was blunted and subcloned into the *EcoR V* site of pBluescript II SK (-) (Stratagene). When linearised with *Hind* III a probe of 320 bases could be generated using T3 RNA polymerase of which 210 bases hybridize to *IGFBP-rP1* specific transcripts.

IGFBP-rP2 (*CTGF*) expression was measured using a 217 base pair *Sma* I fragment from the full length *IGFBP-rP2* (pFastBac1 IGFBPrP2 ref for this plasmid)cloned into the *EcoR* V site of pBluescript II SK (-). Following linearization with *EcoR* I, a probe of 237 bases could be generated of which 217 bases hybridize to *IGFBPrP2* mRNA and protect from RNase.

A template for *IGFBP-rP4* (*Cyr61*) was generated by cloning a 214 base pair *Sma* I/*Pst* I fragment of the full length cDNA from a pBK-CMV plasmid containing the full length Cyr61 mRNA (generous gift from Dr. P. Berta) [14] into pBluescript II SK (-). Following linearization with *EcoR* I a probe of 305 bases could be generated with T3 RNA polymerase of which 214 bases hybridize specifically to *IGFBPrP4* specific mRNA transcripts.

IGFBP-rP5 (*L56/HtraA*) expression was measured by cloning a 186 base pair *Ava* II fragment from a pUC19 plasmid containing the full length cDNA (kind gift of Dr B. Treub) [15] into the *Sma* I site of pGem3Zf(+) (Promega). Following linearization with *EcoR* I a probe of approximately 255 bases could be generated with SP6 of which 186 bases hybridize specifically to *IGFBP-rP5* mRNA transcripts.

All of the plasmids described above were sequenced, in order to ensure that the fragment cloned corresponded to the gene under examination. Sequencing was carried out with T7 Sequenase according to the manufacturers instructions (United States Biochemical). RNase protection was carried out according to the protocol gievn with the RPA II kit (Ambion).

2.4 Analysis of Expression

Quantification of the RPA results was obtained using phosphorimager analysis (BAS-1000, Fuji Photo Film Co., Ltd) with *GAPDH* mRNA levels utilized as the internal control in each case. In each case the values for the gene under scrutiny were normalised to the internal control.

3. Results.

3.1 RNase protection analysis

Following sectioning and histopathological examination (Table I), total RNA was isolated and gene expression was measured using RNase protection analysis. A representative image of the results obtained for each gene examined is shown in Fig. 1. The results of each analysis are described in more detail in the following sections.

3.2 Expression of IGFBP-rP1 (Mac25/TAF/PSF) in Hepatoblastoma.

We examined the mRNA expression levels of *IGFBP-rP1* in a series of matched hepatoblastomas and the corresponding normal liver tissue from patients between the ages of 2 and 54 months. Included in the analysis were some hepatoblastomas with no counterpart normal tissues and fetal liver samples. The results of this analysis are shown in Fig. 2. In four of the eight matched tumours expression of this gene was downregulated when compared to their matched normal counterparts. In the unmatched samples tumours two had expression which was below the average normal liver values. downregulated in the tumours. Thus overall, 6 out of 12 (50%) of the tumours show downregulated expression of this gene. However, in cases 3, 5 and 7 (25% of the tumours) *IGFBP-rP1* is greatly upregulated in these tumours.

3.3 Expression of IGFBP-rP2 (CTGF) in Hepatoblastoma

Next we examined the expression of *IGFBP-rP2* in these samples. One tumour (case 7) showed greatly increased expression over its corresponding normal liver (Fig. 3.). Two other samples (cases 3 and 5) showed slightly elevated levels of expression. Including the unmatched tumours four samples (33%) have upregulated expression of *IGFBP-rP2*. In the matched tumours, downregulated expression of this gene was observed in three tumours (cases 2, 6 and 8). One of the unmatched tumours also showed decresaed expression of this geneand two samples had unaltered expression.

3.4 Expression of IGFBP-rP4 (Cyr61) in Hepatoblastoma

When *IGFBP-rP4* expression was examined most of the tumours were observed to have reduced levels of expression of this gene in comparison with their matched normal liver (Fig. 4.). The exceptions to this were cases 3 and 7 which showed upregulated expression. Of these, case 7 had greatly increased expression of *IGFBP-rP4*. In the unmatched samples two samples have lower levels of expression than the average normal liver value. Overall, 7 of 12 samples or 58% of the hepatoblastomas showed downregulated expression of this gene.

3.5 Expression of IGFBP-rP5 (HTRA/L56) in Hepatoblastoma .

The levels of mRNA transcripts for *IGFBP-rP5* were then measured in these samples. In almost all cases expression of this gene was downregulated in the matched tumour samples compared to their normal liver counterparts (Fig. 5.). Two samples, cases 3 and 5 show an increased level of expression of *IGFBP-rP5*. All of the unmatched tumours have

levels of expression below that of average normal liver. If these are taken into account, 9 out of 12 hepatoblastomas or 75% of the samples had downregulated expression of IGFBP-rP5.

4. Discussion.

In the present study we have examined the mRNA expression of four genes whose products have recently been identified as having the ability to bind IGFs at low affinity in a series of hepatoblastomas in relation to their matched normal tissues (summarized in Table II). Previously we have reported that many members of the IGF-axis have altered expression in these samples including the IGFs which may therefore lead to increased mitogenic signalling within their surroundings [2,7]. IGFBPs are critical regulators of IGF activity, and by binding to IGFs they form biologically inactive complexes which in addition to increasing the half-life of the growth factor, also modulate the binding of the IGFs to their cognate receptors [9,10]. Thus, the newly identified IGFBPrPs may also prove to have important roles in regulating IGF signalling in addition to their other roles [9-12].

IGFBPrP1 has been shown to be a potential tumor suppressor [9,16] and decreased expression of this gene has been observed in higher stage breast cancer [17]. In addition, downregulation of this gene by methylation has been shown to be important for tumorigenesis in a mouse model of liver cancer [18]. As such, the decreased expression of this gene in some of our samples may reflect the loss of tumour suppressive capability. It may also indicate that increased methylation of this gene may be occurring in the hepatoblastomas. Cases 3, 5 and 7 however have greatly increased expression of this gene, and this may indicate an attempt by the tumours to regulate or suppress the tumour.

IGFBP-rP2 or *CTGF* is a major mitogenic factor for connective tissue cells. It has also been shown to be specifically expressed in the maligant lymphoblasts of patients with

acute lymphoblastic leukemia, and also to be expressed in breast cancer cell lines [19,20]. In our samples three tumours have increased expression of this gene, with one sample in particular (case 7), having greatly enhanced expression. This may therefore lead to increased mitogenic signalling in these particular tumours.

(When we tested our samples using immunohistochemistry for IGFBP-rP1 and IGFBP-rP2 we were unable to observe any protein (data not shown). While this may be an artifact of the tissue preparation, it may also indicate the rapid secretion of these proteins into the serum surrounding the tumours .... should we keep this ???)

IGFBP-rP4 (*Cyr61*) has also been implicated in cancer where it has been shown to be downregulated in prostate cancer [21]. However overexpression of this gene in a xenograft model appears to promote tumour growth [22]. In our analysis of hepatoblastomas, one sample (case7) has a very high overexpression of this gene compared to its matched normal liver, and this may be a reflection of increased growth potential in this tumour. However five of the samples also show reduced expression of this gene in a manner similar to that observed for prostate cancer [21].

IGFBP-rP5 (L56/HtrA) is an interesting protein because it has serine protease activity. One feature of the IGF-axis is that the IGFBPs themselves are regulated in part by the actions of serine proteases. The cleavage of such binding proteins could therefore increase the availability of free IGFs, leading to increased mitogenic signalling. IGFBP-rP5 has been shown to be able to cleave IGFBP-5 and as such overexpression of this gene may enhance the mitogenic signalling by IGFs in the vicinity of the tumour [9]. In our samples two hepatoblastomas (cases 3 and 5) show elevated expression of this serine protease. However, in most cases the expression of this gene is reduced, and this may

signal an attempt by the tumours to limit the mitogenic signalling in their vicinity. It is interesting to note that the same samples which show elevated IGFBP-rP5 also have a concommitant overexpression of IGFBP5 indicating that the regulation of IGFBP5 may be linked to IGFBP-rP5 activity [23].

Cases 3 and 5 appear to be of particular interest as in previous reports we have shown that the expression of *IGF1*, *IGF2*, *IGF1R*, *IGFBP5*, *IGFBP6*, *p53*, *pRb*, and *TGFβ1* are all upregulated in these samples when compared to the rest (Gray et al., 2000a; Gray et al., 2000b; von Horn et al., 2001). These changes may be of importance with regard to tumourigenesis in these particular samples. Alternatively, they may also be a reflection of the response to the pre-operative chemotherapy in these individuals.

In conclusion, the data presented indicate that in hepatoblastomas, the IGF-axis is seriously disturbed, extending even to the members of the low affinity insulin-like growth factor binding protein related proteins, confirming the importance of this axis in the pathogenesis of this disease.

Acknowledgements

This work was supported by grants from The Children's Cancer Foundation of Sweden and The Swedish Cancer Foundation. The authors would like to thank Drs B. Treub and P. Berta for their generous gifts of cDNA clones for IGFBPrP4 and IGFBPrP5.

References

[1] G. Perilongo and E.A. Shafford, Liver tumours, *Eur. J. Cancer* 35 (1999) 953-958.

[2] S.G. Gray, W. Hartmann, T. Eriksson, C. Ekstrom, S. Holm, S. Kytola, D. von Schweinitz, T. Pietsch, C. Larsson, P. Kogner, B. Sandstedt and T.J. Ekstrom, Expression of genes involved with cell cycle control, cell growth and chromatin modification are altered in hepatoblastomas, *Int. J. Mol. Med.* 6 (2000) 161-9.

[3] A. Iolascon, L. Giordani, A. Moretti, G. Basso, A. Borriello and F. Della Ragione, Analysis of CDKN2A, CDKN2B, CDKN2C, and cyclin Ds gene status in hepatoblastoma, *Hepatology* 27 (1998) 989-95.

[4] H. Kim, E.K. Ham, Y.I. Kim, J.G. Chi, H.S. Lee, S.H. Park, Y.M. Jung, N.K. Myung, M.J. Lee and J.J. Jang, Overexpression of cyclin D1 and cdk4 in tumorigenesis of sporadic hepatoblastomas, *Cancer Lett.* 131 (1998) 177-83.

[5] S.H. Lee, M.S. Shin, J.Y. Lee, W.S. Park, S.Y. Kim, J.J. Jang, S.M. Dong, E.Y. Na, C.S. Kim, S.H. Kim and N.J. Yoo, In vivo expression of soluble Fas and Fap-1: Possible mechanisms of Fas resistance in human hepatoblastomas, *J. Path.* 188 (1999) 207-212.

[6] S.N. Akmal, K. Yun, J. MacLay, Y. Higami and T. Ikeda, Insulin-like growth factor 2 and insulin-like growth factor binding protein 2 expression in hepatoblastoma, *Hum. Pathol.* 26 (1995) 846-51.

[7] S.G. Gray, T. Eriksson, C. Ekstrom, S. Holm, D. von Schweinitz, P. Kogner, B. Sandstedt, T. Pietsch and T.J. Ekstrom, Altered expression of members of the IGF-axis in hepatoblastomas, *Br. J. Cancer* 82 (2000) 1561-7.

[8] X. Li, G. Adam, H. Cui, B. Sandstedt, R. Ohlsson and T.J. Ekström, Expression, promoter usage and parental imprinting status of insulin-like growth factor II (IGF2) in human hepatoblastoma: uncoupling of IGF2 and H19 imprinting, *Oncogene* 11 (1995) 221-9.

[9] V. Hwa, Y. Oh and R.G. Rosenfeld, The insulin-like growth factor-binding protein (IGFBP) superfamily, *Endocrine Rev.* 20 (1999) 761-787.

[10] L.A. Wetterau, M.G. Moore, L. Kuk-Wah, M.L. Shim and P. Cohen, Novel Aspects of the Insulin-like Growth Factor Binding Proteins, *Mol. Genet. Metab.* 68 (1999) 161-181.

[11] E.E. Moussad and D.R. Brigstock, Connective tissue growth factor: what's in a name?, *Mol. Genet. Metab.* 71 (2000) 276-92.

[12] G.R. Grotendorst, L.F. Lau and B. Perbal, CCN proteins are distinct from and should not be considered members of the insulin-like growth factor-binding protein superfamily, *Endocrinology* 141 (2000) 2254-2256.

[13] P. Chomczynski and N. Sacchi, Single-step method of RNA isolation by acid guanidinium thiocyanate-phenol-chloroform extraction, *Anal. Biochem.*, 162 (1987) 156-9.

[14] P. Jay, J.L. Berge-Lefranc, C. Marsollier, C. Mejean, S. Taviaux and P. Berta, The human growth factor-inducible immediate early gene, CYR61, maps to chromosome 1p, *Oncogene* 14 (1997) 1753-7.

[15] J. Zumbrunn and B. Trueb, Primary structure of a putative serine protease specific for IGF-binding proteins, *FEBS Lett.* 398 (1996) 187-92.

[16] C.C. Sprenger, S.E. Damon, V. Hwa, R.G. Rosenfeld and S.R. Plymate, Insulin-like growth factor binding protein-related protein 1 (IGFBP- rP1) is a potential tumor suppressor protein for prostate cancer, *Cancer Res.* 59 (1999) 2370-5.

[17] G. Landberg, H. Ostlund, N.H. Nielsen, G. Roos, S. Emdin, A.M. Burger and A. Seth, Downregulation of the potential suppressor gene IGFBP-rP1 in human breast cancer is associated with inactivation of the retinoblastoma protein, cyclin E overexpression and increased proliferation in estrogen receptor negative tumors, *Oncogene* 20 (2001) 3497-505.

[18] S. Komatsu, Y. Okazaki, M. Tateno, J. Kawai, H. Konno, M. Kusakabe, A. Yoshiki, M. Muramatsu, W.A. Held and Y. Hayashizaki, Methylation and downregulated expression of mac25/insulin-like growth factor binding protein-7 is associated with liver tumorigenesis in SV40T/t antigen transgenic mice, screened by restriction landmark genomic scanning for methylation (RLGS-M), *Biochem. Biophys. Res. Commun.* 267 (2000) 109-17.

[19] P. Vorwerk, H. Wex, B. Hohmann, Y. Oh, R.G. Rosenfeld and U. Mittler, CTGF (IGFBP-rP2) is specifically expressed in malignant lymphoblasts of patients with acute lymphoblastic leukaemia (ALL), *Br. J. Cancer* 83 (2000) 756-60.

[20] D.H. Yang, H.S. Kim, E.M. Wilson, R.G. Rosenfeld and Y. Oh, Identification of glycosylated 38-kDa connective tissue growth factor (IGFBP-related protein 2) and proteolytic fragments in human biological fluids, and up-regulation of IGFBP-rP2 expression by TGF-beta in Hs578T human breast cancer cells, *J. Clin. Endocrinol. Metab.* 83 (1998) 2593-6.

[21] C.P. Pilarsky, U. Schmidt, C. Eissrich, J. Stade, S.E. Froschermaier, M. Haase, G. Faller, T.W. Kirchner and M.P. Wirth, Expression of the extracellular matrix signaling molecule Cyr61 is downregulated in prostate cancer, *Prostate* 36 (1998) 85-91.

[22] A.M. Babic, M.L. Kireeva, T.V. Kolesnikova and L.F. Lau, CYR61, a product of a growth factor-inducible immediate early gene, promotes angiogenesis and tumor growth, *Proc. Natl. Acad. Sci. U S A*, 95 (1998) 6355-60.

[23] H. von Horn, M. Tally, K. Hall, T. Eriksson, T.J. Ekstrom and S.G. Gray, Expression levels of insulin-like growth factor binding proteins and insulin receptor isoforms in hepatoblastomas, *Cancer Lett.* 162 (2001) 253-60.

Figure 1. RNase protection analysis.

Representative results for each gene examined in the hepatoblastomas. *GAPDH* was used as an internal control in each sample for use in the quantitation of gene expression. *GAPDH* is indicated with an arrow. letters indicate the protected band for each gene as follows: A) *IGFBP-rP1*; B) *IGFBP-rP2*; C) *IGFBP-rP4*; D) *IGFBP-rP5*.

Figure 2. RNase protection analysis of *IGFBP-rP1* expression.

Analysis of total *IGFBP-rP1* transcripts in hepatoblastomas. *GAPDH* expression is used as the internal control for quantification purposes. In all of the following figures the Y-axis units represent the values for each gene divided by the value obtained for the housekeeping gene *GAPDH* (in this case: *IGFBP-rP1/GAPDH*) as determined by phosphorimager analysis and following the adjustments as described in materials and methods. The mean ± standard error of the mean was also calculated for the normal liver (N), and graphed along with the individual samples. Matched tumors are those samples for which normal liver was taken from the same individual at time of surgery. Unmatched tumors are those samples for which normal liver tissue was unavailable. Fetal livers were included to compare against normal liver and tumour expression.

Figure 3. RNase protection analysis of *IGFBP-rP2* expression.

Using RNase protection analysis *IGFBP-rP2* transcripts were quantified and graphed as described in Figure 2.

Figure 4. RNase protection analysis of *IGFBP-rP4* expression.

Quantification of *IGFBP-rP4* transcripts in hepatoblastomas. Following quantification, the results were graphed as described in Figure 2.

Figure 5. RNase protection analysis of *IGFBP-rP5* expression.

Quantification of *IGFBP-rP5* transcripts in hepatoblastomas. Following RNase protection analysis, the results were quantified and graphed as described in Figure 2.

Table I
Clinical data for the tumor samples used in the study

Case no.	*Age at diagnosis (months)*	*Sex*	*Histology*	*Pre-operative chemotherapy*
1	6	M	Epithelial	No
2	19	M	Epithelial	Yes
3	19	M	Epithelial	Yes
4	22	M	Epithelial/mesenchymal	Yes
5	54	M	Epithelial	Yes
6	2	M	Fetal	No
7	12	F	Fetal	Yes
8	36	M	Not available	Yes
9	11	F	Fetal	No
10	13	M	Fetal	No
11	8	F	Epithelial/mesenchymal	No
12	18	M	Not available	Yes

Table II.
Expression patterns of the IGFB-rPs in hepatoblastomas[a]

Case no.	*IGFBP-rP1*	*IGFBP-rP2*	*IGFBP-rP4*	*IGFBP-rP5*
1	N/↑	N	↓	↓
2	↓	↓	↓	↓
3	↑	↑	↑	↑
4	↓	↓/N	↓	↓
5	↑	↑/N	↓/N	↑
6	↓	↓	↓	↓
7	↑	↑	↑	↓
8	↓	↓	↓	↓
9	N	↓/N	↓	↓
10	↓	↓	↓	↓
11	↓	N	↑/N	↓
12	↑	↑	N	n.d.

[a] ↑, increased expression; ↓, decreased expression; N, normal expression; N/↑normal or slightly increased expression; N/↓, normal or slightly decreased expression; n.d., not determined.

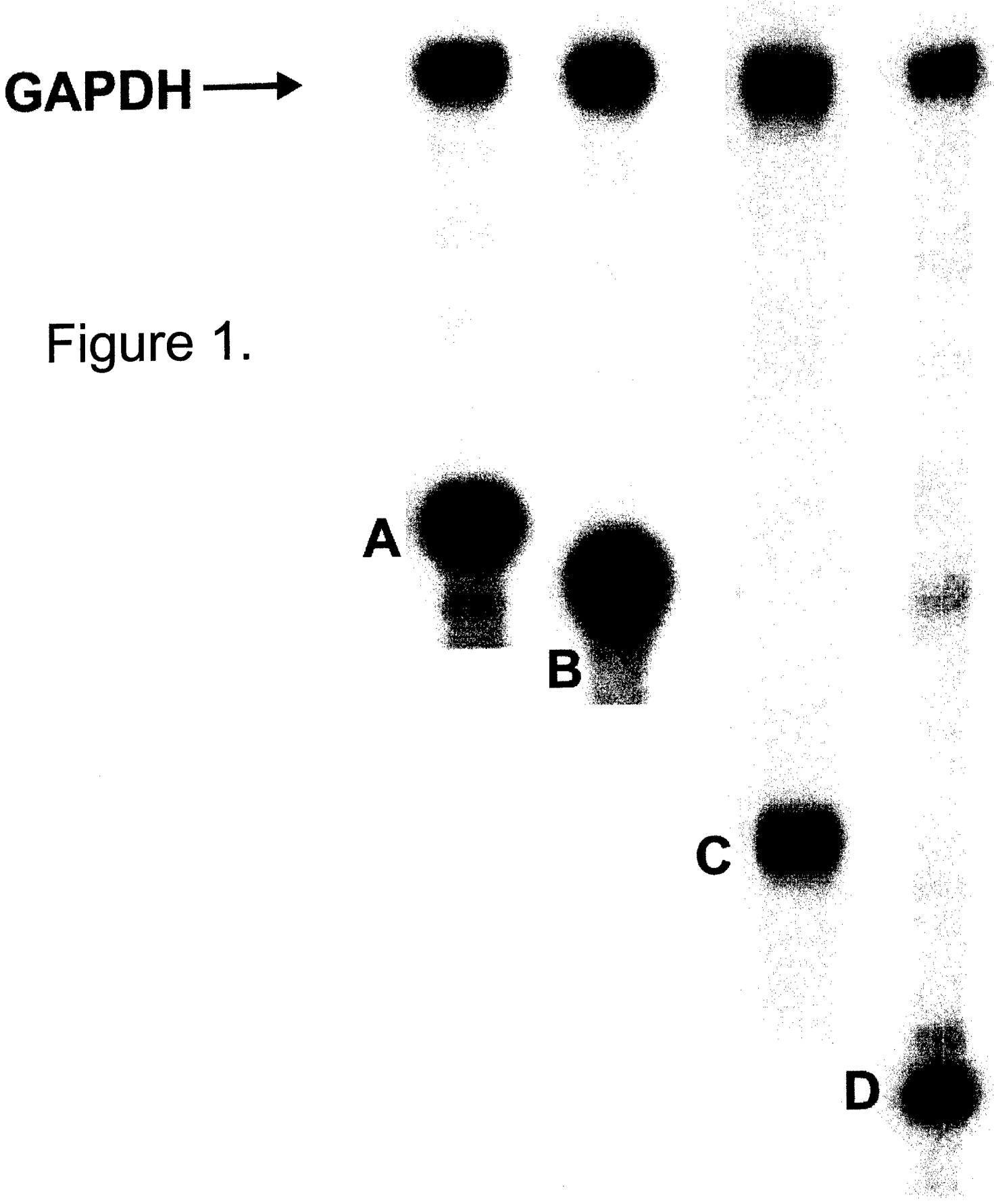

Figure 1.

Figure 2.

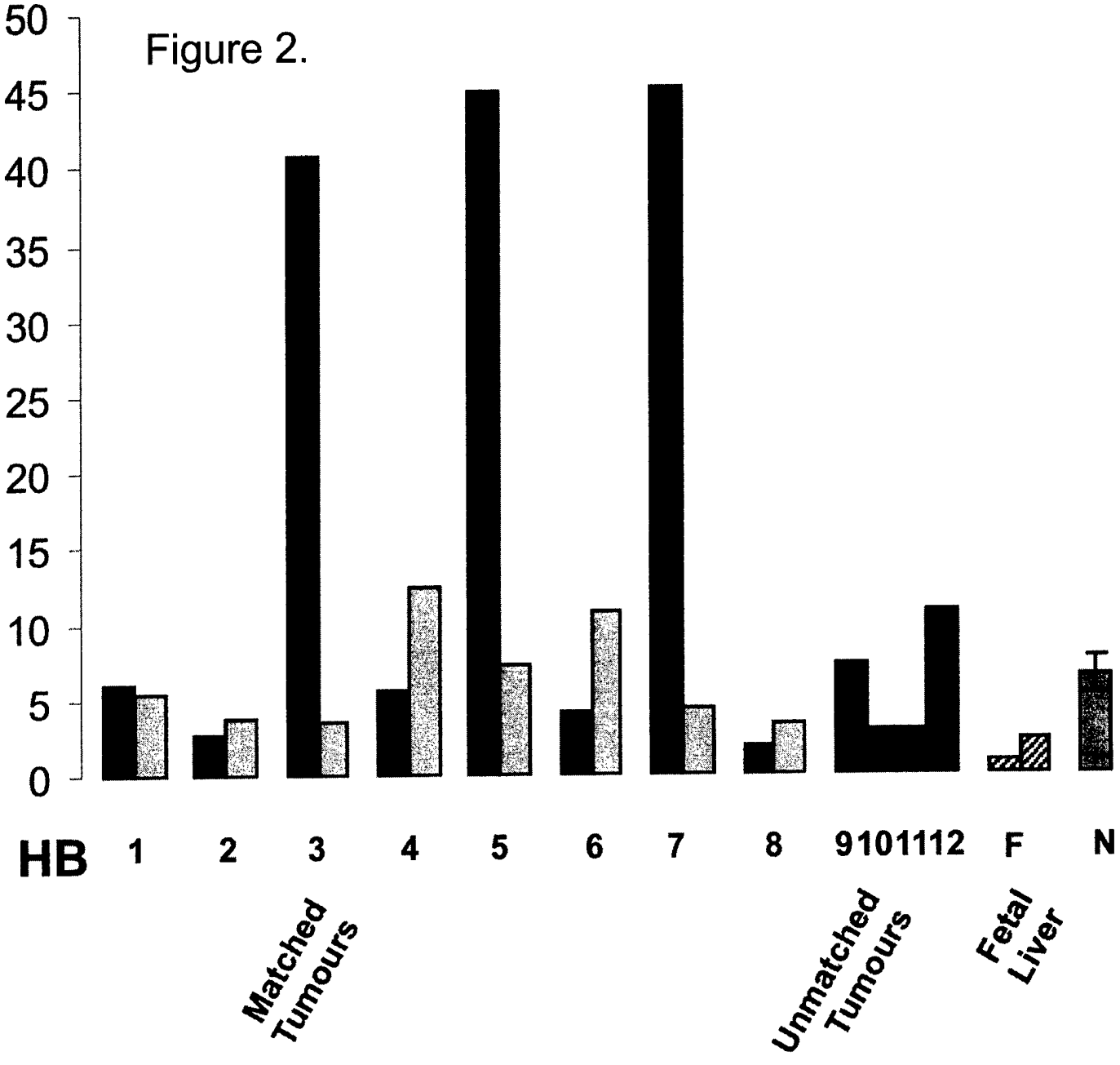
50
45
40
35
30
25
20
15
10
5
0
HB
1
2
3
4
5
6
7
8
9
10
11
12
F
N
Matched Tumours
Unmatched Tumours
Fetal Liver

Figure 3.

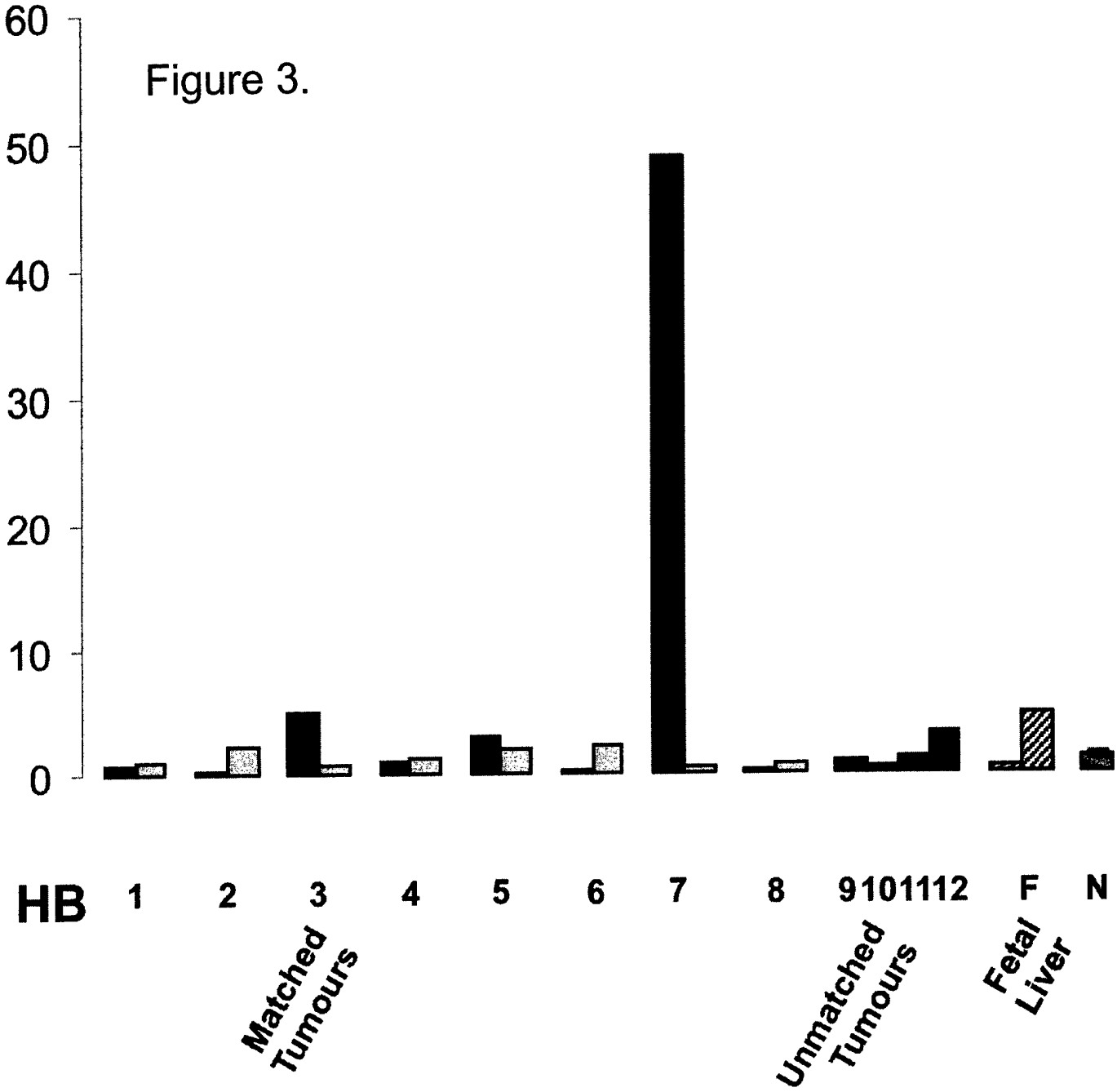
60
50
40
30
20
10
0
HB
1
2
3
4
5
6
7
8
9
10
11
12
F
N
Matched Tumours
Unmatched Tumours
Fetal Liver

Figure 4

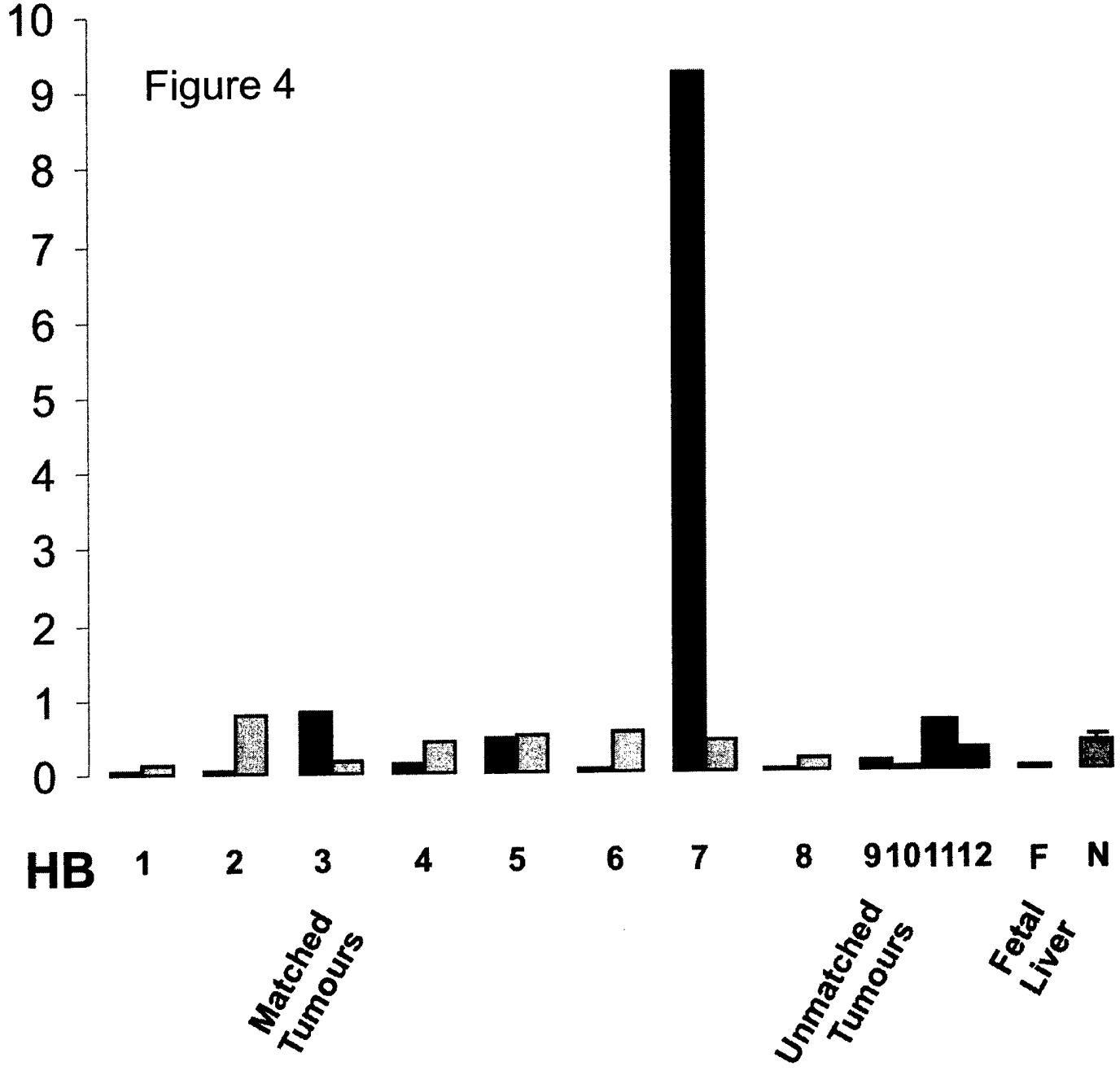
10
9
8
7
6
5
4
3
2
1
0
HB
1
2
3
4
5
6
7
8
9
10
11
12
F
N
Matched Tumours
Unmatched Tumours
Fetal Liver

Figure 5

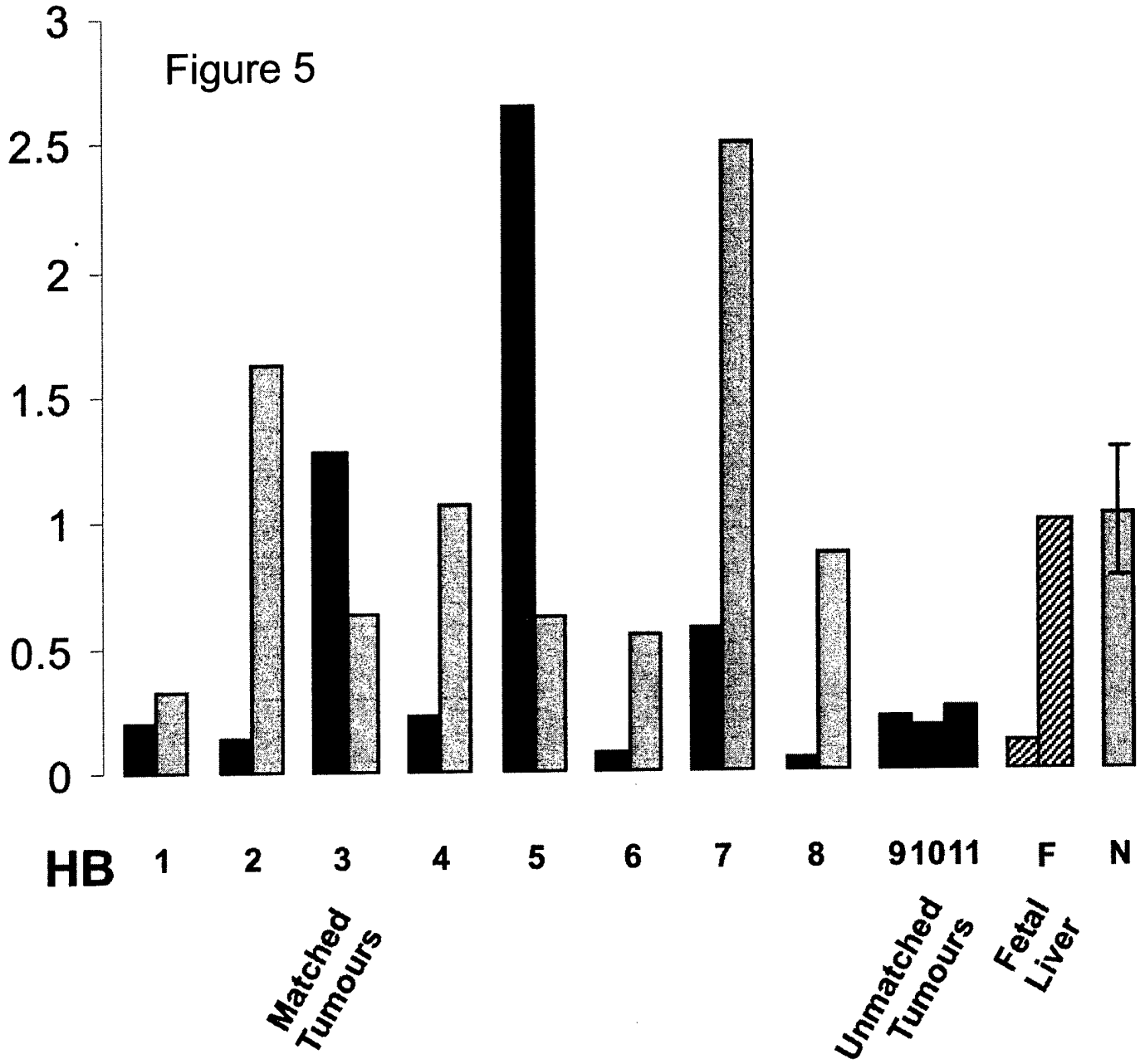
3
2.5
2
1.5
1
0.5
0
HB
1
2
3
4
5
6
7
8
9
10
11
F
N
Matched Tumours
Unmatched Tumours
Fetal Liver

Title

Binding properties of insulin-like growth factor binding protein-3 (IGFBP-3), IGFBP-3 N- and C-terminal fragments, and members of the IGFBP superfamily measured using a biosensor

Running title

Biosensor analysis of IGFBP-3 and IGFBP-rPs

Peter Vorwerk[1], Bianka Hohmann[1], Youngman Oh[2], Ron G. Rosenfeld[2], and Ronald M. Shymko[3]

[1] Otto-von-Guericke University, Dept. Pediatric Oncology, Magdeburg, Germany

[2] Dept. Pediatrics, Oregon Health Sciences University, Portland / OR, USA

[3] Dept. of Scientific Computing, Novo Nordisk A/S, Måløv, Denmark

Corresponding author :

Dr. Peter Vorwerk, M.D., Otto-von-Guericke University, Dept. Pediatric Oncology, Emanuel-Larisch-Weg 17-19, D-39112 Magdeburg, Germany

phone: 49-391-6717223, fax: 49-391-67190562

email: Peter.Vorwerk@medizin.uni-magdeburg.de

Supported by NIH Grants CA-58110 and DK-51513 (RGR), by American Cancer

Society Grant RPG-99-103-01-TBE, Department of the Army grant DAMD 17-00-1-0042 (YO) and a grant from the ministry of culture of Saxonia-Anhalt; Germany (003VE1998; PV).

ABSTRACT

We have measured the binding of IGF-I and IGF-II to recombinant human N-terminal (residues 1-97; rhIGFBP-3^{1-97}) and C-terminal (residues 98-264; rhIGFBP-3^{98-264}) IGFBP-3 fragments, and compared it with IGF binding to intact IGFBP-3, using biosensor analysis. Experiments were carried out in different configurations, either with binding protein or fragment immobilized, or with IGF immobilized. These experiments showed that IGF-I and IGF-II bind to IGFBP-3 with affinities of 4-7 x 10^9 M^{-1}, with IGF-II having a somewhat higher affinity than IGF-I. The association and dissociation kinetics of IGF-II were both slightly slower than those of IGF-I. The affinities of both rhIGFBP-3^{1-97} and rhIGFBP-3^{98-264} for IGF proteins were approximately 3 orders of magnitude less than that of full-length IGFBP-3, with rhIGFBP-3^{1-97} having about 3-5 times the affinity of rhIGFBP-3^{98-264}. These results further support the concept that high-affinity binding of IGF to IGF binding proteins results from a two-site interaction of IGF with both the N and C terminal regions of the binding protein.

Binding of insulin to IGFBP-3 and its N- and C-terminal fragments, and of IGF-I and IGF-II to new members of the IGFBP superfamily, mac25(IGFBP-rP1) and CTGF(IGFBP-rP2) was also investigated. Weak insulin binding to full-length IGFBP-3 could be demonstrated in a few experiments, but we found that binding of IGF-I and IGF-II to mac25(IGFBP-rP1) or CTGF(IGFBP-rP2) was below the detection limit of the biosensor instrument.

Introduction

Insulin-like growth factor binding proteins (IGFBPs) are important regulators of IGF action that act by modulating IGF binding to its receptors. Initially identified as carriers for IGFs in a variety of biological fluids, their presumed function is to protect IGF peptides from degradation and clearance, increase the half-life of IGFs, and deliver them to appropriate tissue receptors (1). A number of IGFBP fragments have been identified in different biological fluids and a variety of specific and nonspecific proteases for IGFBPs have been described (2;3). The concept of IGFBPs as simple carrier proteins has been complicated by the discovery of multiple IGF-independent actions of IGFBPs and the identification of a number of cDNAs encoding proteins that bind IGF with substantially lower affinities than IGFBPs (4). The N-terminal regions of these proteins are structurally homologous to the IGFBPs, with conservation of the cysteine residues and a common N-terminal motif, GCGCCXXC (1). This observation suggests an IGFBP superfamily consisting of the "classical" high affinity IGFBPs and a group of low affinity IGFBP-related proteins (IGFBP-rPs).

IGFBP-3 is the major serum IGFBP and transports 70-90% of the circulating IGFs (5). In target cell systems, it inhibits IGF actions, but also, under specific conditions, potentiates IGF action or exerts IGF-independent effects (5;6). Proteolysis of IGFBP-3 was initially demonstrated in human pregnancy serum, in which circulating IGFBP-3 was found primarily in low-molecular weight forms (7;8). The proteolytic fragments were shown to bind IGF with lower affinities, thereby increasing availability of IGF to target receptors. Subsequent studies demonstrated that limited proteolysis is not restricted to

IGFBP-3, but occurs also in other IGFBP-species, IGFBP-1 through -5 (2;3). As for IGFBP-3, the resulting fragments have a decreased affinity for IGFs and, therefore, more easily release IGF to the target receptors. Furthermore, various IGFBP-fragments are capable of direct stimulatory or inhibitory action at the target cells (9-13).

All members of the IGFBP-superfamily preserve the N-terminal cysteine-rich domain, including the IGFBP-motif GCGCCXXC, but vary in the intermediate region and C-terminal domain of the protein. Only the high affinity IGFBPs also share homology in the cysteine-rich C-terminal domain, which has led to the hypothesis that the conserved N-terminal domain contains the main IGF-binding activity, forming, together with the C-terminal conserved region, the high affinity IGF binding activity in IGFBPs (1;13-15).

With the expression and purification of a variety of recombinant IGFBPs, IGFBP-rPs, and well-defined fragments or mutants, our understanding of structure-function relationships of the members of the IGFBP superfamily has improved (12;13;15-25).

However exact measurement of the binding properties of the various members of the IGFBP superfamily, and especially their proteolytic fragments, has proved difficult. Different methods have been used to estimate the binding affinities: conventional binding assays using radiolabeled IGFs, affinity cross-linking with radiolabeled ligands, gel filtration or western ligand blots using radiolabeled or biotinylated ligands (12-14;17;20;21;26-32). However, it has been difficult to determine accurate affinities of IGFs for IGFBPs using those assays, due to several limiting factors such as quality of labeled ligands, effect of labeling iodine on the affinity and limitation of measurable range of the binding affinity.

In recent years, biosensor instruments using surface plasmon resonance technology have been increasingly used to study biomolecular interactions. We (33-35) and others (15;36-39) have used this technology to study IGFBP interaction with IGFs or their analogues. In the present study, our goal was to make a detailed analysis, using a BIACORE biosensor instrument (Biacore AB, Uppsala, Sweden), of the binding of IGF-I and IGF-II to recombinant IGFBP-3 and fragments of this molecule, and also to new members of the IGFBP superfamily, mac25(IGFBP-rP1) and CTGF(IGFBP-rP2).

Material and Methods

Equipment and reagents

Experiments were done on an upgraded BIACORE™ 1000 instrument (Biacore AB, Uppsala, Sweden). CM5 certified sensor chips, surfactant P20, the amine coupling kit (N-hydroxysuccinimide (NHS), N-ethyl-N'-(3-diethylaminopropyl)carbodiimide (EDC), and ethanolamine hydrochloride were also obtained from Biacore AB. Recombinant human non-glycosylated insulin-like growth factor binding protein-3 (rhIGFBP-3) produced in *E. coli* was a gift from Protegen (Mountain View, CA). N- and C-terminal recombinant fragments, rhIGFBP-3^{1-97} and rhIGFBP-3^{98-264},were produced as previously described (32). IGF-I and IGF-II were purchased from GroPep Pty.Ltd and the biotinylation of IGF-I was performed according to Fowlkes (30).

Immobilization of peptides on the sensor chip

All immobilizations were carried out at 25°C using an amine coupling procedure (33) with a constant flow rate of 5 l/min. A more thorough description of the immobilization procedure can be found elsewhere (40). Equal volumes of 0.1 M NHS and 0.1 M EDC were mixed by the BIACORE system's robotics and injected over the surface of the sensor chip to activate the carboxymethylated dextran. For coupling to the sensor chip, peptides were injected over the activated surface in a 10 mM sodium acetate solution. A solution of 1M ethanolamine was then passed over the surface to deactivate remaining active carboxyl groups and to wash out non-specifically bound protein. Combinations of peptide concentration, pH during coupling, activation time, and

coupling time, respectively, giving a stable surface with satisfactory amounts of the coupled peptide, were as follows: rhIGFBP-3: 10 g/ml, pH 4.5, 3 min, 7min; rhIGFBP-3^{98-264}: 2 g/ml, pH 4.5, 7 min, 7 min; rhIGFBP-3^{1-97}: 20 g/ml, pH 4.0, 10 min, 10 min; IGF-I: 4 g/ml, pH 4.5, 7 min, 7min; IGF-II: 1 g/ml, pH 4.0, 7 min, 7min. All ethanolamine deactivation steps were run for 7 minutes. Immediately after the immobilization procedure, HBS buffer (10 mM Hepes, 150 mM NaCl, 3.4 mM EDTA, 0.05% P20, pH 7.4) was flowed over the sensor chip surface for a minimum of 2 hours to allow the surface to stabilize.

Quality control of immobilized surfaces

In repeated experiments for each peptide, concentration and coupling time were varied to give a range of immobilized peptide coupled to the sensor chip, in order to check for possible mass transport effects, which are expected to be most pronounced at high immobilization levels and high binding affinities (41;42), and also to control for dependence of fitted binding parameters, or of apparent stoichiometry of binding, on immobilization level. We calculate the apparent stoichiometry as the ratio of the maximum achievable analyte bound, measured in the instrument's standard resonance units (RU), to the theoretical maximum, where the theoretical maximum is defined as

ImmobilizedRU * MW(analyte) / MW(immobilized peptide),

where ImmobilizedRU is the amount of peptide immobilized on the sensor chip, also expressed in RU. The apparent stoichiometry gives a good indication of the degree of inactivation of protein due to immobilization, and the steric hindrance of binding due to

overcrowding of immobilized molecules on the surface. Immobilization levels in our experiments were kept low both to give as high apparent stoichiometries as possible, and to reduce steric hindrance effects. Typical apparent stoichiometries for immobilized rhIGFBP-3 were 0.8 to 0.9, whereas those for immobilized IGF-I were about 25% and even lower for IGF-II. Note that a low apparent stoichiometry will still give accurate binding results if the immobilized molecules are all either fully active or fully inactive. Mass transport effects (41;42) were observed when measuring binding of rhIGFBP-3 to immobilized IGF-I or IGF-II, and these effects could not be fully eliminated even at the high flow rates (50 µl/min) used in our experiments. Mass transport effects were not apparent for any of the other tested molecules. In the case of rhIGFBP-3 binding to immobilized IGF-I, analysis of sensorgram data using models including or not including mass transport effects showed only minor differences in estimated binding parameters. These differences were especially minimal in global analyses (i.e. simultaneous analysis of multiple sensorgrams at different analyte concentrations) (43;44). None of the experiments showed a systematic change of binding parameters with immobilization level.

Kinetic assays on the BIACORE

All experiments were carried out at 25 °C, with a constant flow rate of 50 l/min of HBS buffer. This high flow rate was chosen to minimize mass transport effects. Purified analyte was diluted to various concentrations in HBS buffer using the system robotics, and the solution was injected over the peptides coupled to the chip surface for 5

minutes (association phase), followed by 10 minutes flow of HBS buffer alone (dissociation phase). In most experiments, the binding phases were preceded by a 10-minute wash with HBS buffer alone to allow the surface to equilibrate with the buffer. Bound analyte was removed from the coupled peptide by flowing a solution of 100 mM HCl over the surface for 3 minutes. This treatment regenerated the surfaces efficiently without any apparent damage. We observed, however, that IGF-I surfaces immobilized at very low levels tended to be somewhat unstable. In these cases, the surface was regenerated using 50 mM HCl in order to minimize any damaging effects of the regeneration procedure.

In most experiments, a standard intermediate concentration of analyte was first injected over the surface to provide a reference sensorgram. Then a series of varying concentrations of analyte was injected, followed by a second reference injection, a repeat of the concentration series, and a final reference injection. With this procedure the immobilized surface could be monitored for loss of activity, and test results checked for reproducibility.

Solution affinity assays

Solution affinity assays are designed to measure the equilibrium affinity of two molecules in solution, using the BIACORE instrument as a probe to measure the free concentration of one of the molecules (45). In these experiments, rhIGFBP-3 or one of its N- or C-terminal fragments was immobilized on a sensor chip to provide an active surface for measuring the free concentration of IGF-I or IGF-II in a mixture of IGF and

binding protein flowing over the surface. The surface was calibrated by flowing IGF at different (free) concentrations over the surface, recording a sensorgram for each concentration. Mixtures of IGF and binding protein or fragment at various concentrations were flowed over the same surface, and the calibration curve was used to estimate the free IGF remaining in solution for each of the mixed samples. The equilibrium affinity constant K_a was calculated using this estimate plus the known total concentrations of IGF and binding protein, assuming a one-site binding model.

Data analysis

Kinetic analyses were carried out using the BIAEvaluation 3.0 program (Biacore AB), assuming a one-site binding model. If the surface was judged stable by inspection of the repeated series of injected analyte concentrations, all sensorgrams in an experiment were analyzed simultaneously (global analysis). If a surface showed some instability, sensorgrams were analyzed individually, and the results pooled. In all cases, special attention was paid to the fitted R_{max}, which gives the amount of analyte bound at saturation, and is a therefore a measure of the apparent stoichiometry of binding. We have observed that even a visually good fit of a binding model to sensorgram data sometimes gives an unreasonable value of R_{max}, especially when analyzing single sensorgrams. Binding parameter estimates were rejected in such cases.

Model fitting was first done allowing the BIAEvaluation program to estimate the bulk refractive index effect (RI) for each sensorgram. Sensorgrams were then inspected visually to obtain another estimate of these values based on the step up in the

sensorgram at the start of the association phase and the step down at the start of the dissociation phase (33). If the fitted estimates did not correspond to the visual estimates, the fitted estimates were rejected and the fit was redone with the RI values fixed using the visual estimates. In a few experiments, the surface baseline signal (that is, the signal seen when buffer alone flows over the surface) drifted slowly downward through time (baseline drift), evident in the 10-minute pre-association wash and at the end of the dissociation phase. In these cases, the downward drift rate was estimated by fitting a straight line to the 10-minute wash, and the sensorgram was corrected for this drift during the fitting.

Results

Binding of IGF-I and IGF-II to rhIGFBP-3 and its N- and C-terminal fragments

With the BIACORE instrument, a binding reaction can be measured with either of the reacting pair immobilized, and the other injected over the immobilized surface. In this study, we attempted to measure all binding reactions in both orientations, which would be expected to give comparable results if the experimental conditions are suitable. Figure 1 shows the binding of IGF-I to rhIGFBP-3 with either rhIGFBP-3 immobilized (412 RU, Fig. 1a) or IGF-I immobilized (256 RU, Fig. 1b). These sensorgrams show the typical protocol used in these studies: a 10-minute wash to allow the surface to equilibrate with the buffer, followed by a 10-minute association phase and a 10-minute dissociation phase. The short downward spikes seen in the sensorgrams are disturbances resulting from opening and closing of valves in the BIACORE instrument's flow system. A sharp rise in signal at the beginning of the association phase and a corresponding sharp drop at the beginning of the dissociation phase are due to a small refractive index difference between buffer alone and buffer containing the analyte protein.

In both Fig. 1a and 1b, the concentration of analyte was 20 nM. The difference in maximum analyte bound (75 RU IGF-I vs. 200 RU rhIGFBP-3) is due to the difference in molecular weight. The linearity of the initial portion of the association phase of the sensorgram in Fig. 1b indicates the presence of mass transport effects. However, analyses of these experiments with or without including mass transport in the model gave comparable results, which were also in agreement with results obtained with

rhIGFBP-3 immobilized and IGF-I as analyte (e.g. Fig. 1a).

Figure 2 shows the results of similar experiments using the binding protein fragments rhIGFBP-3^{1-97} and rhIGFBP-3^{98-264}. For each of the fragments, the shapes of the sensorgrams are similar whether the fragment or IGF-I is immobilized. The rhIGFBP-3^{1-97} and rhIGFBP-3^{98-264} sensorgrams have different general shapes because both the kinetic association and dissociation constants are slower for rhIGFBP-3^{98-264} than for rhIGFBP-3^{1-97} (see Table I). Note that there is a downward or upward drift in signal during the initial wash stage in the experiments with binding protein fragments immobilized. This was a general observation during these studies; that is, sensor chip surfaces immobilized with binding protein fragment tend to be more unstable than those immobilized with full-length rhIGFBP-3, or with IGF-I.

In Figure 3 is shown a comparison of the measured binding affinity for IGF-I binding to full-length rhIGFBP-3 or to the binding protein fragments, either with binding protein immobilized or with IGF-I immobilized. The data are plotted with a logarithmic ordinate, and the results show that the affinity of IGF-I for either rhIGFBP-3^{1-97} or rhIGFBP-3^{98-264} is approximately 1000-fold lower than the affinity for full-length rhIGFBP-3, with rhIGFBP-3^{98-264} having a somewhat lower affinity than rhIGFBP-3^{1-97}. The figure also shows that experiments in either immobilization orientation give similar measured affinities.

Whenever possible, binding parameter estimates were obtained from global fitting to multiple sensorgrams at different analyte concentrations. An example of such an experiment is shown in Fig. 4. In this experiment, rhIGFBP-3 was immobilized at 726

RU, and IGF-I at concentrations from 0.5 – 50 nM was flowed over the immobilized surface. Because of the high affinity of IGF-I for rhIGFBP-3, binding is affected by mass transport limitation, which is most pronounced at lower analyte concentrations. The entire set of sensorgram data was fitted using a model that includes mass transport effects, and for comparison was re-fitted using an ordinary one-site (Langmuir) binding model. For this experiment, the computed binding affinities for the two different models were 5.6×10^9 M^{-1} and 5.8×10^9 M^{-1}, respectively. The respective kinetic association constants were 8.3×10^5 $M^{-1}s^{-1}$and 6.4×10^5 $M^{-1}s^{-1}$, and the dissociation constants were 1.4×10^{-4} s^{-1} and 1.2×10^{-4} s^{-1}. Other global experiments also showed a close correspondence between the results using the two different models, indicating that the estimated binding parameters, especially the equilibrium constants, are not especially sensitive to mass transport effects when global fitting is used.

Binding of IGF-II or biotinylated IGF-I to rhIGFBP-3 and its fragments

All of the above experiments were repeated using IGF-II instead of IGF-I. In all experiments, the sensorgrams for IGF-II were visually very similar to those for IGF-I, and calculated binding parameters were also similar, although IGF-II showed a slightly higher affinity for rhIGFBP-3. Figure 5 shows sensorgrams for IGF-I and IGF-II, as well as a biotin-labeled IGF-I, all at 50 nM, binding to the same immobilized rhIGFBP-3 surface. These sensorgrams were taken from a larger experiment designed for global analysis. The top two sensorgrams are those for IGF-I and IGF-II. Note that in the association phase the IGF-I signal is higher than that for IGF-II, which is due solely to a

slightly higher refractive index of the IGF-I-containing buffer. In the dissociation phase, where both surfaces are exposed to the same buffer, the IGF-II signal is slightly higher, indicative of its higher affinity. The affinities for IGF-I and IGF-II in this experiment, calculated by global analysis, were 2.1 x 10^9 M^{-1} and 3.0 x $10^9 M^{-1}$, respectively. Table I gives the summary of the calculated binding parameters for IGF-I and IGF-II binding to immobilized rhIGFBP-3 or its N- or C-terminal fragments. The table only includes results from experiments using immobilized binding protein and fragments, as the experiments with the immobilized IGFs were judged to be less reliable, primarily due to possible self-association of binding proteins (see later discussion).

In this experiment, we also tested the binding of biotin-labeled IGF-I to immobilized rhIGFBP-3. The lowest of the curves in Fig. 5 shows the binding of biotin-IGF-I to rhIGFBP-3. In this experiment, using global analysis, the affinity of biotin-IGF-I was calculated to be 1.1 x 10^9 M^{-1}.

Binding of human insulin to rhIGFBP-3 and its N- and C-terminal fragments

In this study we tested the binding of human insulin to rhIGFBP-3 and its fragments, with either binding protein or insulin immobilized on the sensor chip. In most experiments, the observed binding was very weak or absent in either configuration, and reasonable estimates of binding parameters could not be made, nor could comparisons be made of the relative affinities of insulin binding to full-length rhIGFBP-3 or its fragments. Apparent binding was observed in a few experiments, and by comparing this binding with control runs using IGF-I, we could estimate equilibrium K_a's less than 10^6

M^{-1}. Figure 6 shows an example of the weak binding of human insulin (2 μM) to immobilized rhIGFBP-3. For this sensorgram, the equilibrium K_a was estimated to be less than 10^5 M^{-1}, assuming that insulin binds with the same stoichiometry as IGF-I.

Binding of IGF-I and IGF-II to mac25(IGFBP-rP1) and CTGF(IGFBP-rP2)

We also tested the binding of IGF-I, IGF-II and human insulin to new members of the IGFBP superfamily, mac25(IGFBP-rP1) and CTGF(IGFBP-rP2). In no case could we unambiguously demonstrate binding of IGF or insulin molecules to these proteins. Figure 7 shows examples of tests of mac25(IGFBP-rP1) and CTGF(IGFBP-rP2) binding to immobilized IGF-I.

Self-association of IGFBP and its fragments

Most of our experiments using immobilized IGFs gave consistent results, with calculated binding parameters very similar to those for the experiments with IGFBP immobilized (see Fig. 3). However, because of potential inaccuracies in binding parameter determinations due to the two-dimensional geometry of binding, we also attempted to measure equilibrium binding affinities using solution affinity assays on the BIACORE. Our observations in some of these experiments revealed apparent self-aggregation of the IGF binding protein and its fragments. Figure 8 shows one such experiment, in which IGF-I at 20 nM was incubated with varying concentrations (2-200 nM) of rhIGFBP-3 for 15-20 min at 25 °C, after which the solution was passed over an rhIGFBP-3-immobilized sensor chip to record a sensorgram. These sensorgrams were

interleaved with sensorgrams in which solutions of pure IGF-I at varying concentrations between 0 and 20 nM were injected over the rhIGFBP-3 surface, and the pure-IGF-I sensorgrams were used to construct a calibration curve of signal vs. free IGF-I concentration. The goal was to use the calibration curve to determine the free concentration of IGF-I in the mixed solution, and, along with the known total concentrations of IGF-I and rhIGFBP-3 in solution, to perform an equilibrium analysis to determine the solution equilibrium binding affinity. Because increasing concentrations of rhIGFBP-3 should decrease the free IGF-I concentration, the signal in the mixed protein sensorgrams would be expected to decrease at higher rhIGFBP-3 concentrations. Instead, as shown in Fig. 8, we observed that the signal remained constant or dropped slightly for rhIGFBP-3 concentrations up to 20 nM, but at higher concentrations the signal increased instead of falling. The most straightforward interpretation of this was that the rhIGFBP-3 was itself binding to the rhIGFBP-3 immobilized surface, and therefore solution assays could not be done in this system.

We then investigated directly the binding of rhIGFBP-3 and its fragments to each other. Figure 9 shows an example of binding of rhIGFBP-3 or rhIGFBP-3^{98-264} to a surface immobilized with rhIGFBP-3^{98-264}, in which binding is clearly evident. From experiments using all combinations of immobilized and solution proteins, we observed that rhIGFBP-3 and rhIGFBP-3^{98-264} bind weakly to themselves and to each other (apparent K_a ~ 8-30 x 10^6 M^{-1}; that is, more than 100-fold lower affinity than that of IGF-I for rhIGFBP-3), whereas rhIGFBP-3^{1-97} binds very weakly or not at all to itself and to the other proteins (Ka ~ 0-3 x 10^6 M^{-1}). Because rhIGFBP-3 and rhIGFBP-3^{98-264} would be expected to

aggregate also in the flow-through solution in these assays, these results are approximate.

Discussion

If the N- and C- terminal regions of IGFBP-3 combine to form a high-affinity binding site for IGF molecules (1;14;15), one would expect that the N- or C-terminal fragments of IGFBP-3 might individually bind IGF-I or IGF-II, but with lower affinity than the full-length binding protein. The binding regions on the two fragments could combine to form a single larger high-affinity site, or could interact with two separate regions on the IGF molecule to result in high affinity binding. This last mechanism has been suggested, for example, for insulin binding to the insulin receptor (46;47). Our results here show that IGF-I and IGF-II bind the N- and C-terminal recombinant fragments rhIGFBP-3^{1-97} and rhIGFBP-3^{98-264} with affinities approximately 1000-fold lower than that of the IGFs for full-length rhIGFBP-3. These results are consistent with the idea that the combination of the two sites results in high-affinity binding, but do not distinguish whether there is a single high-affinity binding site or two separate sites.

Recently, Galanis *et al* (38) studied the binding of IGF-I and IGF-II to N-terminal (1-88) and C-terminal (165-264) IGFBP-3 fragments using a BIACORE instrument. For the N-terminal fragment, they measured equilibrium affinities of 1.03×10^7 M^{-1} and 6.16×10^7 M^{-1} for IGF-I and IGF-II binding, respectively, as compared to our measurements of about 0.6×10^7 M^{-1} for both IGF-I and IGF-II. They did not quote an affinity for IGF-I or IGF-II binding to their C-terminal fragment using the BIACORE, but were able to observe binding using solution assays. Interestingly, they found that the 1-88 N-terminal fragment could not be immobilized using the amine coupling method, and that the 165-264 C-terminal fragment could be immobilized, but was inactive in BIACORE assays. In

contrast, both our 1-97 N-terminal and 98-264 C-terminal fragments could be immobilized and retained activity, and both were also active in binding to immobilized IGF-I (38).

Our measurements of the binding of IGF-I and IGF-II to full-length rhIGFBP-3 indicate equilibrium affinities in the range of 4-5 x 10^9 M^{-1}. These estimates are lower than those measured using ^{125}I-labeled IGFs, where affinities between 8 x 10^9 M^{-1} and 152 x 10^9 M^{-1} have been reported (quoted and summarized in (36)). We had observed a similar difference in an earlier study of IGF analogue binding to IGFBP-3 (33), but it is not clear whether this is due to the different conditions of binding, or to differences in analytical methods.

Wong et al (36), using a BIACORE instrument, calculated an affinity of 18.4 x 10^9 M^{-1} for IGF-I binding to a human recombinant IGFBP-3. These results are apparently the average of separate determinations of the kinetic binding parameters from individual sensorgrams, whereas our results for IGF-I binding to immobilized rhIGFBP-3 are derived from global analyses (43;44), in which a binding model is fitted simultaneously to data from multiple sensorgrams at different analyte concentrations. Global analyses should be more accurate, since they assume a common value in all sensorgrams for R_{max}, the maximum analyte bound at saturation, whereas analyses of single sensorgrams from the same experiment can yield different apparent values of R_{max}, which is unrealistic.

Galanis *et al* (38) also determined a high affinity (1 x 10^{11} M^{-1}) for full-length IGFBP-3 binding to immobilized IGF-I, as compared to our estimate of 7 x 10^9 M-1 under similar

conditions. Their high affinity was primarily due to a very low kinetic k_d (1×10^{-6} s^{-1} compared to 3×10^{-4} s^{-1} in our experiments). One explanation we can offer for the difference is that Galanis *et al* conducted their assays at a flow rate of 5 µl/min, whereas ours were done at 50 µl/min. It is well-known (48;49) that for high-affinity interactions such as that between IGF-I and IGFBP-3, there can be significant rebinding of analyte during the dissociation phase, and this can be expected to decrease the apparent dissociation rate.

Here, and in our previous study 3 (33), our data show that IGF-II binds rhIGFBP-3 with slightly higher affinity than does IGF-I, which was also observed in other studies in the literature (50).

Our measurements of binding of biotinylated IGF-I to rhIGFBP-3, using global analysis, show that the kinetic association constant is reduced by a factor of 3, and the kinetic dissociation constant increased by a factor of 1.4 relative to non-biotinylated IGF-I. This results in a 4-fold reduction in the apparent equilibrium affinity of biotinylated IGF-I relative to non-biotinylated IGF-I. These are relatively small differences, indicating that biotinylation of IGF-I does not greatly interfere with its binding to IGFBPs. It is of note that labeling with iodine resulted in an affinity change of labeled IGFs to IGFBP-3 (51). Thus, the biotinylated IGF-I could be a better alternative to ^{125}I-IGF-I in experiments requiring labeled hormone.

With the BIACORE instrument, there is always the concern that the two-dimensional binding geometry can lead to inaccuracies in binding parameter measurements, for example from mass transport limitation or steric hindrance (52), or because of

inactivation of ligands due to immobilization on the sensor chip surface. In order to test the magnitude of such possible effects, we attempted to measure binding affinities in solution. For such an experiment to give reliable results, one of the requirements is that the signal observed when flowing the mixed sample over the surface is due only to the free IGF in solution. As shown earlier (see Figs. 8 and 9), this requirement does not hold for rhIGFBP-3 and rhIGFBP-3^{98-264}, since these molecules bind to each other in BIACORE assays and presumably self-associate in solution. Therefore the solution assay cannot reliably be used for these molecules. Although solution assays might be possible for rhIGFBP-3^{1-97}, since its self-association is much less than that of rhIGFBP-3 or rhIGFBP-3^{98-264}, we did not systematically investigate this.

The observation of self-association also raises questions about the accuracy of binding results obtained using binding proteins in the flow solution and, for example, immobilized IGF. At high concentrations, there could be a significant amount of self-aggregated binding protein in solution, which could introduce errors in the binding analysis. Furthermore, there is the possibility that binding protein might bind to other binding protein molecules already associated to the immobilized IGF. To analyze these phenomena in detail would require further investigation, but these observations suggest that binding analyses with immobilized binding proteins, such as the results shown in Table 1, should be more reliable than those with immobilized IGFs.

On the basis of evidence that activation of the insulin receptor is inhibited by IGFBPs, and that mac25(IGFBP-rP1) is able to bind insulin (13), we tested the binding of human insulin to rhIGFBP-3, and to the recombinant mac25(IGFBP-rP1) and CTGF(IGFBP-

rP2) molecules using the BIACORE instrument. We also tested insulin binding to the IGFBP recombinant fragments rhIGFBP-3^{1-97} and rhIGFBP$^{98-264}$. Most experiments could not confirm binding, but in a few experiments the binding of insulin to rhIGFBP-3 (see Fig. 6) was detectable, indicating that insulin may bind IGFBP-3 with low affinity, as we had previously observed (33). We could not detect binding of insulin to the IGFBP-related proteins, nor to the rhIGFBP-3 fragments, in these biosensor assays.

We tested the binding of IGF-I and IGF-II to the mac25(IGFBP-rP1) and CTGF(IGFBP-rP2) molecules, with either the BP-rP or the IGF molecules immobilized, at analyte concentrations up to 500 nM. In no case could we detect binding using the biosensor instrument (see Fig. 7). These results were unexpected, since there is evidence for binding of both IGF-I and insulin to the binding protein molecules, from studies using radiolabeled IGF molecules (13;20). However, since binding affinities less than about 10^5 M^{-1} or 10^6 M^{-1} are difficult to detect using the biosensor, we cannot rule out that there is weak binding below the detection limit of the instrument. There is an indication from affinity cross-linking studies that IGF-I binding affinity for mac25(IGFBP-rP1) may be higher than these values (13;53) so it remains to be determined whether our inability to detect binding on the biosensor instrument is because of differences in binding conditions, or because cross-linking experiments are in fact measuring extremely low binding affinities.

References

1. **Rosenfeld RG, Hwa V, Wilson L, Lopez-Bermejo A, Buckway C, Burren C, Choi WK, Devi G, Ingermann A, Graham D, Minniti G, Spagnoli A, Oh Y** 1999 The Insulin-like Growth Factor Binding Protein Superfamily: New Perspectives. Pediatrics 104:1018-1021

2. **Binoux M, Lalou C, Mohseni-Zadeh S** 1999 Biological actions of proteolytic fragments of the IGF binding proteins. In: Rosenfeld RG, Roberts Jr ChT (eds). The IGF-System, Molecular Biology, Physiology, and Clinical Applications.Humana Press, Totowa, NJ, USA:281-313

3. **Maile LA, Holly JM** 1999 Insulin-like growth factor binding protein (IGFBP) proteolysis: occurrence, identification, role and regulation. Growth Hormone and IGF Research 9:85-95

4. **Oh Y, Rosenfeld RG** 1999 IGF-independent actions of the IGF binding proteins. In: Rosenfeld RG, Roberts Jr ChT (eds). The IGF-System, Molecular Biology, Physiology, and Clinical Applications.Humana Press, Totowa, NJ, USA:257-272

5. **Jones JI, Clemmons DR** 1995 Insulin-like growth factors and their binding proteins: biological actions. Endocr Rev 16:3-34

6. **Oh Y, Muller HL, Lamson G, Rosenfeld RG** 1993 Insulin-like growth factor (IGF)-independent action of IGF-binding protein-3 in Hs578T human breast cancer cells. Cell surface binding and growth inhibition. Journal of Biological Chemistry 268:14964-14971

7. **Hossenlopp P, Segovia B, Lassarre C, Roghani M, Bredon M, Binoux M** 1990 Evidence of enzymatic degradation of insulin-like growth factor-binding proteins in the 150K complex during pregnancy. J Clin Endocrinol Metab 71:797-805

8. **Giudice LC, Farrell EM, Pham H, Lamson G, Rosenfeld RG** 1990 Insulin-like growth factor binding proteins in maternal serum throughout gestation and in the puerperium: effects of a pregnancy- associated serum protease activity. J Clin Endocrinol Metab 71:806-816

9. **Andress DL, Birnbaum RS** 1992 Human osteoblast-derived insulin-like growth factor (IGF) binding protein-5 stimulates osteoblast mitogenesis and potentiates IGF action. Journal of Biological Chemistry 267:22467-22472

10. **Lalou C, Lassarre C, Binoux M** 1996 A proteolytic fragment of insulin-like growth factor (IGF) binding protein-3 that fails to bind IGFs inhibits the mitogenic effects of IGF- I and insulin. Endocrinology 137:3206-3212

11. **Angelloz-Nicoud P, Lalou C, Binoux M** 1998 Prostate carcinoma (PC-3) cell

proliferation is stimulated by the 22-25-kDa proteolytic fragment (1-160) and inhibited by the 16-kDa fragment (1-95) of recombinant human insulin-like growth factor binding protein-3. Growth Horm IGF Res 8:71-75

12. **Vorwerk P, Yamanaka Y, Spagnoli A, Oh Y, Rosenfeld RG** 1998 Insulin and IGF binding by IGFBP-3 fragments derived from proteolysis, baculovirus expression and normal human urine. J Clin Endocrinol Metab 83:1392-1395

13. **Yamanaka Y, Wilson EM, Rosenfeld RG, Oh Y** 1997 Inhibition of insulin receptor activation by insulin-like growth factor binding proteins. Journal of Biological Chemistry 272:30729-30734

14. **Spencer EM, Chan K** 1995 A 3-dimensional model for the insulin-like growth factor binding proteins (IGFBPs); supporting evidence using the structural determinants of the IGF binding site on IGFBP-3. Prog Growth Factor Res 6:209-214

15. **Carrick FE, Forbes BE, Wallace JC** 1999 Recreating a high affinity insulin-like growth factor binding protein using discrete N- and C-terminal fragments. Growth Hormone and IGF Research 9:317-318

16. **Vorwerk P, Oh Y, Lee PD, Khare A, Rosenfeld RG** 1997 Synthesis of IGFBP-3 fragments in a baculovirus system and characterization of monoclonal anti-IGFBP-

3 antibodies. J Clin Endocrinol Metab 82:2368-2370

17. **Yang DH, Kim HS, Wilson EM, Rosenfeld RG, Oh Y** 1998 Identification of glycosylated 38-kDa connective tissue growth factor (IGFBP-related protein 2) and proteolytic fragments in human biological fluids, and up-regulation of IGFBP-rP2 expression by TGF-beta in Hs578T human breast cancer cells. J Clin Endocrinol Metab 83:2593-2596

18. **Firth SM, Baxter RC** 1999 Characterisation of recombinant glycosylation variants of insulin-like growth factor binding protein-3. J Endocrinol 160:379-387

19. **Firth SM, Ganeshprasad U, Baxter RC** 1998 Structural determinants of ligand and cell surface binding of insulin- like growth factor-binding protein-3. Journal of Biological Chemistry 273:2631-2638

20. **Kim HS, Nagalla SR, Oh Y, Wilson E, Roberts CTJ, Rosenfeld RG** 1997 Identification of a family of low-affinity insulin-like growth factor binding proteins (IGFBPs): characterization of connective tissue growth factor as a member of the IGFBP superfamily. Proc Natl Acad Sci U S A 94:12981-12986

21. **Burren CP, Wilson EM, Hwa V, Oh Y, Rosenfeld RG** 1999 Binding properties and distribution of insulin-like growth factor binding protein-related protein 3 (IGFBP-rP3/NovH), an additional member of the IGFBP Superfamily. J Clin

Endocrinol Metab 84:1096-1103

22. **Forbes BE, Turner D, Hodge SJ, McNeil KA, Forsberg G, Wallace JC** 1998 Localization of an insulin-like growth factor (IGF) binding site of bovine IGF binding protein-2 using disulfide mapping and deletion mutation analysis of the C-terminal domain. Journal of Biological Chemistry 273:4647-4652

23. **Sommer A, Maack CA, Spratt SK, Mascarenhas D, Tressel TJ, Rhodes ET, Lee R, Roumas M, Tatsuno GP, Flynn JA, Gerber N, Taylor J, Cudny H, Nanncy L, Hunt TK, Spencer EM** 1991 Molecular genetics and actions of recombinant insulin-like growth factor binding protein-3. In: Spencer EM (ed). Modern concepts of Insulin-like growth factors.Elsevier Science Publishing Co.,Inc.,715-728

24. **Spencer EM, Steenfos H, Strathearn M, Spratt SK, Hunt TK** 1989 Molecular biology and physiology of the insulin-like growth factor binding protein 3, the acid-stable unit of the 150k serum insulin-like growth factor binding komplex. In: Drop SL, Hintz RL (eds). Insulin-like growth factor binding proteins.Elsevier Science Publishers Biomedical Division,73-79

25. **Chernausek SD, Smith CE, Duffin KL, Busby WH, Wright G, Clemmons DR** 1995 Proteolytic cleavage of insulin-like growth factor binding protein 4 (IGFBP-4). Localization of cleavage site to non-homologous region of native IGFBP-4. Journal

of Biological Chemistry 270:11377-11382

26. **Kiefer MC, Schmid C, Waldvogel M, Schlapfer I, Futo E, Masiarz FR, Green K, Barr PJ, Zapf J** 1992 Characterization of recombinant human insulin-like growth factor binding proteins 4, 5, and 6 produced in yeast. Journal of Biological Chemistry 267:12692-12699

27. **Bach LA, Hsieh S, Sakano K, Fujiwara H, Perdue JF, Rechler MM** 1993 Binding of mutants of human insulin-like growth factor II to insulin- like growth factor binding proteins 1-6. Journal of Biological Chemistry 268:9246-9254

28. **Clemmons DR, Dehoff ML, Busby WH, Bayne ML, Cascieri MA** 1992 Competition for binding to insulin-like growth factor (IGF) binding protein-2, 3, 4, and 5 by the IGFs and IGF analogs. Endocrinology 131:890-895

29. **Oh Y, Muller HL, Lee DY, Fielder PJ, Rosenfeld RG** 1993 Characterization of the affinities of insulin-like growth factor (IGF)- binding proteins 1-4 for IGF-I, IGF-II, IGF-I/insulin hybrid, and IGF-I analogs. Endocrinology 132:1337-1344

30. **Fowlkes JL, Serra D** 1996 A rapid, non-radioactive method for the detection of insulin-like growth factor binding proteins by Western ligand blotting. Endocrinology 137:5751-5754

31. **Op De Beeck L, Verlooy JE, Van Buul-Offers SC, Du CM** 1997 Detection of serum insulin-like growth factor binding proteins on western ligand blots by biotinylated IGF and enhanced chemiluminescence. J Endocrinol 154:R1-R5

32. **Devi GR, Yang DH, Rosenfeld RG, Oh Y** 2000 Differential effects of insulin-like growth factor (IGF)-binding protein-3 and its proteolytic fragments on ligand binding, cell surface association, and IGF-I receptor signaling. Endocrinology 141:4171-4179

33. **Heding A, Gill R, Ogawa Y, De Meyts P, Shymko RM** 1996 Biosensor measurement of the binding of insulin-like growth factors I and II and their analogues to the insulin-like growth factor-binding protein-3. Journal of Biological Chemistry 271:13948-13952

34. **Shymko RM, Hohmann B, Vorwerk P** 1999 Biosensor analysis of insulin-like growth factor/insulin-like growth factor binding protein interactions. Growth Hormone and IGF Research 9:323

35. **Vorwerk P, Hohmann B, Oh Y, Rosenfeld RG, Shymko RM** 1999 Biosensor measurement of IGF-binding to N- and C-terminal recombinant human IGFBP-3 fragments. Growth Hormone and IGF Research 9:363

36. **Wong MS, Fong CC, Yang M** 1999 Biosensor measurement of the interaction

kinetics between insulin-like growth factors and their binding proteins. Biochim Biophys Acta 1432:293-301

37. **Marinaro JA, Jamieson GP, Hogarth PM, Bach LA** 1999 Differential dissociation kinetics explain the binding preference of insulin-like growth factor binding protein-6 for insulin-like growth factor-II over insulin-like growth factor-I. FEBS Lett 450:240-244

38. **Galanis M, Firth SM, Bond J, Nathanielsz A, Kortt AA, Hudson PJ, Baxter RC** 2001 Ligand-binding characteristics of recombinant amino- and carboxyl-terminal fragments of human insulin-like growth factor-binding protein-3. J Endocrinol 169:123-133

39. **Kalus W, Zweckstetter M, Renner C, Sanchez Y, Georgescu J, Grol M, Demuth D, Schumacher R, Dony C, Lang K, Holak TA** 1998 Structure of the IGF-binding domain of the insulin-like growth factor-binding protein-5 (IGFBP-5): implications for IGF and IGF-I receptor interactions. EMBO J 17:6558-6572

40. **Johnsson B, Lofas S, Lindquist G** 1991 Immobilization of proteins to a carboxymethyldextran-modified gold surface for biospecific interaction analysis in surface plasmon resonance sensors. Analytical Biochemistry 198:268-277

41. **Schuck P** 1996 Kinetics of ligand binding to receptor immobilized in a polymer

matrix, as detected with an evanescent wave biosensor. I. A computer simulation of the influence of mass transport. Biophys J 70:1230-1249

42. **Myszka DG** 1997 Kinetic analysis of macromolecular interactions using surface plasmon resonance biosensors. Curr Opin Biotechnol 8:50-57

43. **Schuck P** 1997 Reliable determination of binding affinity and kinetics using surface plasmon resonance biosensors. Current Opinion in Biotechnology 8:498-502

44. **Karlsson R, Falt A** 1997 Experimental-design for kinetic-analysis of protein-protein interactions with surface-plasmon resonance biosensors. Journal Of Immunological Methods 200:121-133

45. **Karlsson R, Kullman-Magnusson M, Hamalainen MD, Remaeus A, Andersson K, Borg P, Gyzander E, Deinum J** 2000 Biosensor analysis of drug-target interactions: Direct and competitive binding assays for investigation of interactions between thrombin and thrombin inhibitors. Analytical Biochemistry 278:1-13

46. **Schäffer L** 1994 A model for insulin binding to the insulin receptor. European Journal of Biochemistry 221:1127-1132

47. **De Meyts P, Ursø B, Christoffersen CT, Shymko RM** 1995 Mechanism of insulin

and IGF-I receptor activation and signal transduction specificity. Receptor dimer cross-linking, bell- shaped curves, and sustained versus transient signaling. Annals of the New York Academy of Sciences 766:388-401

48. **Glaser RW** 1993 Antigen-antibody binding and mass transport by convection and diffusion to a surface: A two-dimensional computer model of binding and dissociation kinetics. Analytical Biochemistry 213:152-161

49. **Schuck P, Minton AP** 1996 Analysis of mass transport-limited binding-kinetics in evanescent-wave biosensors. Analytical Biochemistry 240:262-272

50. **Martin JL, Baxter RC** 1986 Insulin-like growth factor binding proteins from human plasma. Journal of Biological Chemistry 261:8754-8760

51. **Suikkari AM, Baxter RC** 1991 Insulin-like growth factor (IGF) binding protein-3 in pregnancy serum binds native IGF-I but not iodo-IGF-I. J Clin Endocrinol Metab 73:1377-1379

52. **Schuck P** 1997 Use of surface plasmon resonance to probe the equilibrium and dynamic aspects of interactions between biological macromolecules. Annual Review of Biophysics and Biomolecular Structure 26: 541-566

53. **Oh Y, Nagalla SR, Yamanaka Y, Kim HS, Wilson E, Rosenfeld RG** 1996

Synthesis and characterization of insulin-like growth factor-binding protein (IGFBP)-7. Recombinant human mac25 protein specifically binds IGF-I and -II. Journal of Biological Chemistry 271:30322-30325

Table Legend

Table I. Binding parameters (S.E.) for IGF-I and IGF-II binding to immobilized rhIGFBP-3, rhIGFBP-3^{1-97} and rhIGFBP-3^{98-264}. a) Equilibrium affinity, K_a (M^{-1}) b) Kinetic association constant, k_a ($M^{-1}\,s^{-1}$) c) Kinetic dissociation constant, k_d (s^{-1}).

Figure Legends

Figure 1: a) IGF-I (20 nM) binding to immobilized full-length rhIGFBP-3 (412 RU). HBS buffer was flowed over the surface for 12 minutes, followed by 5 minutes of association and 10 minutes of dissociation of IGF-I. b) Full-length rhIGFBP-3 (20 nM) binding to immobilized IGF-I (256 RU).

Figure 2. a) IGF-I (1000 nM) binding to immobilized rhIGFBP-3^{1-97} (1245 RU). b) rhIGFBP-3^{1-97} (200 nM) binding to immobilized IGF-I (532 RU). c) IGF-I (100 nM) binding to immobilized rhIGFBP-3^{98-264} (2253 RU) d) rhIGFBP-3^{98-264} (1000 nM) binding to immobilized IGF-I (191 RU).

Figure 3. Comparison of measured IGF-I binding affinities in opposite immobilization orientations. Solid bars: Binding protein or fragment immobilized, IGF-I in the flow-through buffer. Open bars: IGF-I immobilized, binding protein or fragment in the flow-through buffer. Error bars show standard deviations.

Figure 4. Example of a data set used for global binding analysis: IGF-I (bottom to top curves - 0.5, 1, 2, 5, 10, 20, 50 nM) binding to immobilized full-length rhIGFBP-3 (726 RU). The linearity of the early part of the association phases, most pronounced at low concentrations, indicates mass transport limitation.

Figure 5. Sensorgrams for IGF-I, IGF-II and biotinylated IGF-I, all at 50nM, binding to immobilized full-length rhIGFBP-3 (158 RU). Solid line: IGF-I; dashed line: IGF-II; dotted line: biotinylated IGF-I. The IGF-I curve is higher than that for IGF-II in the association phase because of a difference in refractive index of the two solutions. In

the dissociation phase, where the flow-through buffers are identical, the IGF-II curve is higher, indicating that more IGF-II than IGF-I was bound to the surface.

Figure 6. Interaction of human insulin (2000 nM) with full-length rhIGFBP-3 (412 RU). The rising association phase and falling dissociation phase indicate apparent binding, but with very low affinity, and near the detection limit of the instrument.

Figure 7. Interaction of a) mac25 (IGFBP-rP1) and b) CTGF (IGFBP-rP2), with immobilized IGF-I (532 RU). Binding is below the detection limit of the instrument.

Figure 8. Interaction of a mixture of IGF-I (20 nM) and full-length rhIGFBP-3 (0-200 nM) with a sensor chip surface on which full-length rhIGFBP-3 is immobilized (522 RU). Solid lines: 20 nM IGF-I plus 0-20 nM rhIGFBP-3; Dotted lines: 20 nM IGF-I plus, bottom to top, 50, 100, 200 nM rhIGFBP-3.

Figure 9. Interaction of full-length rhIGFBP-3 and rhIGFBP-3^{98-264} with immobilized rhIGFBP-3^{98-264} (2307 RU). Solid lines: rhIGFBP-3 (bottom to top: 50, 200, 500 nM). Dashed lines: rhIGFBP-3^{98-264} (bottom to top: 50, 200, 500 nM).

Tables

Table Ia, b, c: IGF-I and IGF-II binding to immobilized binding protein or fragments

Ka values: Units = 1/M, errors are S.E.s

	rhIGFBP-3	rhIGFBP-3$^{1-97}$	rhIGFBP-3$^{98-264}$
IGF-I	4.13 0.71 x10^{9}	6.14 1.98 x10^{6}	1.80 0.84 x10^{6}
IGF-II	4.68 0.83 x10^{9}	5.89 1.09 x10^{6}	1.01 0.89 x10^{7}

ka values: Units = 1/M.s, , errors are S.E.s

	rhIGFBP-3	rhIGFBP-3$^{1-97}$	rhIGFBP-3$^{98-264}$
IGF-I	7.87 ± 1.00 x10^{5}	3.22 ± 1.11 x10^{4}	2.54 ± 2.15 x10^{3}
IGF-II	7.63 ± 1.60 x10^{5}	3.63 ± 2.67 x10^{4}	2.17 ± 1.61 x10^{4}

kd values: Units = 1/s, , erors are S.E.s

	rhIGFBP-3	rhIGFBP-3$^{1-97}$	rhIGFBP-3$^{98-264}$
IGF-I	2.09 ± 0.35 x10^{-4}	5.55 ± 1.40 x10^{-3}	1.09 ± 0.69 x10^{-3}
IGF-II	1.78 ± 0.53 x10^{-4}	5.48 ± 3.52 x10^{-3}	3.18 ± 1.19 x10^{-3}